DOCTORAL DISSERTATION

Study on the Properties of Organic Molecule / Nano-Carbon Conjugates

有機分子／ナノカーボン複合体の物性研究

Ahmed Ibrahim Ahmed Abd El-Mageed

2016

Department of Chemistry, Graduate School of Science

Osaka University

ACKNOWLEDGMENT

First of all, I would like to thank my **GOD** for giving me the opportunity and well power to accomplish my PhD thesis.

I really would like to express my deepest and full gratitude to my research advisor ***Prof. Takuji Ogawa,*** Professor of Physical Organic Chemistry, Department of Chemistry, Graduate School of Science, Osaka University, for his generous, kind and continuous support, help, advice, guidance and ongoing encouragement along my study. It is my great honor to have the opportunity to join in his group and being one of his students. Through him you are not only learning science but also the ethics of it, I have really learned a lot of valuable things, gained a lot of experiences during my study in Japan which are of great importance to my skill, career and also for my life.

I wish to express my deepest gratefulness and gratitude to ***Prof. Fouad Taha***, Professor of Physical Chemistry, Minia University, Egypt, ***Prof. Amro Dyab***, Associate Professor of Physical Chemistry, Minia University, Egypt, and ***Prof. Hisham Essawy***, Professor of Physical Chemistry, National Research Center, Egypt, for their substantial assistance, kind help and support during my study in master as well as in PhD. I'm really lucky to have such kind of these respected, affectionate supervisors.

I am grateful from my deepest heart to ***Mrs. Ryoko Takeda*** for the great support and also her kind help not only for my study but also for my administrative affairs and my daily life. She is really awesome; I'll never forget her and her kindness with me and my family during my stay in Japan.

I would like to express my deeply thank to my former Assistant Professors, ***Prof. Hirofumi Tanaka*** and ***Prof. Daisuke Tanaka*** for all their help, useful discussion and suggestions in my study and experimental work in Japan.

I would like to express my sincerely thank to my Associate Professor ***Dr. Ken-ichi Yamashita***, my Assistant Professor ***Dr. Yosuke Tani***, my wonderful senior ***Dr. Murni Handayani***, for all their kind help and support during my study.

I would like to sincerely thank the present lab (Laboratory of Physical Organic Chemistry) members including ***Mr. Minoru Fukumori***, ***Mr. Takashi Tamaki***, ***Mrs. Sunri Lee, Mr. Ari Yustisia Akbar, Mrs. Nunik Nurhayati, Mr. Yuki kawakami, Mr. Fumito Ishimura, Mrs. Yukiko Okimura, Mr. Shohei Hasegawa, Mr. Yoshito Yamazaki, Mr. Yudai Yamamoto, Mr. Zhijin Chen, Mr. Yuya Otani, Mrs. Kaya Ogawa, Mr. Yusuke Goto, Mr. Akira Shimojitosho, Mr. Kazuhito Furutani and Mrs. Yosephin Dewiani Rahmayanti, Mr. Hiroki Taniguchi, Mrs. Takayo Yamanaka, Mr. Zhao Wenyan, Mrs. Carolin Gruner***, for their friendliness and their help to my study.

I am really grateful to the past lab members including ***Dr. Tomoko Inose, Mrs. Mayuko Ojima, Mr. Nobuto Sumitani, Mr. Naoki Aketa, Mr. Sinichi Katayoshe, Mr. Satsuki Shimono, Mr. Naoya Sakata, Mr. Fumiya Miyamoto***, for all they have helped to my study.

I would like to express thanks to ***Mr. Akihiro Ito*** for kind help in Mass spectroscopy measurements and TEM training, ***Mr. Yasuto Todokoro*** and ***Mr. Naoya Inazumi*** for their help in NMR measurement.

I'm really grateful to ***Minia University***, Egypt and ***Osaka University***, Japan, for being part of them.

I would like to sincerely thank all the present and past ***staff of the Office for International Students and International Affairs,*** and ***Office of Graduate Admissions*** in Graduate School of Science, Osaka University, especially ***Mrs. Mizuho Suzuki,*** for their kind help and support during my study in Japan.

I would like to express thank to the ***Cultural Affairs and Missions Sector, Ministry of Higher Education, Arab Republic of Egypt***, for the scholarship (JS Scholarship) support for my study.

Also, I would like to express my deeply appreciation the all the past and present staff of ***Egyptian Cultural and Educational Bureau in Tokyo and all stuff,*** for their kind help, support and cooperation during my study.

I would like to express thanks to ***Ministry of Education, Culture, Sport and Science and Technology of Japan***, for the scholarship support for my study.

I would like to thank to all ***my Egyptian and Foreign Friends*** and ***kind Japanese people*** who have helped me and supported my study and my life in Japan.

And finally and most importantly, I would like to especially thank to ***my big and small families*** especially ***my parents***, ***my brothers***, ***my sister***, ***my wife*** and ***my little daughters***, for their never-ending love and support.

Ahmed Ibrahim Ahmed

Department of Chemistry, Graduate School of Science

Osaka University

August, 2016

Table of Contents

Chapter I. General Introduction

1.1. Molecular Electronics

1.1.1. Brief History

In 1974, the relationship between the electron transportation and the molecular structure in single molecule based devices has been initially investigated by Arieh Aviram and Mark Ratner[1]. They succeed to fabricate the first rectifier model as very simple electronic devices by using single organic molecules composed of donor - σ spacer (insulator) - acceptor system (i.e. molecular *p-n* junction). Two molecules were used by Aviram and Ratner, which illustrated in Figure 1. The first molecule is tetracyanoquinodimethane (TCNQ) tetrathiofulvalene (TTF) or TCNQ-TTF henceforth, in which TCNQ portion is used as an acceptor part while TTF portion is the donor part and both donor and acceptor parts are separated by three methylene bridges (to be more rigid) as an insulator or spacer to prevent overlapping between the two π – systems of the donor and acceptor ; however the second molecule is hemiquinone in which the quino groups (= O) are electron withdrawing groups so they decrease the π - electron density and elevate the electron affinity, hence make the left part of the molecule behaves as an acceptor part whereas the presence of the methoxy groups (− OCH_3) in the right part as an electron donating groups will increase the π - electron density and minimize the ionization potential making the right part of the molecule as the donor part, again the donor and acceptor parts are totally separated by single methylene bridge a spacer.

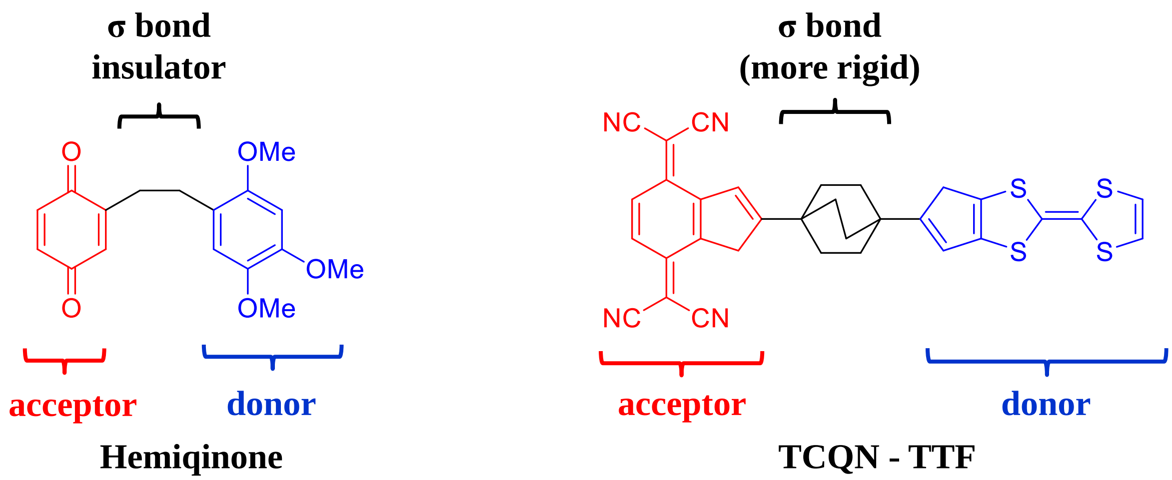

Figure 1. Two examples of single molecules can be used as rectifiers, proposed by Aviram and Ratner[1], composed of acceptor - σ spacer (insulator) - donor systems.

The rectification mechanism proposed by Aviram and Ratner is depicted in Figure 2, in which the molecule and its molecular orbitals are located in between two metal electrodes, the donor and acceptor parts of the molecule are totally separated by internal tunneling barrier which represents σ bridging bonds. As shown in Figure 2a, the energy diagram at no applied bias voltage in which LUMO of the acceptor (the lowest unoccupied molecular orbital) is located at or slightly above the Fermi energy level of the electrodes and obviously above the HOMO (the highest occupied molecular orbital) of the donor which is definitely appropriate to the rectifier behavior.

By applying an external field to the system, this is will cause an overlapping between the Fermi energy level of the cathode with the LUMO of the acceptor, at the same time the HOMO of donor would be also overlapped with the Fermi energy level of the anode. Under the forward applied bias voltage (VF), an electron can tunnel from the Fermi energy level of the cathode to the LUMO of the acceptor, consequentially an electron tunnels from the HOMO of the donor to the anode. Therefore, the electron tunneling process will occur from LUMO of acceptor to HOMO of donor, as demonstrated in Figure 2b.

Under reverse bias conditions, the electron tunneling from the cathode to the anode is no longer possible as the LUMO of donor is located higher than the Fermi energy level of the cathode (and significantly higher than the HOMO of the acceptor), also the HOMO of the acceptor is slightly lower than the Fermi energy level of the anode. If the reverse bias voltage becomes high enough, current will start to flow from the anode to the cathode through the π - system that means the tunneling mechanism would be same as forward case however higher bias voltage (backward bias V_B) is needed $V_B >> V_F$ (Figure 2c). As there is no current will flow in the backward case, the device will show rectification behavior. In an ideal rectification behavior, the electrical current should be passed in only one direction.

Accordingly since Aviram and Ratner's proposal, the molecular electronics field (occasionally also referred as *moletronics*[2]) has significantly expanded and attracted interest of many researchers[3-11]. Consequently numerous models of single molecule electronic devices have been actively designed and developed with a wide range of characteristic functions including diodes[12-15], memories[16-18], switches[19-23], logic gates[24-27], negative differential resistance[28], transistors[29-31] and wires[32].

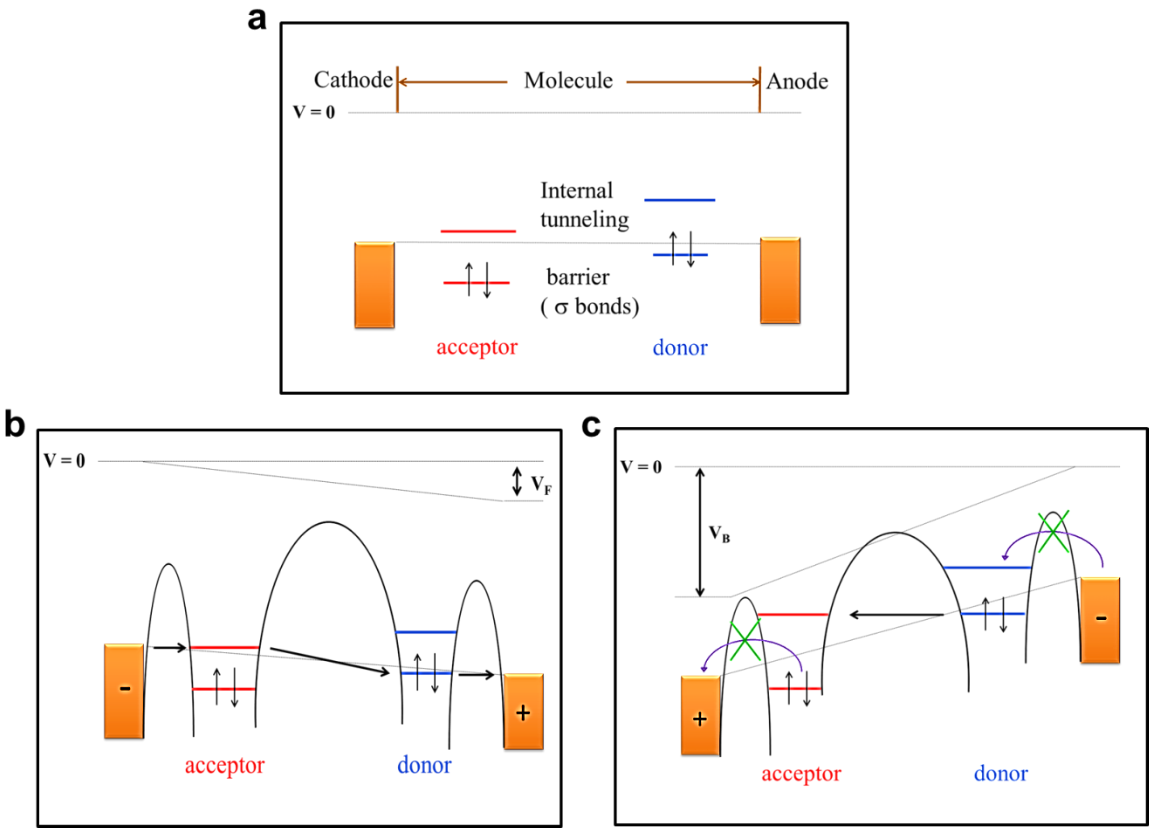

Figure 2. Schematic diagram illustrating Aviram-Ratner[1] rectifier model and the rectification mechanism **a**, Energy diagram at zero applied bias voltage, in which molecular orbitals of the molecule were located between two metal electrodes, the acceptor and donor parts are separated by internal tunneling barrier which represents σ bonds **b**, Forward applied bias voltage in which the rectification direction in the system as follows cathode ⟶ acceptor ⟶ donor ⟶ anode **c**, Reverse (backward) applied bias voltage, in which electron transfer is irreversible.

1.1.2. Concept

Molecular electronics is an interdisciplinary theme in nanotechnology, which can be also related to chemistry, physics, materials science and sometimes to biosciences[11,33]. The term molecular electronics is describing the field in which single molecules, small group of molecules or nanoscale objects can be utilized to perform electronic functions as the main active components in the electronic devices[3,7]. There is a wide variety of molecular building blocks, which can be used for the fabrication of electronic components i.e. molecules, nanoparticles, nanotubes and nanowires to form new devices and circuit architectures[34]. These molecular building blocks can be designed and/or assembled in such a way that they have properties which resemble traditional electronic components i.e. wire, transistor, rectifier, memory and switch. By emerging the properties inherent in single molecule components for fabricating a functional device; this will offer unlimited possibilities for technological development because the potentially diverse electronic functions of the component molecules[8].

Another approach to fabricate molecular electronic devices can be attained by using supramolecular chemistry techniques and/or self-assembly of organic molecules, carbon nanotubes, proteins and others. Self-assembly is a phenomenon in which atoms, molecules or groups of molecules can be arranged spontaneously into regular patterns without interference from outside. Interestingly, in molecular electronic devices, the electrochemically active molecules can change their behavior dramatically depending on the surrounded environment whether by electrodes or by other materials, where the molecules can either serve as conduits of electrical current or influence the charge transport properties of the electrodes to which they are connected[7,35]. Molecular electronic can be subdivided into two categories; *Molecular materials for electronics* in which the bulk properties of a material can be affected by utilizing the molecules properties, while *molecular scale electronics* mainly concentrate on single-molecule applications[36,37].

1.1.3. Why Molecular Electronics?

Although the complementary metal-oxide-semiconductors (CMOS henceforth) are being considered as the main solid state components for the modern integrated electronic circuitry; there has been considerable interest in finding out alternative electronic devices, which can display more significant applications, to replicate solid state components usage. In this regard, single molecules have been considered as effective and valuable building blocks for the future nanoelectronics systems, to overcome rising difficulties and substantial limitations that CMOS technology facing upon further downscaling for investigating higher performance[7,8].

When compared to the traditional inorganic materials i.e. silicon; organic semiconductors molecules (like π-conjugated organic molecules and polymers) have a very unique advantages and properties such as their low cost, low-temperature processing on flexible substrates, high-speed fabrication and tunable electronic properties. Furthermore, single molecules provide ideal systems to investigate charge transport on the molecular scale. In addition by using the chemical synthesis, very interesting devices and promising collections can be obtained such as nanocarbon materials / molecular junctions. Moreover, by using the physical and electronic properties of organic molecules designed by synthetic methods, chemical engineering can bring a novel dimensions in design flexibility that doesn't existent in typical inorganic electronic materials. Finally, the amalgamation of molecules and other nanoscale structures has led to a number of demonstrations of new and potentially useful applications. All of these aspects render single molecules a promising candidate for the next generation of electronics, so this is where the richness of molecular electronics emerges[7,8,35].

Since the main subject-matter in molecular electronics is the concept of size decreasing offered by molecular level control of properties even by individual molecules or by the use of small ensembles as functional building blocks in electronic device. It is well known that solid-state devices are fabricated from the "top-down" approach which utilizes an assortment of sophisticated lithographic techniques in order to pattern a substrate and this approach has become increasingly challenging as feature size decreases. On the other hand, the molecules are synthesized and designed from "bottom-up" approach that emerges small structures from the atomic, molecular, or single device level which offers a very precise design of atoms and molecules with specific and significant functionalities.

1.2. Porphyrins as Efficacious Components in Molecular Devices Design

1.2.1. Background and Importance

The word porphyrin comes from an old Greek word "*porphura*", where this ancient word was used for describing the purple color. Porphyrins are indeed a very large class of naturally occurring or synthetic deeply colored organic dyes[38,39]. As they are found naturally in two of very well-known important biological compounds; porphyrins are playing a vital role in the metabolism and biochemical processes in *vivo*. Haemoglobin is containing porphyrin as ligand complexed with iron II (haem), however reduced porphyrin ligand (chlorin) is complexing with magnesium II giving chlorophyll (Figure 3). Subsequently, without porphyrins and their metal derivatives, life would be impossible. Therefore, being aware with these porphyrin systems, will led us to further understanding wide variety of many important biological processes i.e. biological catalysis, oxygen binding in haemoglobin and light absorption step in photosynthesis.

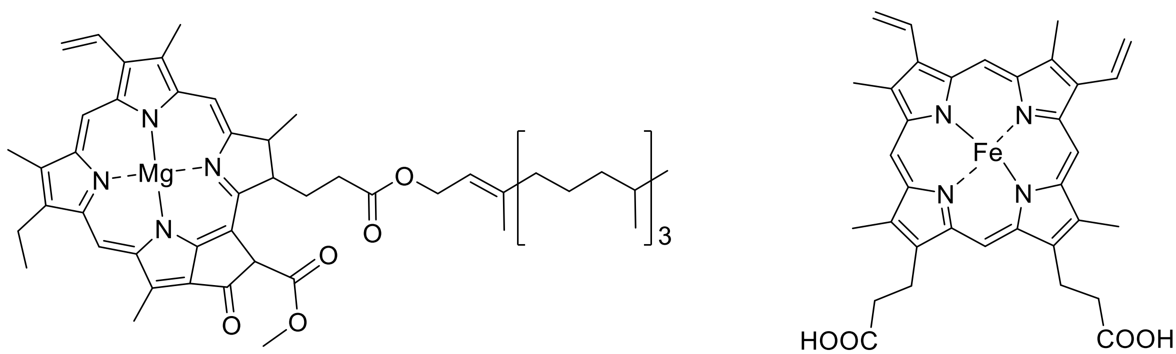

Chlorophyll **Haem**

Figure 3. Chemical structure of Chlorophyll (left) and Haem (right).

In addition to their naturally occurring; porphyrins and their derivatives can be also synthesized with a wide variety of functional groups, even with different anchoring groups which can be directly attached to metal electrodes. This is because porphyrins are architecturally adaptable and there are many chemical protocols in which various building blocks can be used in the synthesis schemes i.e. aldehydes, pyrroles, dipyrromethanes, dipyrromethenes and linear tetrapyrroles. Moreover porphyrins are very stable even in solution and/or at high temperatures, furthermore porphyrins can be dissolved in both aqueous and organic solvents[40].

1.2.2. Porphyrin Structure

The fundamental structure of porphyrin macrocycle is consisting of four pyrrole rings (marked with blue color) linked together through four methine (CH_2 = CH-) bridges (marked with green). The basic structure of porphyrin (also known as porphine), together with the IUPAC numbering system of its ring, is displayed in Figure 4.

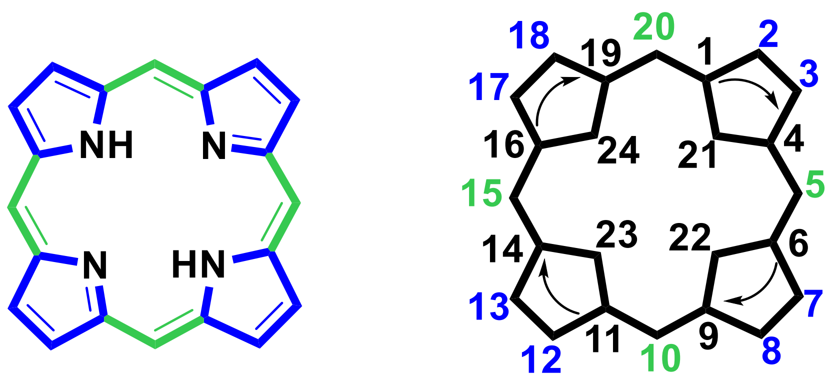

Figure 4. Porphyrin structure and its IUPAC numeration system

In the IUPAC numbering system, carbons at positions 2, 3, 7, 8, 12, 13, 17 and 18 are indicated to the *β*-positions, carbons at positions 1, 4, 6, 9, 11, 14, 16 and 19 are referred to the *α*-positions, however carbons at positions 5, 10, 15 and 20 are known as *meso* -positions. There are four nitrogen atoms in porphyrin structure; two of them are pyrrolenine nitrogen atoms (positions 21 and 23) which have the ability to accept two protons giving dication structure. On the other hand, the other two nitrogen atoms in NH groups (positions 22 and 24) can form dianion structure by losing the two protons under basic conditions. Such kind of porphyrin dianion is capable of coordinate with numerous of metals inside the porphyrin macrocycle giving very wide variety of metalloporphyrins[38,39,41]. The coordination of porphyrins with different metal centers resulting in different geometries i.e. regular (in-plane) and sitting-atop (out-of-plane) based on the size and charge of the metal ions[42]

Another important feature for porphyrin NHs that their signals in NMR spectra always observed at very high field with negative chemical shift (shielding effect); the reason is these protons are located as exocyclic (out of current) with respect to the local pyrrole ring currents and endocyclic (in current) with respect to the macrocyclic current, in consequent shielding effect could be occurred. It is worth to mention that, the *β*-protons and *meso*-protons signals are always observed at low field with positive chemical shift, this is due to they are located excocyclic with respect to the macrocyclic and local pyrrole currents, hence desheilding effect would be happened[43,44].

The tetrapyrrole macrocycle planar structure of porphyrin is containing 22 π-electrons; only 18 of them are delocalized. Accordingly the molecule is highly conjugated and aromatic as it obeys to Hückel rule of aromaticity (4n+2 delocalized π-electrons, where n=4 in porphyrin). Two conjugated forms can be formed due to the tautomerism of porphyrins as a result for the presence delocalized 18 π-electrons. The possible conjugation pathway is shown in Figure 5 and can be described using E. Vogel [18] annulene model[45] in which porphyrin behaves as a bridged diaza [18] annulene.

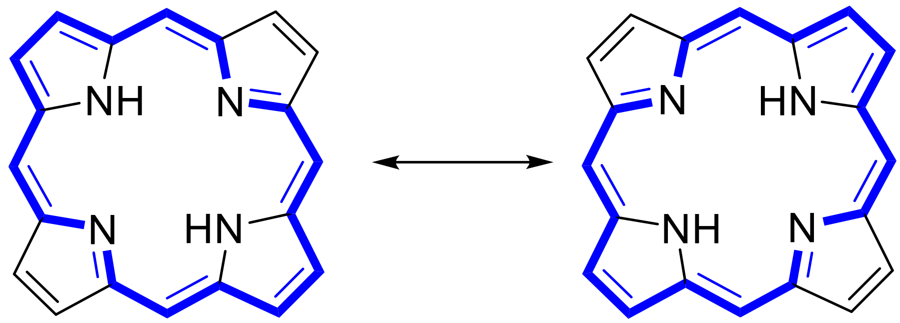

Figure 5. Conjugation pathway and tatuomerism in porphyrin system.

1.2.3. UV- Visible Spectra and Electronic Structure of Porphyrins

Since porphyrins have a highly conjugated π-electron system; they always have an intense colors derived from that spacious conjugation (Fig. 5). As a result, one of the most substantial features for characterizing porphyrins is the UV / Visible electronic absorption spectra which consisting of two distinguished zones in the ultraviolet and visible regions. Figure 6 displays the UV / Visible absorption spectra of i.e. 5,15-bisdodecylporphyrin (C12P) (left) and 5,15-bisdodecylporphyrin (Ni (II)-C12P) (right). It is illustrated from the figure that the electronic absorption spectra of a typical porphyrins composed of two zones; the first one is around 400 nm and called the Soret or B band region which is attributed to the electronic transition from the ground state to the second excited state ($S_0 \rightarrow S_2$). The second zone is between 500 – 650 nm and called the Q-band region which is referred to the electronic transitions from the ground state to the first excited state ($S_0 \rightarrow S_1$). The absorption spectrum of porphyrins can be theoretically clarified by using "Gouterman four orbital model"[46].

.

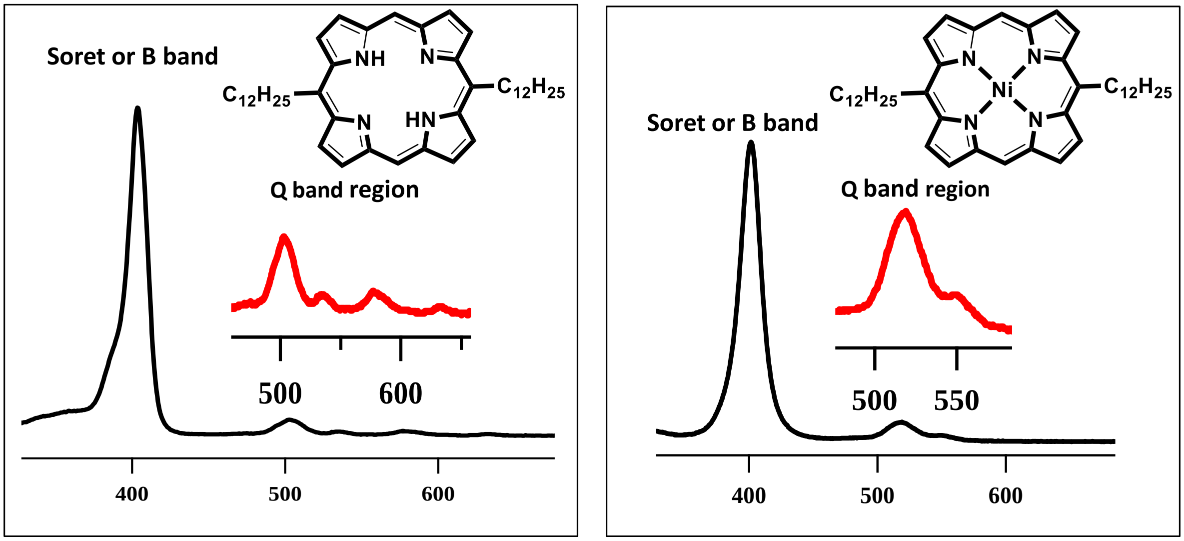

Figure 6. UV-Visible spectra of C12P (left) and Ni (II)-C12P (right) including enlargement of the Q region.

Gouterman proposed that the two absorption bands (B and Q) originate from $\pi \rightarrow \pi^*$electronic transitions between four orbitals (two HOMOs and two LUMOs). The two HOMOs are referred to a_{1u} and a_{2u} orbitals (π-orbitals), while the two LUMOs are degenerate and referred to e_{gx} and e_{gy} orbitals (π^*-orbitals). Since a_{1u} has similar energy of a_{2u} and because of the degeneracy of e_{gx} and e_{gy}; a strong configurational interaction between the $a_{1u} \rightarrow e_g$ and the $a_{1u} \rightarrow e_g$ transitions. Consequently, two bands would be originated with different wavelengths and intensities. The strong short-wavelength B-band will be originated as a result for constructive interference, whilst destructive combinations produced the weak long-wavelength Q-bands (Fig. 7). The spectrum in the visible region can be changed, giving two or four Q-bands, by insertion of metal center atoms inside the macrocycle of porphyrins or by protonation of the two inner nitrogen atoms. There are many factors which can effect on the absorption spectra of porphyrins like temperature, pH change, solvent type, metalation and/or protonation.

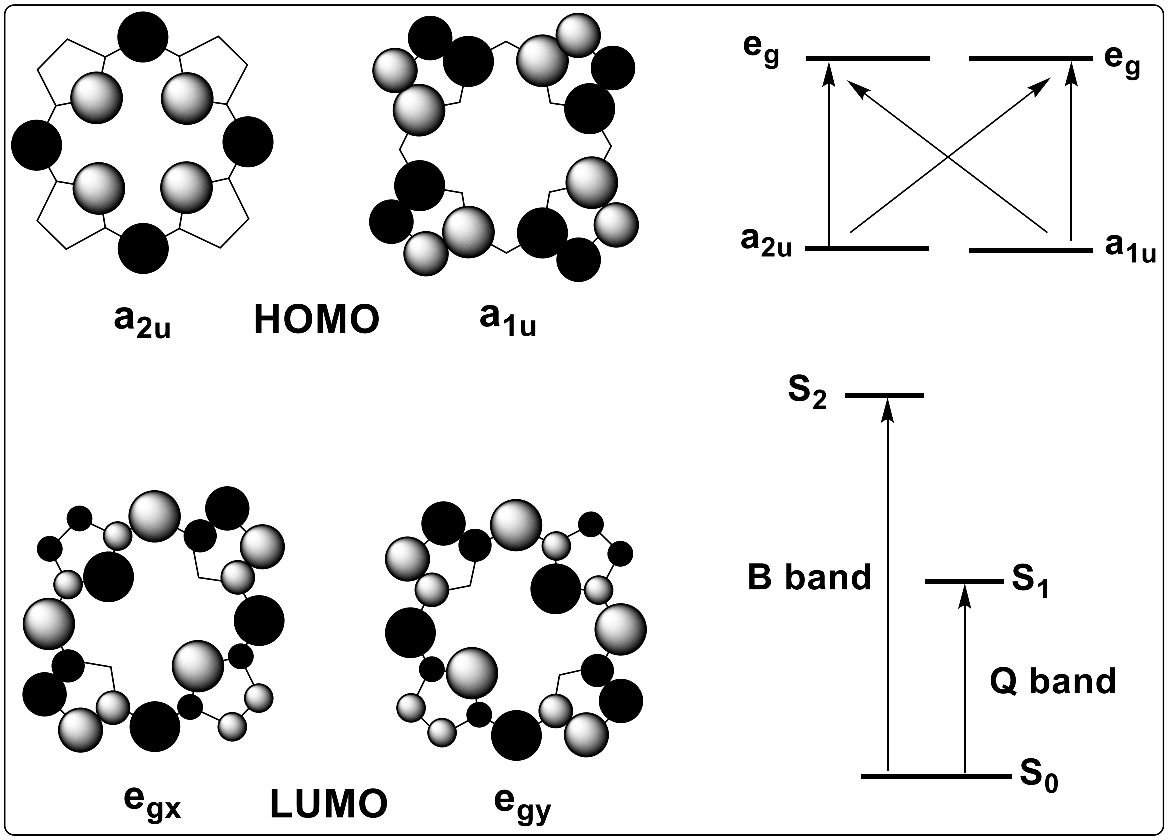

Figure 7. The Gouterman four orbital model[46].

1.2.4. Porphyrins for Molecular Devices Design

Since porphyrins can show promising physical and optoelectronic properties; so they can be utilized in many fantastic applications i.e. enzymes simulation, catalysis, solar cells fabrication and energy conversion, light harvesting and molecular electronics applications. Focusing on the latter type of applications; as porphyrins have a characteristic, reversible and rich redox chemistry which enhances employ as switches, wires, junctions, transistors and photodiodes. The physical and electronic properties of porphyrins are controlled by the substituents which can bind to *β*- and/or *meso*- positions, and also by the type of metal ions which can be incorporated inside the porphyrin macrocycle. As divalent ligands, porphyrins can be coordinated with almost every metal in the periodic table, which leads to further modification and enhancement the optoelectronic properties of porphyrins[47,48].

The photoelectronic properties of a given porphyrin in materials are extremely depend on the surrounding environment around porphyrin i.e. number, conductivity, connectivity, relative orientation and the intermolecular interactions. As they possess adaptable photonic properties, high stability, and synthesis availability, porphyrins and its related materials are highly recommended to be used as main components of organic light emitting devices, sensors, solar cells, and photocatalysts. There are two common ways through which porphyrins can be organized onto material surfaces, the first one in which the porphyrin active molecules can be covalently attached to the surface via well-established surface chemistries, this way is known as self-assembled monolayers (SAMs). In the second way porphyrins can be self-organized giving two dimensional arrays and/or layers via non-covalent adsorption onto surfaces. In the two cases, the molecular structure, surface chemistry and energetics are playing essential roles in the fabrication and organization of the final photonic materials[47,48].

1.3. Nano-carbon Materials (Nanocarbons)

Nanocarbons are carbon materials in the nanometer scale composed of benzene hexagons (mainly made of sp^2-hybridized carbon atoms) with a very well-defined geometric patterns and unique repeated decorative design. They are exhibiting gorgeous properties i.e. electrical conductivity, emitting and absorbing light, thermal conductivity, acting as hosts to other molecules, in addition to very interesting magnetic properties. There are many examples for nanocarbons[49] for instance, carbon nanotubes, CNTs hereafter, which discovered in 1991[50] (cylindrical shape), fullerene C60 which discovered was in 1985[51] (spherical shape), graphene which discovered in 2004[52] (sheet structure), and graphite (layered structure) which first named by Abraham Gottlob Werner in 1789[53].

According to their dimensional structure, nanocarbons can be classified as follows: 0D structure i.e. fullerenes, 1D structure i.e. CNTs, 2D structure like graphene and graphene nanoribbons (GNRs), and 3D structure i.e. Mackay crystals or graphite structure (Fig. 8). It is worthy to mention that, CNTs and GNR aren't considered as structurally pure molecules as they were synthesized with some defects in their structure[49,50,52].

There are many forms, or allotropes, of carbon, of which graphite and diamond are the most popular naturally occurring and thermodynamically stable. Such kinds of these allotropies have immensely different alignment of carbon atoms which has a great effect on the properties of the carbon based-materials. Discovering of nanocarbons has opened the gates towards novel and advanced technologies. Since they have unique properties, so nanocarbons can be used in extensive applications in the field of material science i.e. electronics, organic bioelectronics and bio-imaging, giving a promising and unexpected outcome[49]. In this thesis since the supramolecular structures of some organic molecules on some nanocarbon surfaces like CNTs and highly oriented pyrolytic graphite (HOPG hereafter) have been studied, so structure and properties of CNTs and HOPG will be discussed with more details.

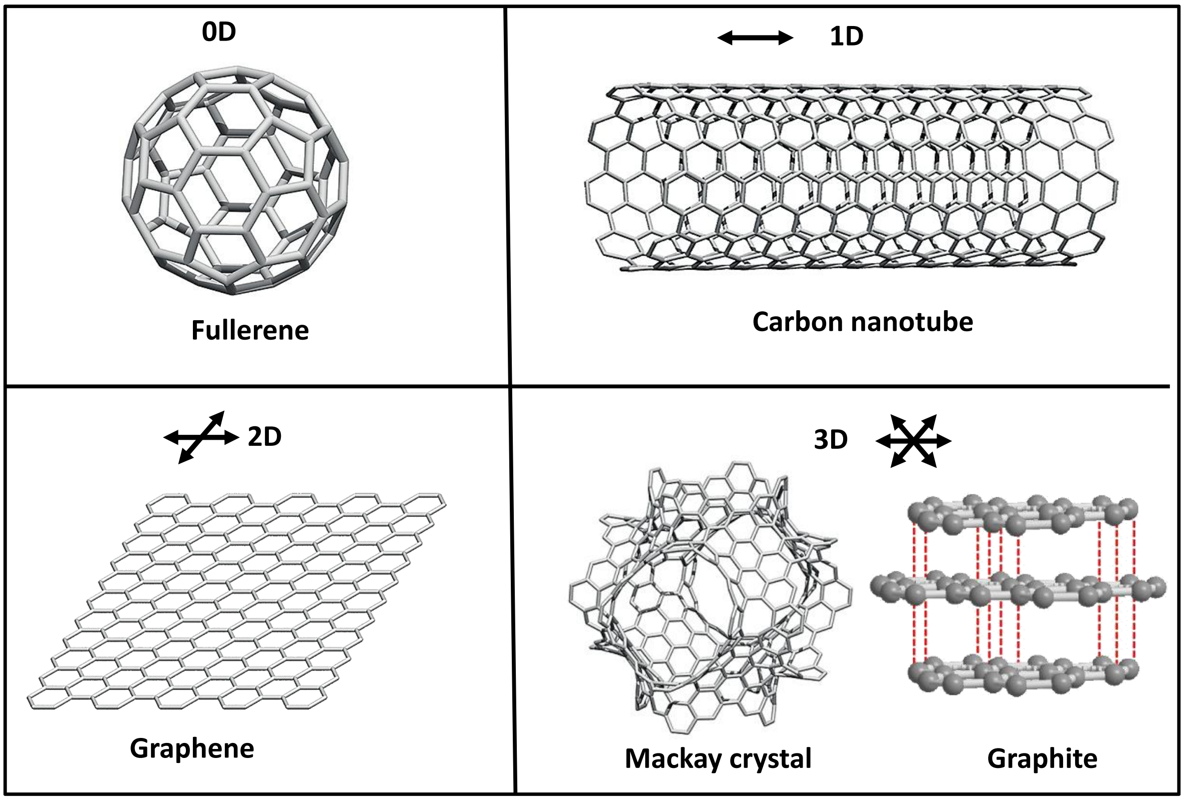

Figure 8. Types of nanocarbons which classified based on their dimensionality i.e. fullerenes, carbon nanotubes, graphene, Mackay crystals and graphite which representing 0D, 1D, 2D and 3D structures of nanocarbons, respectively. Adapted by permission from Macmillian Publishers Ltd: Nature Reviews Materials, copy right 2016[49].

1.3.1. Highly Oriented Pyrolytic Graphite (HOPG)

Usually the typical structure of natural graphite is deficient due to abundance of defect and the presence of some impurities. Therefore in order to prepare almost ideal and perfect structure of graphite; there are some special preparation techniques have been developed to achieve that purpose. One of the most common and effective technologies is organic compounds pyrolysis. With a view to approach an ideal structure of graphite, according to the graphite nature, annealing at higher temperatures and longer times is needed to minimize the structure defects and mosaicity of the material.

HOPG is highly ordered form of high-purity pyrolytic graphite which produced by annealing (at very high temperature around 3000 º C) of pyrolytic graphite under very high uniaxial pressure. As a result, graphite will be obtained with a very well crystallographic orientation. Since the defects, mosaicity and granular structure of graphite are mainly depending on the annealing parameters, so based on the deformation percent and annealing temperature and time, graphite can be produced with diverse mosaic diffusion, defects amounts and granular structures. As a standard, HOPG production companies should take in consideration the correlation between mosaic spreads, defects and granular structures[54].

HOPG has a lamellar structure composed of multilayered stacked parallel graphene planes which attached together by π-π stacking. Each graphene sheet composed of network of carbon atoms covalently linked forming hexagons. The hexagonal lattices of two successive graphene sheets are arranged as ABAB stacking. The distance between two adjacent carbon atoms in the same plane and between three neighboring carbon atoms (C–C–C) equals 1.42 and 2.46 Å, respectively, however the distance between two successive graphene planes equal to 3.35 Å (Fig. 9). As the interaction between carbon atoms within one graphene plane (covalent bonding) is much stronger than the interactions between the adjacent planes (i.e. Van der Waals forces); this elucidates the distinctive cleaving behavior of graphite[54].

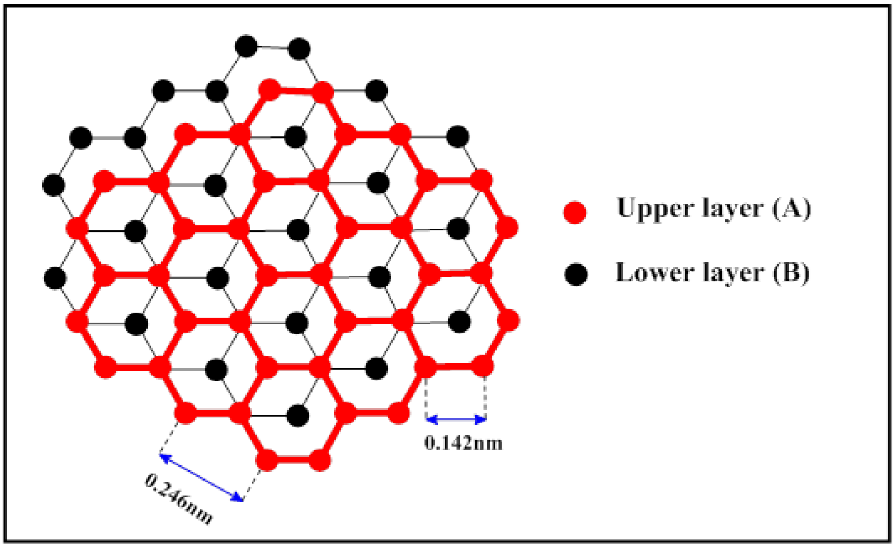

Figure 9. Schematic representation of HOPG structure which formed from alternative successions of graphene layers as ABABAB… structure attached via π-π stacking. The distances between two neighboring carbons, and between three adjacent carbon atoms equal 1.42 and 2.46 Å, respectively, however the distance between two successive graphene planes equal to 3.35 Å.

HOPG is used as one of the most common substrates in scanning tunneling microscopy (STM) measuments due to its relatively high stability, so it can be used under a wide variety of conditions i.e. under ambient conditions, under high vacuum, under high temperatures and using different liquid environments. In addition to its smooth, flat, uniform and renewable surface which can be straightforwardly obtained by simple cleaving. Consequently, HOPG can be used in very wide range of applications especially in electronics, biomaterials and catalysis.

1.3.2. Carbon Nanotubes (CNTs)

1.3.2.1. CNT Discovery and Classifications

Historically during the synthesis of fullerene via arc discharge method, Iijima had discovered for the first time multi-walled carbon nanotubes (MWNT) in 1991; directly after two years, he also succeed in generating single-walled carbon nanotubes (SWNT) in 1993[50,55]. Carbon nanotubes are hollow seamless cylindrical shaped tubes of sp^2 carbon atoms, with radius of some nanometers and a few micrometers in length[56].

Since it is well known that graphite consists of many basal planes of carbons called graphene, CNTs also can be composed either from single graphene sheet or multi-layered graphene sheets. Based on how many graphene sheets from which carbon nanotubes can be formed; CNTs can be classified into three categories, single-walled carbon nanotube (SWNT) if the tube consists of one rolled-up graphene sheet, double-walled carbon nanotubes (DWNT) which composed of two rolled-up graphene layers, and multi-walled carbon nanotubes (MWNT) which formed from multi-cylinders of graphene (more than two) and have the “Russian doll” configuration. This can be shown in Fig. 10 , in which the three types are identified. Generally the lengths of all the types can be extremely varied based on the synthesis methods, usually the tube lengths are in the microscopic scale rather than the nanoscopic one.

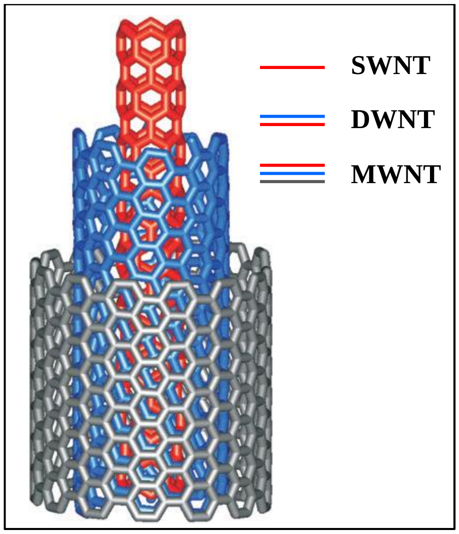

Figure 10. Classification of carbon nanotubes based on the number of rolled-up graphene sheets; single-walled carbon nanotube (SWNT) marked by red, double-walled carbon nanotubes (DWNT) marked by blue and red, and multi-walled carbon nanotubes (MWNT) marked by red, blue and gray. Adapted by permission from copy right 2005 Wiley[57].

1.3.2.2. CNT Properties and Applications

As they have a unique structure and extraordinary intrinsic properties i.e. structural, mechanical, and electronic properties, CNTs are one of the most commonly effective building blocks in the field of nanotechnology. CNTs seems an excellent materials as they possess thermal conductivity better than all but the purest diamond, very high electrical conductivity with the ability to carry much higher current (due to the high carrier mobility they can produce a streams of electrons very efficiently) than copper, and they have a remarkable tensile strength higher than steel. Therefore, they are stronger than steel, harder than diamond, higher electro-conductive than copper, and higher thermo-conductive than diamond[58].

Due to their adorable and remarkable properties i.e. high surface area, chemical stability, unique electronic and physical properties, high electrical and thermal conductivity, CNTs are being used in a wide potential applications in many fields for instance, nano electronics, microelectronics, molecular electronics, optoelectronics, sensors, energy storage materials, gas storage materials, catalysis, polymer reinforcements, composite materials, nano-biotechnology, and nano-medicine. Consequently, they become one of the most attractive materials in the field of nanotechnology[59-62].

1.3.2.3. CNT Synthesis

In general there are three main different processes through which carbon nanotubes can be synthesized, usually CNTs can be produced by arc discharge of graphite, laser ablation, or gas-phase catalytic growth from different carbon sources and carbon monoxide. The produced raw materials usually contain nanotubes mixed with some impurities like amorphous carbon and catalytic metal particles. Of course these processes are frequently varied with respect to the produced nanotube type, purity, quality and scalability[60]. The first process is arc discharge method (AD); by this method Iijima[50] accidently succeed in the discovery of carbon nanotubes during fullerene synthesis. After that discovery within a few years another two new methods have been introduced known as laser ablation (LA)[63] and chemical vapor deposition (CVD)[64] as well as some more recent methods operating using high pressure of the carbon monoxide or some unique catalytic mixtures. . In arc discharge and laser ablation methods high temperatures are being used, on the other hand CVD method can be proceed at relatively lower temperatures. Each method, along with its advantages and disadvantages, will be discussed in more details in the following part.

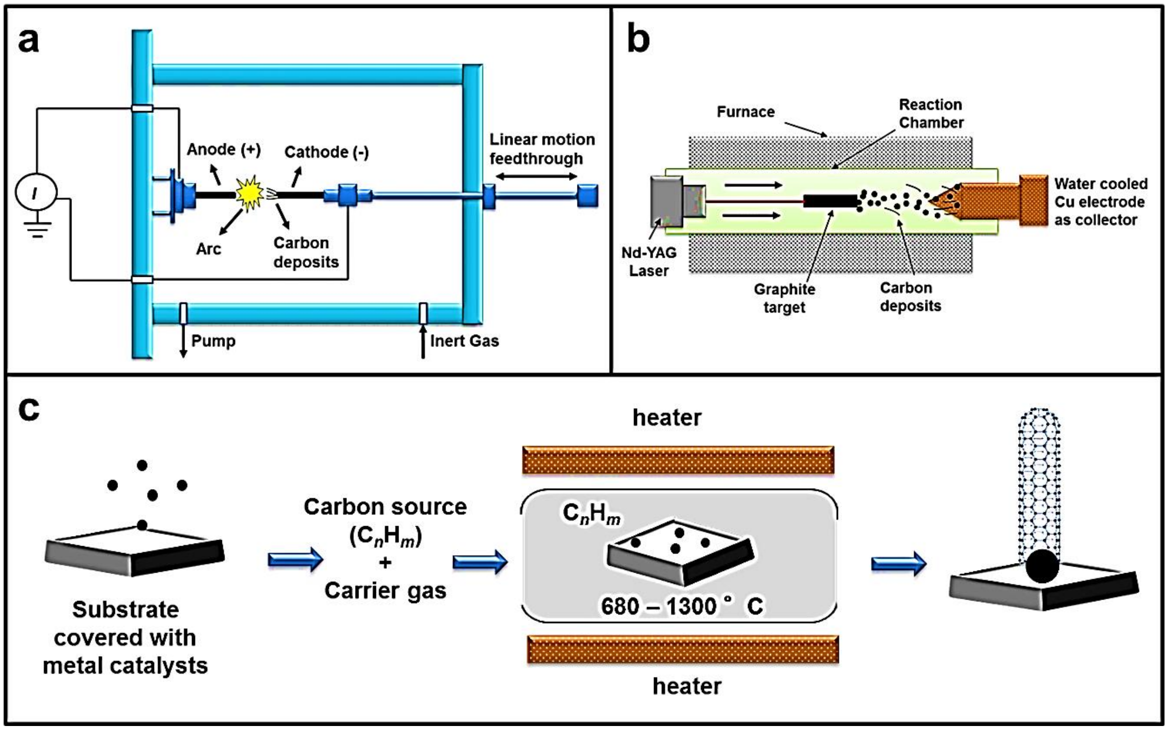

Figure 11. Schematic representation for carbon nanotubes synthesis methods **a**, Arc discharge **b**, Laser ablation **c**, Chemical vapor deposition.

1.3.2.3.1. Arc Discharge (AD) Method

In this method an arc is originated in between two electrodes made from graphite rods, where the two rods are placed in closed system filled with an inert gas i.e. argon or helium or nitrogen, at low pressure. Typically the anode is often filled with a catalyst, and it should be smaller in size than the cathode, as a consumable electrode. By approaching anode to cathode an arc is struck and the anode is being evaporated and deposited upon the cathode surface. After depressurizing and cooling the interaction chamber, the CNTs along with by-products can be collected from the cathode surface. A schematic representation of the experimental setup is shown in Fig. 11a. This method is suitable for producing SWNT, MWNT and sometimes bundles of SWNTs, with a conversion yield up to 60 % [65]. Many factors can effect on this method for instance, the arching current, the temperature, the inert gas type and the gap between anode and cathode.

1.3.2.3.2. Laser Ablation (LA) Method

In 1995 Smalley and his coworkers for the first time have used the laser ablation method for synthesizing CNTs[66]. In this method a metal-graphite composite target rod is placed inside a tube furnace, and then ablated by an intense laser beam in the presence of an inert gas like helium or argon (as a carrier gas), resulting formation of carbon nanotubes. During the process the carbon target rod is preheated at 1200 °C in the furnace, and then struck by an intense laser beam. As the surface temperature of the rod rises up to be 6000 °C (after being struck by the laser pulses), carbon vapor formed around the rod surface, and these carbon species is carried via the inert gas flow, to be condensed and deposited on the copper collector surface. After cooling down the chamber, CNTs and other carbon species can be collected. A schematic representation of the process setup is illustrated in Fig. 11b. Some parameters should be controlled to give the high yield of CNTs like the furnace temperature and flowing rate of the inert gas[67].

The two previous methods (arc discharge and laser ablation) are no longer used nowadays as they need very high temperatures to be processed, as a result the carbon sources are often evaporated, in addition to the resultant CNTs are structurally disordered (containing many structure defects), sometimes short (due to the short time of the processes), with high contents of impurities so high purification techniques are needed.

1.3.2.3.3. Chemical Vapor Deposition (CVD) Method

Compared to the previous methods, CVD is a low temperature method for producing CNTs, in which the carbon source is thermally decomposed producing the carbon species and CNTs in ultimate. This method can be processed using template (like aluminum oxide) or substrate (like Si-wafer, metal foils, quartz glass), in the presence of catalyst. Wide range of carbon sources can be used in this process for instance; normal hydrocarbons i.e. methane, ethane, propylene, also carbon monoxide can be also used as a carbon precursor. Many types of catalysts are often used in CVD method; the most popular among them are transition metals and some of their carbonyl complexes i.e. Fe, Co and Ni. The CVD temperature mainly depends the carbon precursor type, the general range of CVD temperature is in between 700 – 1300 °C for producing good quality of CNTs. The schematic experimental setup of CVD method is explained in Fig. 11c, at first the substrate or template covered with the catalyst is inserted into tubular oven, heated to the desired temperature. At the desired temperature, mixture of the carrier gases and carbon sources are introduced to the oven. By cooling down the oven to room temperature, a good quality CNTs can be obtained through this method[67-69].

Although CVD method is often produced a good quality CNTs, but there is some limitations regarding broad distribution of the tube diameter and length, therefore there are some modified CVD methods have been reported to overcome that limitations of normal CVD method. Some of these methods are water assisted chemical vapor deposition (WCVD)[70], hi-pressure carbon monoxide method (HiPCO)[71,72], and CoMoCAT method[73].

In water assisted chemical vapor deposition method CNTs can be grown up to a millimeter length, so it is a unique method. It is almost same as normal CVD method but with one modification, during the synthesis in addition to the synthesis components (hydrocarbon, argon and hydrogen gas, catalyst and substrate), a small amount of water vapor is supplied to that mixture. However the change is trivial but it very substantial to keep the catalyst activity for longer time, so the CNT growth will be continue for longer period. The catalyst activity and refining can be preserved by using water as a weak oxidant[67]. There are some research groups have reported this process in growing SWNT and MWNT, and also for tuning the CNT diameter and morphology[70,74].

Another intrinsic method for producing very high quality CNTs is the high pressure carbon monoxide process or HiPCO. In this process after heating the oven to 1100 – 1300 °C, a mixture of carbon monoxide gas and iron pentcarbonyl [$Fe(CO)_5$] is pumped to the oven. Small iron nanoparticles are produced from the iron complex cracking and interacting with the gas to produce very high quality, low structurally defected, highly selective SWNTs. The resultant SWNTs produced by HiPCO with purification yield up to 90 % [65].

In 2002 kitiyanan[73] and his coworkers reported one more method for CNTs synthesis, known as CoMoCAT. In this method carbon monoxide along with unique catalyst mixture of cobalt and molybedenum are used to produce very high purity CNTs. Throughout this process carbon monoxide is thermally decomposed at 700 – 950 °C into carbon dioxide and simple carbon. The main advantage of this process is high purity level and prohibition of by-products of the resultant CNTs.

1.3.2.4. Growth Mechanism of CNT

There are two possible mechanisms for growing CNTs; the first one is known as tip-growth (Fig. 12a), in which a bulk diffusion is occurred where the metal particles are located at the tip of the CNTs, however in the second mechanism which known as base-growth (Fig. 12b), the metal particles are located at the base of CNTs, therefore a surface diffusion is occurred. In the tip-growth, the metal particles detach from the substrate surface, and remain on the top of the growing nanotubes. On the other hand, in the base-growth, the metal particles remain attached to the substrate surface and the nanotubes grow upwards from the metal particle surface[59]. Another important factor which mainly determines the mechanism type is the metal-support interaction strength, where CNTs can grow via the base-growth mechanism as a result for strong metal-support interaction, or via the tip-growth mechanism due to weak metal-support interaction.

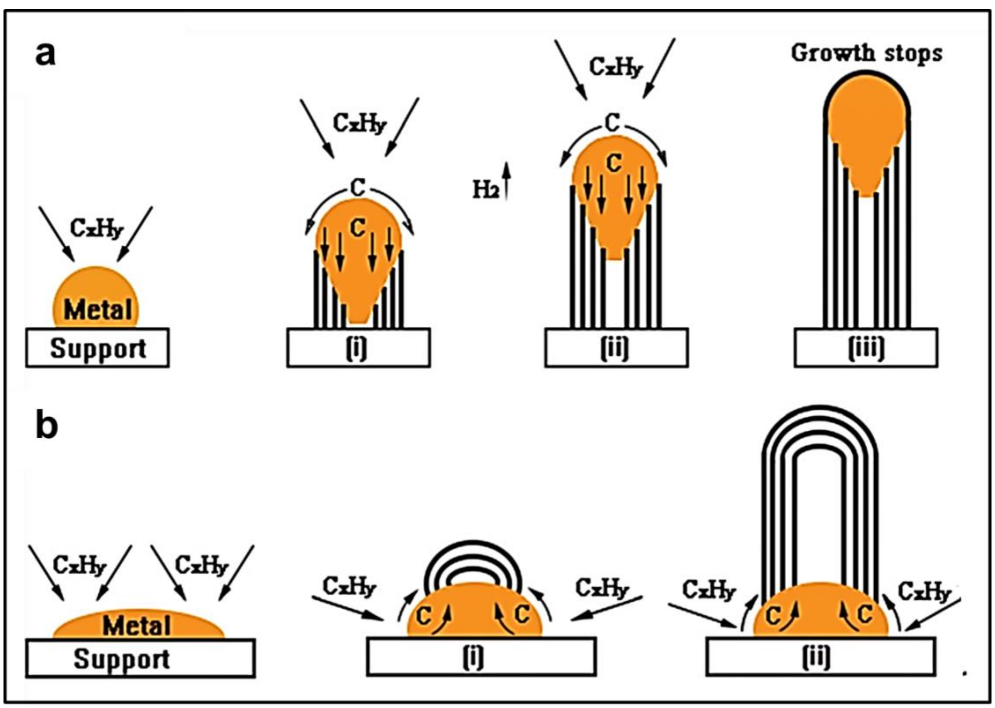

Figure 12. Growth mechanisms for CNTs **a**, tip-growth mechanism **b**, base-growth mechanism. Adapted with permission of the Royal Society of Chemistry[59].

1.3.2.5. SWNT Functionalization

The chemical modification of CNTs by interacting with something else i.e. organic molecules or surrounding polymer and so on, is known as functionalization. There are many approaches through which SWNT can be functionalized in both molecular and supramolecular chemistry; for instance, defect functionalization, covalent sidewalls functionalization, non-covalent exohedral functionalization (i.e. formation of supramolecular adducts with surfactants or polymers or some organic molecules), and endohedral functionalization with for example, C_{60}.[75]

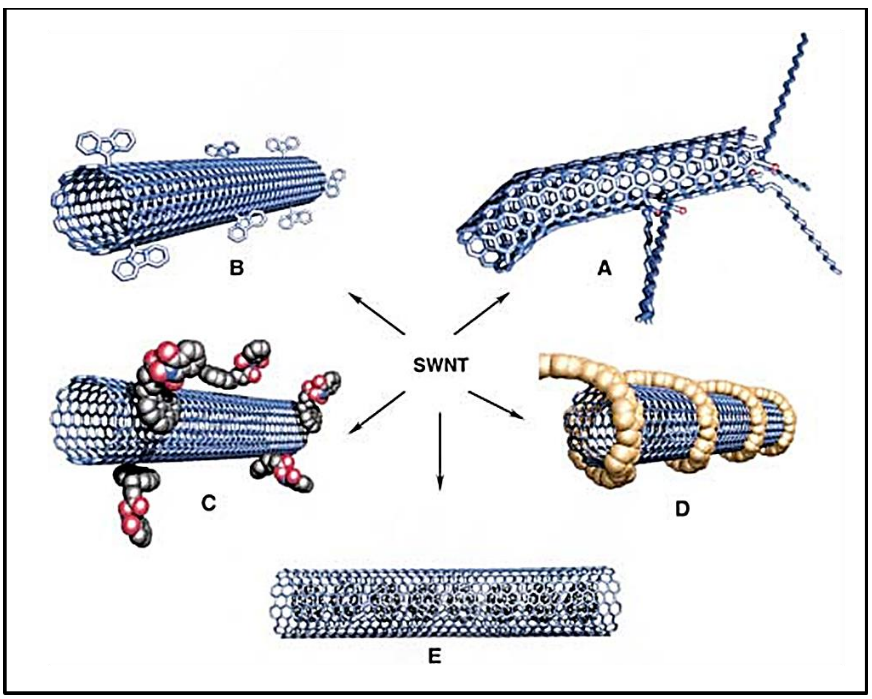

Figure 13. Functionalization possibilities for SWNTs **a**, defect-group functionalization **b**, covalent sidewall functionalization **c**, non-covalent exohedral functionalization with

surfactants **d,** non-covalent exohedral functionalization with polymers **e,** endohedral functionalization with, for example, C_{60}. Adapted by permission from copy right 2002 Wiley[75].

As it is clearly appeared from Fig. 13, CNTs can be functionalized mainly by two broad approaches, covalent and non-covalent (supramolecular). Although, covalent functionalization of CNTs has been widely investigated and yield a wide variety of modified nanotube structures conjugated with both small molecules and polymers, but some covalently modified-SWNTs aren't suitable to be used in some applications which based on the high conductivity or mechanical strength of SWNTs. This is because the covalent functionalization strategy significantly disorganizes the conjugated pi-system of the CNT; consequently, result in spectacular alternations in its electronic and structural properties. On the other hand, the non-covalent functionalization includes molecular adsorption on the tube surface via pi-stacking or Van der Waals interactions with pi-conjugated sidewall of the tube. As a result, this strategy can maintain both the electronic and structural impartiality of SWNTs, allowing the employ of both conductivity and strength properties in definitive application, and this is the richness and power of supramolecular approach[76].

In this thesis, SWNT is non-covalently functionalized by some porphyrins via non-covalent interactions i.e. Van der Waals interactions and π-π stacking, allowing us to study some important properties of the eventual complex.

1.3.2.6. SWNT Chirality

1.3.2.6.1. (*n, m*) Indices Chirality

Since SWNT cylindrical structure can be simply identified as a rolled up graphene sheet, so the structure can be defined by a roll-up vector $\boldsymbol{C}_h$; this vector is given as $\boldsymbol{C}_h$=. $n\boldsymbol{a_1} + m\boldsymbol{a_2}$, where $\boldsymbol{a_1}$ and $\boldsymbol{a_2}$ are the unit vectors of a 2D-graphene sheet, however n and m are integers and are referred to the roll-up index (*n,m*) and/or Chiral index, whilst $\boldsymbol{C}_h$ is referred to Chiral vector[77,78]. The electronic and optical properties of SWNTs are mainly depend on their structures, in other words mainly depends on (*n,m*) values[79,80].

CNTs properties are mainly depend upon three important structural parameters; tube diameter, (*n,m*) indices chirality, and handedness chirality (this kind of chirality exits only in chiral CNTs which define right- and left-handed helical structures of SWNTs, the handedness chirality will be discussed in details later), where diameter is the geometrical dimension of the tube, chirality or chiral angle (θ) is the angle by which the hexagon structure can be rotated along the main axis of the tube . Based on (*n,m*) chirality, the chiral angle, and rolling up direction of the honeycomb structure; SWNT can be classified into three types i.e. armchair (*n,n*) where $n = m$ & θ = 30 °, zigzag (*n,0*) where $m= 0$ & θ = 0 ° and chiral CNTs (*n,m*) where $n \neq m$ & θ = 0 ° to 30 °. This is can be clearly illustrated in Fig. 14.

On the basis of the hexagon orientation with respect to the main axis of the tube, the three types can be readily distinguished. The chiral angle (θ) value will reflect the honeycomb orientation. In armchair and zigzag types at least one c-c atom in the hexagon will be either parallel or perpendicular to the tube axis. This type of chirality is always described by two integers placed between two brackets (*n*,*m*). Based on *n*, *m* and chiral angle (θ) values, one can easily identify the CNT type. i.e. armchair (*n*,*n*) where $n = m$ & θ = 30 ° or zigzag (*n*,*0*) where $m = 0$ & θ = 0 ° or chiral (*n*,*m*) where $n \neq m$ & θ = 0 ° to 30 °. Furthermore, those indices can uniquely determine whether the CNT is metallic or semiconductor, as well as its band gabs, when $n - m = 3l$, then it will be metallic CNT, whilst CNT will be semiconductor if $n - m = 3l \pm 1$, where *l* is integer.

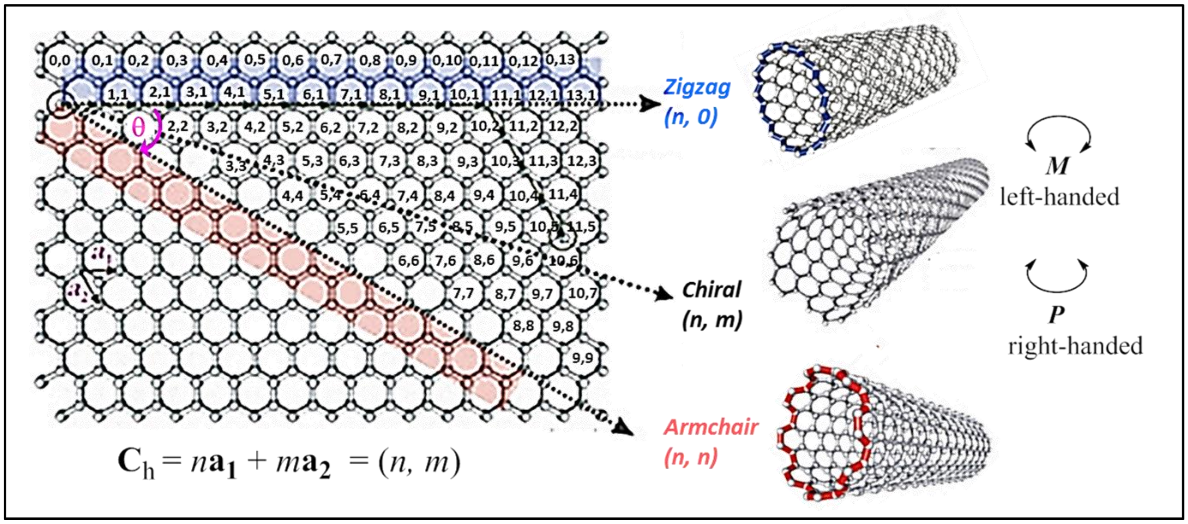

Figure 14. Rolling-up of graphene sheet along the roll-up vector C_h using two unit vectors, a_1 and a_2 and chiral angle (θ), which lead to three different types of CNTs i.e. armchair (*n*,*n*), zigzag (*n*,*0*) and chiral (*n*,*m*). The ***M*** and ***P*** handedness chirality (which define left- and right-handed helical structures of SWNTs) of chiral CNTs is also visualized by rolling up clockwise, indicated as , and anticlockwise, indicated by , respectively. Adapted by permission from copy right 2005 Wiley[57].

1.3.2.6.2. Handedness Chirality

Even after Strano[81] stated that in order to define carbon nanotubes structures, a systematic nomenclature should be sought; the stereochemistry of carbon nanotubes[82] and a new methodologies for Sorting, separating and extracting DWNTs[83] and SWNTs[84] based on the handedness using chiral biological molecules[85], chiral diporphyrin nanotweezers[86-92], chiral dipyrene nanotweezers[93], chiral nanocalipers[94,95], chiral monoporphyrin[96], different metalloporphyrins[97], chiral polymer wrapping[98], or by electron diffraction[99] have been widely studied.

Since SWNT cylindrical structure can be defined by the chiral vector $\boldsymbol{C}_h$, considering that the meaning of "chiral" here isn't proportionate with the fundamental meaning identified by International Union of Pure and Applied Chemistry (IUPAC) which is "the geometric property of a rigid object of being non-superposable on its mirror image"[100]; despite that the chiral molecules should contain optically active centers; the molecules which don't have optically active centers might have an axial chirality. One sort of axial chirality is helicity or helical chirality or handedness chirality; which represents right- and left-handed enantiomers. The later type of chirality presents in some biological molecules i.e. amino acids, where these molecules can be found in two forms right (R) and left (L) mirror image structures[101].

Carbon nanotubes (CNTs) belong to the latter kind of handedness chirality, as they can be formed in two ways; either right or left handed helix cylindrical shapes. Except Armchair and zigzag structures (as they don't have their non-superposable mirror image); all the SWNTs have a helical chirality[84,91,102]. ***P*** (plus) and ***M*** (Minus) terminology would be used to define right- and left-handed helical structures of SWNTs (Fig. 14), respectively[82]. Although *(n,m)* indices of SWNTs can be identified using spectroscopic techniques, such as UV-Vis., Raman, and photoluminescence (PL) spectroscopy, the identification of handedness chirality (***P***, ***M***) of SWNT is not established yet. In this thesis, we are focusing on investigation of the absolute handedness chirality of SWNT and its effective role on the alignment of organic molecules on its surfaces, using scanning tunneling microscopic (STM) technique.

1.4. Scanning Probe Microscopy (SPM)

Scanning probe microscopy (SPM) is one of the foremost substantial and effective tools which are used for imaging, measuring, characterizing and manipulating matter in the field of nanotechnology and material science. SPM is microscopic branch by which images of surfaces can be obtained, using a physical probe that can scan the specimen surface. The exceedingly common types of SPM, is atomic force microscopy (AFM) and scanning tunneling microscopy (STM).

1.4.1. Atomic Force Microscopy (AFM)

AFM is a very high resolution of scanning probe microscope. It scans within a fraction of a nanometer. Using of a probe allows obtaining resolution higher than optical diffraction limit. Atomic force microscope is misleading name since it does not actually see the surface but rather feels the surface; i.e. the information is gathered by "feeling" the surface with a mechanical probe. AFM works by measuring atomic forces, such as mechanical contact force, Van der Waals forces, capillary forces, chemical bonding, electrostatic forces, magnetic forces and other atomic forces. Most common use is still to analyze how the surface looks like.

A cantilever that has a very small probe (tip) which interacts with the atomic surface, a laser is focused on the tip, a photodiode to which a light is reflected. Piezoelectric (PZT) components are used to either move the stage or the cantilever in x, y and z directions. When the tip is brought into a sample surface, forces between the tip and the sample lead to a deflection of the cantilever according to Hooke's law (F= *k*X). Typically, the deflection is measured using a laser spot reflected from the top surface of the cantilever into an array of photodiodes. AFM, like a record player, moves the tip across the surface. PZT are used to either move the platform or the cantilever. PZT on a cantilever allow motion in z direction useful for contact scans. The tip is usually made of silicone or silicon nitride, and is on scale of several nanometers. The laser is used to measure change in force on the tip or the vibration of the tip. Another part of most AFM is a feedback system that interprets all the data and prevents the tip from crashing and breaking.

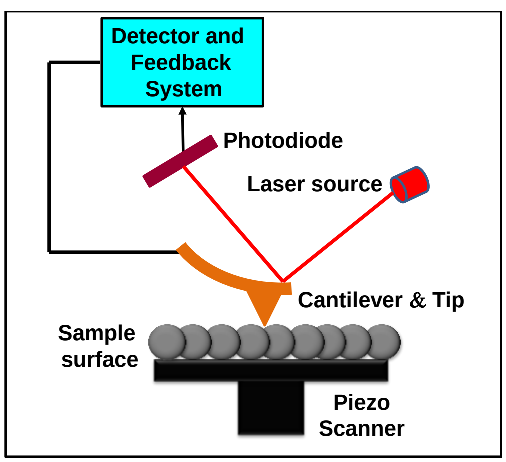

Figure 15. Schematic representation of atomic force microscope components and working mechanism by detecting the laser beam deflection.

There are two basic scanning modes for AFM; dynamic and static modes. In static mode, also is known as contact mode, the force is kept constant while height above the sample changes. So in static mode the z coordinate changes to keep the force constant. This mode gives good, high resolution results but have some disadvantages. First it is slower than dynamic mode; because the tip has to be lowered till the desired force is reached, like trial and error method. Second disadvantage is that it is easier to break the tip, especially on rougher surfaces. The atomic forces are very strong when tip is near the surface and may cause tip to crash into surface and break. So static, constant force, mode is slower and has a risk of damaging the tip and the surface, but gives high quality results. However, in dynamic mode (tapping mode) the tip isolates at its, or close to its, resonance frequency. The atomic forces from the surface change the frequency, computer analyses the data allowing measuring the force. Dynamic mode is faster and safer because the tip does not come too close to the surface, like in static mode.

The data from both dynamic and static mode can be used to find the shape of the surface. Static mode uses z coordinates data and keeps force constant. In dynamic mode, z coordinate is constant and the changes in oscillation frequency are used to find the force. Also in both cases PZT is used to move the cantilever over the surface and to move it into z direction or to oscillate the cantilever. Laser is used to measure the changes in oscillation frequency or to measure the force on the tip.

1.4.2. Scanning Tunneling Microscopy (STM)

Since, G. Binnig and H. Rohrer[103-105] had performed the first scanning tunneling microscope (STM), which provided the first observation of vacuum tunneling between a sharp STM tip and the (110) surfaces of $CaIrSn_4$ and Au; STM became the most appropriate tool for manipulating and imaging such kind of these supramolecular structures and interactions of different organic molecules with different types of large flat surfaces whatever metallic[106-111], or nanocarbon materials[112-117], as well as curved surfaces too[118,119].

Generally it is a vital and indispensable technique in the nanoelectronics and surface science research fields[120-127], as by using STM the vacuum tunneling between the conductive tip and conductive surfaces can be observed with this tunneling effect atoms could be distinguished in real space. In addition to the atomic resolution imaging capability of STM, tunnel currents could be studied with this tool in a spectroscopy manner providing insight into the local density of state (LDOS) of material surfaces.

STM is based on a quantum mechanical phenomenon, called tunneling (The tunnel effect, describes the ability of an electron to tunnel through a vacuum barrier from one electrode to the other). In quantum mechanics, small particles like electrons exhibit wave-like properties, allowing them to "penetrate" potential barriers. In general, STM involves a very sharp conductive tip that is brought within tunneling distance (sub-nanometer) of a conductive sample surface, thereby creating a metal-insulator-metal (M-I-M) configuration. In the representation of one-dimensional tunneling (Figure 16a), the tunneling wave of the sample electrons, Ψs, and the wave of a STM tip electrons, Ψt, overlap in the insulating gap (vacuum level) , allowing a current to flow[120,128-134].

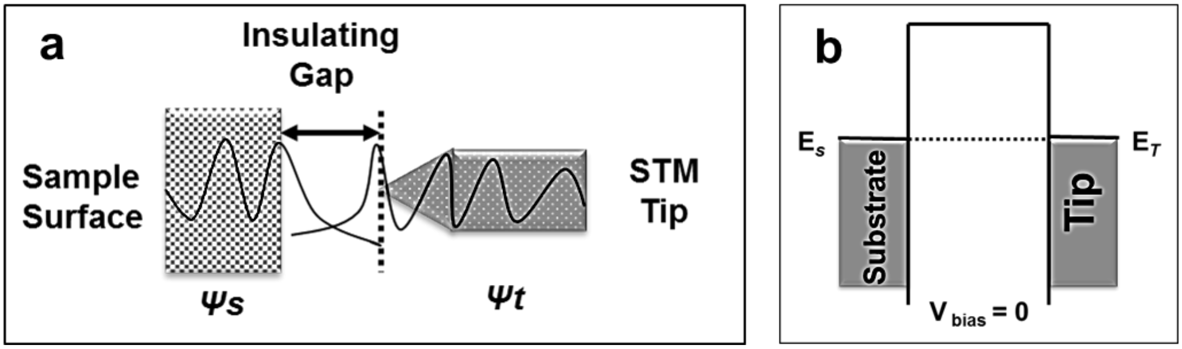

Figure 16. a, Schematic of STM one-dimensional tunneling configuration, where *Ψs* is the tunneling wave of the sample electrons, and *Ψt* is the tunneling wave of a STM tip electrons **b,** Schematic of a metal-insulator-metal tunneling junction at zero bias voltage.

To achieve some understanding of the physical meaning of the wave-function *Ψ*, we consider the square magnitude of it, which represents the probability of finding an electron at a given location. Generally, this is visualized with electron clouds for atoms or molecules, or for condensed phases with energy levels, as illustrated with the gray shaded areas in Figure 16b. In metals, electrons fill the continuous energy levels up to the Fermi level, E_f, which defines an upper boundary, similar to the sea level. Above E_f we find electrons that are activated (e.g., thermally). We can raise the Fermi level (e.g., of the sample) in regards to a second material (e.g., tip) by applying a voltage. The tunneling current between a metallic tip and a metallic surface is proportional to the surface local density of states (LDOS) at the Fermi level, E_f, evaluated at the location of the tip.

Thus, to observe the tunneling current (*I*) of electrons through the vacuum gap between the sample and the tip, a bias voltage, V_{bias}, is applied, as shown in Figure 17. This Figure illustrates the energies of the adsorbate states need to be placed with respect to the energies of the substrate surface states. In addition to, the frontier orbitals of the molecular adsorbate, i.e., the highest occupied molecular orbital, HOMO, and the lowest unoccupied molecular orbital, LUMO[134].

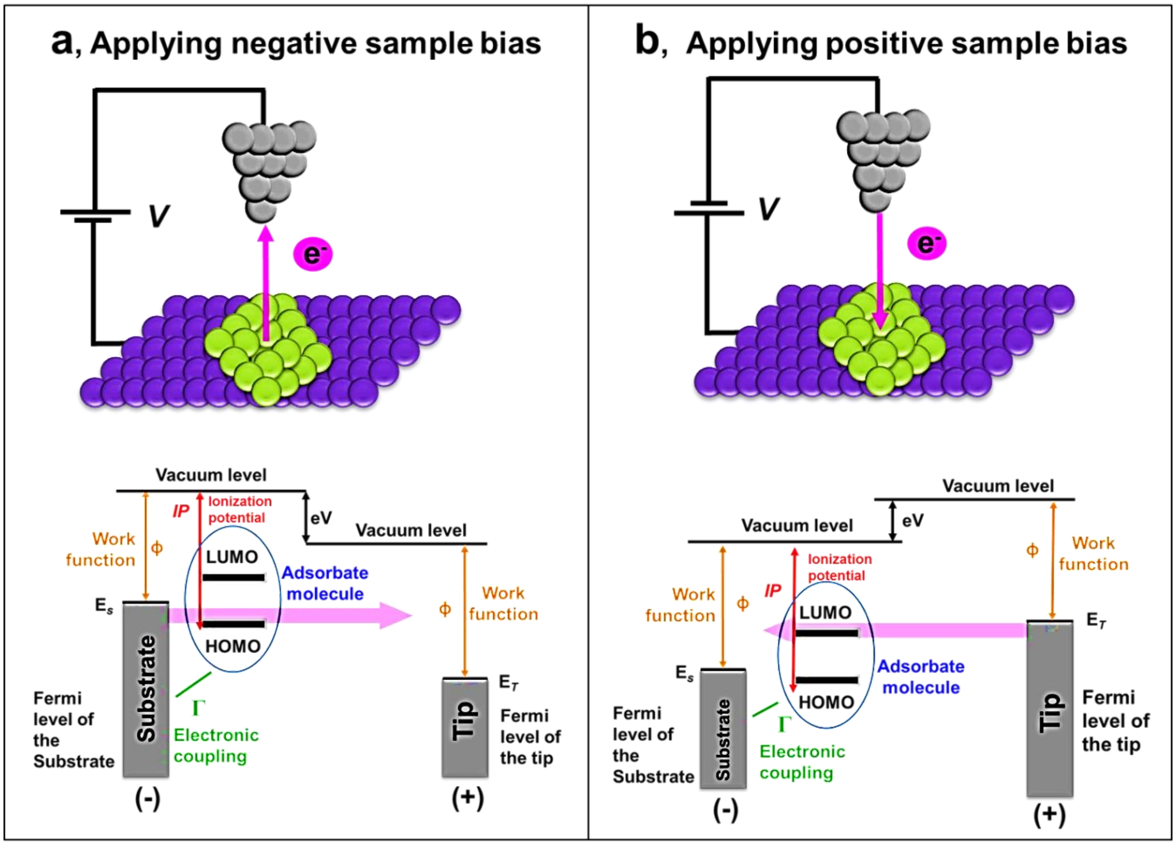

Figure 17. Schematic representation of the energy diagram for an STM junction when applying negative or positive sample bias as in **a** and **b**, respectively. The position of molecular frontier orbitals (HOMO and LUMO) and Fermi levels of substrate (E_S) and tip (E_T) are indicated. While molecular energy levels are broadened and shifted due to electronic coupling (Γ) to substrate states (and other phenomena), their approximate position can be evaluated by pinning the vacuum level of the isolated molecule to that of the substrate.

The Fermi level of the substrate and the HOMO of a free molecule are referred to the vacuum level by the work-function, Φ, and ionization potential, *IP*, respectively. However, a quantitative treatment will have to take into account shifts (and broadening) of energy levels due to effects such as the electronic coupling, Γ, between adsorbate and substrate states, the presence of any solvent (typically lowering the energy of ions), and the electric field in the vicinity of the STM tip[134].

When the surface adsorbate exhibits electronic states near the Fermi level (i.e., for a moderate HOMO-LUMO gap), then individual molecular orbitals may dominate in the mediation of the electron transmission. At $V_{bias} = 0$, the electrons can't flow in either direction since the Fermi level, E_f, of both the tip and the sample is equal i.e. the gradient is zero. For negative sample bias $V_{bias} < 0$, the Fermi level of the sample is raised by V_{bias}, therefore electrons from filled surface states tunnel to the tip. As illustrated in Figure 17a, mediation of this process is dominated by the HOMO of the adsorbate, if the HOMO is situated near the Fermi level. Conversely, electrons tunnel from occupied state of the tip into empty surface states for positive sample bias $V_{bias} > 0$. As illustrated in Figure 17b, the LUMO may play a dominant role in this case if it is located near the Fermi level. Thus, with appropriately chosen bias voltages STM images can reveal the shape of individual molecular orbitals[134].

References

1 Aviram, A. & Ratner, M. A. Molecular rectifiers. *Chemical Physics Letters* **29**, 277-283 (1974).

2 Lent, C. S. Bypassing the transistor paradigm. *Science* **288**, 1597 (2000).

3 Carroll, R. L. & Gorman, C. B. The genesis of molecular electronics. *Angewandte Chemie International Edition* **41**, 4378-4400 (2002).

4 Andrews, D. Q., Solomon, G. C., Van Duyne, R. P. & Ratner, M. A. Single molecule electronics: increasing dynamic range and switching speed using cross-conjugated species. *J. the American Chemical Society* **130**, 17309-17319 (2008).

5 Moth-Poulsen, K. & Bjørnholm, T. Molecular electronics with single molecules in solid-state devices. *Nature nanotechnology* **4**, 551-556 (2009).

6 Kaneko, S. *et al.* Site selection in single-molecule junction for highly reproducible molecular electronics. *Journal of the American Chemical Society* (2016).

7 Heath, J. R. Molecular electronics. *Annual Review of Materials Research* **39**, 1-23 (2009).

8 Song, H., Reed, M. A. & Lee, T. Single molecule electronic devices. *Advanced Materials* **23**, 1583-1608 (2011).

9 Huang, Z., Chen, F., Bennett, P. A. & Tao, N. Single molecule junctions formed via Au-thiol contact: Stability and breakdown mechanism. *Journal of the American Chemical Society* **129**, 13225-13231 (2007).

10 Heath, J. R. & Ratner, M. A. Molecular electronics. (2003).

11 Tour, J. M. Molecular electronics. Synthesis and testing of components. *Accounts of Chemical Research* **33**, 791-804 (2000).

12 Metzger, R. M. *et al.* Unimolecular electrical rectification in hexadecylquinolinium tricyanoquinodimethanide. *Journal of the American Chemical Society* **119**, 10455-10466 (1997).

13 Metzger, R. M. Unimolecular electrical rectifiers. *Chemical reviews* **103**, 3803-3834 (2003).

14 Elbing, M. et al. A single-molecule diode. Proceedings of the National Academy of Sciences of the United States of America **102**, 8815-8820 (2005).

15 Hihath, J. *et al.* Inelastic transport and low-bias rectification in a single-molecule diode. *ACS nano* **5**, 8331-8339 (2011).

16 Flood, A. H., Stoddart, J. F., Steuerman, D. W. & Heath, J. R. Whence molecular electronics? *Science* **306**, 2055-2056 (2004).

17 Waser, R. & Aono, M. Nanoionics-based resistive switching memories. *Nature materials* **6**, 833-840 (2007).

18 Liu, Z., Yasseri, A. A., Lindsey, J. S. & Bocian, D. F. Molecular memories that survive silicon device processing and real-world operation. *Science* **302**, 1543-1545 (2003).

19 Liljeroth, P., Repp, J. & Meyer, G. Current-induced hydrogen tautomerization and conductance switching of naphthalocyanine molecules. *Science* **317**, 1203-1206 (2007).

20 Koumura, N., Zijlstra, R. W., van Delden, R. A., Harada, N. & Feringa, B. L. Light-driven monodirectional molecular rotor. *Nature* **401**, 152-155 (1999).
21 Browne, W. R. & Feringa, B. L. Making molecular machines work. *Nature nanotechnology* **1**, 25-35 (2006).
22 Dulić, D. *et al.* One-way optoelectronic switching of photochromic molecules on gold. *Physical review letters* **91**, 207402 (2003).
23 Auwärter, W. *et al.* A surface-anchored molecular four-level conductance switch based on single proton transfer. *Nature nanotechnology* **7**, 41-46 (2012).
24 Okawa, Y. *et al.* Chemical wiring and soldering toward all-molecule electronic circuitry. *Journal of the American Chemical Society* **133**, 8227-8233 (2011).
25 Collier, C. *et al.* Electronically configurable molecular-based logic gates. *Science* **285**, 391-394 (1999).
26 Kompa, K. & Levine, R. A molecular logic gate. *Proceedings of the National Academy of Sciences* **98**, 410-414 (2001).
27 Joachim, C., Renaud, N. & Hliwa, M. The different designs of molecule logic gates. *Advanced Materials* **24**, 312-317 (2012).
28 Lam, H. Y. & Natelson, D. Transport in single-molecule transistors: Kondo physics and negative differential resistance. *Nanotechnology* **15**, S517 (2004).
29 Kubatkin, S. *et al.* Single-electron transistor of a single organic molecule with access to several redox states. *Nature* **425**, 698-701 (2003).
30 van der Zant, H. S. *et al.* Molecular three-terminal devices: fabrication and measurements. *Faraday discussions* **131**, 347-356 (2006).
31 Liang, W., Shores, M. P., Bockrath, M., Long, J. R. & Park, H. Kondo resonance in a single-molecule transistor. *Nature* **417**, 725-729 (2002).
32 Staykov, A., Areephong, J., R. Browne, W., L. Feringa, B. & Yoshizawa, K. Electrochemical and photochemical cyclization and cycloreversion of diarylethenes and diarylethene-capped sexithiophene wires. *ACS nano* **5**, 1165-1178 (2011).
33 Mallajosyula, S. S. & Pati, S. K. Effect of protonation on the electronic properties of DNA base pairs: applications for molecular electronics. *The Journal of Physical Chemistry B* **111**, 11614-11618 (2007).
34 Vuillaume, D. Molecular nanoelectronics. *Proceedings of the IEEE* **98**, 2111-2123 (2010).
35 Ratner, M. A. *et al.* Molecular wires: Charge transport, mechanisms, and control. *Annals of the New York Academy of Sciences* **852**, 22-37 (1998).
36 Gergel-Hackett, N. *et al.* Vapor phase deposition of oligo (phenylene ethynylene) molecules for use in molecular electronic devices. *Journal of Vacuum Science & Technology B* **25**, 252-257 (2007).
37 Kamenetska, M. *et al.* Conductance and geometry of pyridine-linked single-molecule junctions. *Journal of the American Chemical Society* **132**, 6817-6821 (2010).
38 Milgrom, L. R. The colours of life: an introduction to the chemistry of porphyrins and related compounds. (1997).
39 R. Bonnett. Dolphin, D. The Porphyrins, Vols. I. *Academic Press, New York*, 1-27 (1978).

40 Tanaka, T. & Osuka, A. Conjugated porphyrin arrays: synthesis, properties and applications for functional materials. *Chemical Society Reviews* **44**, 943-969 (2015).
41 J. W. Buchler. Dolphin, D. The Porphyrins, Vols. I. *Academic Press, New York*, 389-483 (1978).
42 Giovannetti, R. The use of Spectrophotometry UV-Vis for the Study of Porphyrins. *Macro to Nano Spectroscopy* **1**, 87-108 (2012).
43 Mamardashvili, N. Z. & Golubchikov, O. A. Spectral properties of porphyrins and their precursors and derivatives. *Russian Chemical Reviews* **70**, 577-606 (2001).
44 Zabardasti, A. Molecular Interactions of Some Free Base Porphyrins with σ-and π-Acceptor Molecules. (INTECH Open Access Publisher, 2012).
45 Vogel, E., Haas, W., Knipp, B., Lex, J. & Schmickler, H. Tetraoxaporphyrin Dication. *Angewandte Chemie International Edition in English* **27**, 406-409 (1988).
46 Gouterman, M. Spectra of porphyrins. *Journal of Molecular Spectroscopy* **6**, 138-163 (1961).
47 Jurow, M., Schuckman, A. E., Batteas, J. D. & Drain, C. M. Porphyrins as molecular electronic components of functional devices. *Coordination chemistry reviews* **254**, 2297-2310 (2010).
48 Smith, K. M. & Falk, J. E. *Porphyrins and metalloporphyrins*. (Elsevier Amsterdam, 1975).
49 Segawa, Y., Ito, H. & Itami, K. Structurally uniform and atomically precise carbon nanostructures. *Nature Reviews Materials* **1**, 15002 (2016).
50 Iijima, S. Helical microtubules of graphitic carbon. *nature* **354**, 56-58 (1991).
51 Kroto, H. W., Heath, J. R., O'Brien, S. C., Curl, R. F. & Smalley, R. E. C 60: buckminsterfullerene. *Nature* **318**, 162-163 (1985).
52 Terrones, H., Lv, R., Terrones, M. & Dresselhaus, M. S. The role of defects and doping in 2D graphene sheets and 1D nanoribbons. *Reports on Progress in Physics* **75**, 062501 (2012).
53 Evans, J. W. V.—THE MEANINGS AND SYNONYMS OF PLUMBAGO. *Transactions of the Philological Society* **26**, 133-179 (1908).
54 Teobaldi, G., Inami, E., Kanasaki, J., Tanimura, K. & Shluger, A. Role of applied bias and tip electronic structure in the scanning tunneling microscopy imaging of highly oriented pyrolytic graphite. *Physical Review B* **85**, 085433 (2012).
55 Iijima, S. & Ichihashi, T. Single-shell carbon nanotubes of 1-nm diameter. (1993).
56 Dresselhaus, M., Dresselhaus, G. & Jorio, A. Unusual properties and structure of carbon nanotubes. *Annu. Rev. Mater. Res.* **34**, 247-278 (2004).
57 Balasubramanian, K. & Burghard, M. Chemically functionalized carbon nanotubes. *Small* **1**, 180-192 (2005).
58 Kumar, M. & Ando, Y. Chemical vapor deposition of carbon nanotubes: a review on growth mechanism and mass production. *Journal of nanoscience and nanotechnology* **10**, 3739-3758 (2010).
59 Yan, Y. *et al.* Carbon nanotube catalysts: recent advances in synthesis, characterization and applications. *Chemical Society Reviews* **44**, 3295-3346 (2015).
60 Singh, P. *et al.* Organic functionalisation and characterisation of single-walled carbon nanotubes. *Chemical Society Reviews* **38**, 2214-2230 (2009).

61 Gao, C., Guo, Z., Liu, J.-H. & Huang, X.-J. The new age of carbon nanotubes: an updated review of functionalized carbon nanotubes in electrochemical sensors. *Nanoscale* **4**, 1948-1963 (2012).
62 Paul Holister, T. E. H. a. C. R. V. Nanotubes. *CMP-Científica*, 1-13. (2003).
63 Thess, A., Lee, R., Nikolaev, P. & Dai, H. Crystalline ropes of metallic carbon nanotubes. *Science* **273**, 483 (1996).
64 Ren, Z. *et al.* Synthesis of large arrays of well-aligned carbon nanotubes on glass. *Science* **282**, 1105-1107 (1998).
65 Isaacs, J., Tanwani, A., Healy, M. & Dahlben, L. Economic assessment of single-walled carbon nanotube processes. *Journal of Nanoparticle Research* **12**, 551-562 (2010).
66 Guo, T. *et al.* Self-assembly of tubular fullerenes. *The Journal of Physical Chemistry* **99**, 10694-10697 (1995).
67 Joshi, M. S. R. K. Synthesis, alignment, growth mechanism and functional properties of carbon nanotubes and their hybrid materials with inorganic and biomaterials. *PhD dissertation* (2010).
68 Walker Jr, P., Rakszawski, J. & Imperial, G. Carbon formation from carbon monoxide-hydrogen mixtures over iron catalysts. I. Properties of carbon formed. *The Journal of Physical Chemistry* **63**, 133-140 (1959).
69 José- Yacamán, M., Miki- Yoshida, M., Rendon, L. & Santiesteban, J. Catalytic growth of carbon microtubules with fullerene structure. *Applied physics letters* **62**, 202-204 (1993).
70 Hata, K. *et al.* Water-assisted highly efficient synthesis of impurity-free single-walled carbon nanotubes. *Science* **306**, 1362-1364 (2004).
71 Nikolaev, P. *et al.* Gas-phase catalytic growth of single-walled carbon nanotubes from carbon monoxide. *Chemical physics letters* **313**, 91-97 (1999).
72 Smalley, R. E. & Yakobson, B. I. The future of the fullerenes. *Solid state communications* **107**, 597-606 (1998).
73 Resasco, D. *et al.* A scalable process for production of single-walled carbon nanotubes (SWNTs) by catalytic disproportionation of CO on a solid catalyst. *Journal of Nanoparticle Research* **4**, 131-136 (2002).
74 Ci, L., Manikoth, S. M., Li, X., Vajtai, R. & Ajayan, P. M. Ultrathick freestanding aligned carbon nanotube films. *Advanced Materials* **19**, 3300-3303 (2007).
75 Hirsch, A. Functionalization of single- walled carbon nanotubes. *Angewandte Chemie International Edition* **41**, 1853-1859 (2002).
76 Cheng, F. & Adronov, A. Noncovalent functionalization and solubilization of carbon nanotubes by using a conjugated Zn–porphyrin polymer. *Chemistry–A European Journal* **12**, 5053-5059 (2006).
77 Samsonidze, G. G. *et al.* Interband optical transitions in left-and right-handed single-wall carbon nanotubes. *Physical Review B* **69**, 205402 (2004).
78 Sánchez-Castillo, A., Román-Velázquez, C. & Noguez, C. Optical circular dichroism of single-wall carbon nanotubes. *Physical Review B* **73**, 045401 (2006).
79 Kataura, H. *et al.* Optical properties of single-wall carbon nanotubes. *Synthetic metals* **103**, 2555-2558 (1999).

80 G. Liu, F. W., X. Peng, A. F. M. M. Rahman, A. K. Bauri and N. Komatsu. *Handbook of Carbon Nano Materials, ed. F. D'Souza and K. M. Kadish, World Scientific* **3**, 203–232 (2012).

81 Strano, M. S. Carbon nanotubes: Sorting out left from right. *Nature nanotechnology* **2**, 340-341 (2007).

82 Komatsu, N. Stereochemistry of carbon nanotubes. *Japanese Journal of Applied Physics* **49**, 02BC01 (2010).

83 Liu, Z. *et al.* Determination of optical isomers for left-handed or right-handed chiral double-wall carbon nanotubes. *Physical review letters* **95**, 187406 (2005).

84 Liu, G. *et al.* Simultaneous discrimination of diameter, handedness, and metallicity of single-walled carbon nanotubes with chiral diporphyrin nanocalipers. *Journal of the American Chemical Society* **135**, 4805-4814 (2013).

85 Komatsu, N. & Wang, F. A comprehensive review on separation methods and techniques for single-walled carbon nanotubes. *Materials* **3**, 3818-3844 (2010).

86 Ju, S.-Y., Abanulo, D. C., Badalucco, C. A., Gascón, J. A. & Papadimitrakopoulos, F. Handedness enantioselection of carbon nanotubes using helical assemblies of flavin mononucleotide. *Journal of the American Chemical Society* **134**, 13196-13199 (2012).

87 Wang, F., Matsuda, K., Rahman, A. M., Kimura, T. & Komatsu, N. Improved selectivity in discriminating handedness and diameter of single-walled carbon nanotubes with N-substituted 3, 6-carbazolylene-bridged chiral diporphyrin nanotweezers. *Nanoscale* **3**, 4117-4124 (2011).

88 Liu, G. *et al.* Preferential extraction of left-or right-handed single-walled carbon nanotubes by use of chiral diporphyrin nanotweezers. *Organic & biomolecular chemistry* **10**, 5830-5836 (2012).

89 Peng, X., Komatsu, N., Kimura, T. & Osuka, A. Improved optical enrichment of SWNTs through extraction with chiral nanotweezers of 2, 6-pyridylene-bridged diporphyrins. *Journal of the American Chemical Society* **129**, 15947-15953 (2007).

90 Peng, X., Komatsu, N., Kimura, T. & Osuka, A. Simultaneous enrichments of optical purity and (n, m) abundance of SWNTs through extraction with 3, 6-carbazolylene-bridged chiral diporphyrin nanotweezers. *ACS nano* **2**, 2045-2050 (2008).

91 Peng, X. *et al.* Optically active single-walled carbon nanotubes. *Nature Nanotechnology* **2**, 361-365 (2007).

92 Peng, X., Wang, F., Bauri, A. K., Rahman, A. M. & Komatsu, N. Optical Resolution of Single-Walled Carbon Nanotubes through Molecular Recognition with Chiral Diporphyrin Nanotweezers. *Chemistry Letters* **39**, 1022-1027 (2010).

93 Wang, F. *et al.* Simultaneous discrimination of handedness and diameter of single-walled carbon nanotubes (swnts) with chiral diporphyrin nanotweezers leading to enrichment of a single enantiomer of (6, 5)-swnts. *Journal of the American Chemical Society* **132**, 10876-10881 (2010).

94 Rahman, A. M., Wang, F., Matsuda, K., Kimura, T. & Komatsu, N. Diameter-based separation of single-walled carbon nanotubes through selective extraction with dipyrene nanotweezers. *Chemical Science* **2**, 862-867 (2011).

95 Liu, G. *et al.* Bis (tert- butylpyrene) Nanotweezers and Nanocalipers: Enhanced Extraction and Recognition Abilities for Single- Walled Carbon Nanotubes. *Chemistry–A European Journal* **19**, 16221-16230 (2013).
96 Peng, X., Wang, F., Kimura, T., Komatsu, N. & Osuka, A. Optical resolution and diameter-based enrichment of single-walled carbon nanotubes through simultaneous recognition of their helicity and diameter with chiral monoporphyrin. *The Journal of Physical Chemistry C* **113**, 9108-9113 (2009).
97 Li, Y. *et al.* Enrichment of large-diameter single-walled carbon nanotubes (SWNTs) with metallo-octaethylporphyrins. *Materials* **6**, 3064-3078 (2013).
98 Deria, P. *et al.* Single-handed helical wrapping of single-walled carbon nanotubes by chiral, ionic, semiconducting polymers. *Journal of the American Chemical Society* **135**, 16220-16234 (2013).
99 Liu, Z. & Qin, L.-C. A practical approach to determine the handedness of chiral carbon nanotubes by electron diffraction. *Chemical physics letters* **405**, 265-269 (2005).
100 Saito, R., Dresselhaus, G. & Dresselhaus, M. S. *Physical properties of carbon nanotubes*. Vol. 35 (World Scientific, 1998).
101 Moss, G. Basic terminology of stereochemistry (IUPAC Recommendations 1996). *Pure and applied chemistry* **68**, 2193-2222 (1996).
102 Barlow, S. M. & Raval, R. Complex organic molecules at metal surfaces: bonding, organisation and chirality. *Surface Science Reports* **50**, 201-341 (2003).
103 Binning, G., Rohrer, H., Gerber, C. & Weibel, E. in *Scanning Tunneling Microscopy* 31-35 (Springer, 1982).
104 Binnig, G. & Rohrer, H. Scanning tunneling microscopy. (1982).
105 Binnig, G., Rohrer, H., Gerber, C. & Weibel, E. 7× 7 reconstruction on Si (111) resolved in real space. *Physical review letters* **50**, 120 (1983).
106 Teugels, L. G., Avila-Bront, L. G. & Sibener, S. Chiral domains achieved by surface adsorption of achiral nickel tetraphenyl-or octaethylporphyrin on smooth and locally kinked Au (111). *The Journal of Physical Chemistry C* **115**, 2826-2834 (2011).
107 Murphy, B. *et al.* Growth and ordering of Ni (II) diphenylporphyrin monolayers on Ag (111) and Ag/Si (111) studied by STM and LEED. *Journal of Physics: Condensed Matter* **24**, 045005 (2012).
108 Haq, S. *et al.* Versatile bottom-up construction of diverse macromolecules on a surface observed by scanning tunneling microscopy. *ACS nano* **8**, 8856-8870 (2014).
109 Yoshimoto, S. & Itaya, K. Advances in supramolecularly assembled nanostructures of fullerenes and porphyrins at surfaces. *Journal of Porphyrins and Phthalocyanines* **11**, 313-333 (2007).
110 Phan, T. H., Kosmala, T. & Wandelt, K. Potential dependence of self-assembled porphyrin layers on a Cu (111) electrode surface: In-situ STM study. *Surface Science* **631**, 207-212 (2015).
111 Phan, T. H. & Wandelt, K. Self-assembly of metal free porphyrin layers at copper-electrolyte interfaces: Dependence on substrate symmetry. *Surface Science* **607**, 82-91 (2013).

112 Zhang, X. *et al.* Solvent dependent supramolecular self-assembly and surface reversal of a modified porphyrin. *Physical Chemistry Chemical Physics* **15**, 12510-12515 (2013).
113 Oncel, N. & Bernasek, S. L. The effect of molecule-molecule and molecule-substrate interaction in the formation of Pt-octaethyl porphyrin self-assembled monolayers. *Applied Physics Letters* **92**, 133305 (2008).
114 Ikeda, T. *et al.* STM observation of alkyl-chain-assisted self-assembled monolayers of pyridine-coordinated porphyrin rhodium chlorides. *Langmuir* **20**, 5454-5459 (2004).
115 Ikeda, T., Asakawa, M., Miyake, K., Goto, M. & Shimizu, T. Scanning tunneling microscopy observation of self-assembled monolayers of strapped porphyrins. *Langmuir* **24**, 12877-12882 (2008).
116 Ogunrinde, A., Hipps, K. & Scudiero, L. A scanning tunneling microscopy study of self-assembled nickel (II) octaethylporphyrin deposited from solutions on HOPG. *Langmuir* **22**, 5697-5701 (2006).
117 Shen, Y. *et al.* Self-assembling in fabrication of ordered porphyrins and phthalocyanines hybrid nano-arrays on HOPG. *CrystEngComm* **15**, 5526-5531 (2013).
118 Basiuk, V. A. & Bassiouk, M. Nanoassembly of meso-tetraphenylporphines on surfaces of carbon materials: initial steps as studied by molecular mechanics and scanning tunneling microscopy. *Journal of nanoscience and nanotechnology* **8**, 259-267 (2008).
119 Basiuk, E. V., Basiuk, V. A., Santiago, P. & Puente-Lee, I. Noncovalent functionalization of carbon nanotubes with porphyrins: meso-tetraphenylporphine and its transition metal complexes. *Journal of nanoscience and nanotechnology* **7**, 1530-1538 (2007).
120 Tersoff, J. & Hamann, D. in *Scanning Tunneling Microscopy* 59-67 (Springer, 1985).
121 Lang, N. Spectroscopy of single atoms in the scanning tunneling microscope. *Physical Review B* **34**, 5947 (1986).
122 Feenstra, R. M., Stroscio, J. A. & Fein, A. Tunneling spectroscopy of the Si (111) 2× 1 surface. *Surface Science* **181**, 295-306 (1987).
123 Kuwabara, M., Clarke, D. R. & Smith, D. Anomalous superperiodicity in scanning tunneling microscope images of graphite. *Applied physics letters* **56**, 2396-2398 (1990).
124 Kano, S., Tada, T. & Majima, Y. Nanoparticle characterization based on STM and STS. *Chemical Society Reviews* **44**, 970-987 (2015).
125 Christensen, P. Electrochemical aspects of STM and related techniques. *Chem. Soc. Rev.* **21**, 197-208 (1992).
126 Rohrer, H. Scanning tunneling microscopy: a surface science tool and beyond. *Surface science* **299**, 956-964 (1994).
127 Wiesendanger, R. Scanning probe microscopy and spectroscopy: methods and applications. (Cambridge University Press, 1994).

128 Tersoff, J. & Hamann, D. Theory and application for the scanning tunneling microscope. *Physical review letters* **50**, 1998 (1983).
129 Giancarlo And, L. C. & Flynn, G. W. Scanning tunneling and atomic force microscopy probes of self-assembled, physisorbed monolayers: Peeking at the peaks. *Annual review of physical chemistry* **49**, 297-336 (1998).
130 Giancarlo, L. C. & Flynn, G. W. Raising flags: Applications of chemical marker groups to study self-assembly, chirality, and orientation of interfacial films by scanning tunneling microscopy. *Accounts of chemical research* **33**, 491-501 (2000).
131 Poirier, G. E. Characterization of organosulfur molecular monolayers on Au (111) using scanning tunneling microscopy. *Chemical reviews* **97**, 1117-1128 (1997).
132 Magonov, S. N. & Whangbo, M.-H. Surface analysis with STM and AFM: experimental and theoretical aspects of image analysis. (John Wiley & Sons, 2008).
133 Claypool, C. L. *et al.* Source of image contrast in STM images of functionalized alkanes on graphite: A systematic functional group approach. *The Journal of Physical Chemistry B* **101**, 5978-5995 (1997).
134 Müller, T. scanning tunneling microscopy: a tool for studying self-assembly and model systems for molecular devices. *bruker corporation.* (2010).

Copyright Clearance Center | RightsLink® | Home | Account Info | Help | Live Chat

npg nature publishing group

Title:	Structurally uniform and atomically precise carbon nanostructures
Author:	Yasutomo Segawa, Hideto Ito, Kenichiro Itami
Publication:	Nature Reviews Materials
Publisher:	Nature Publishing Group
Date:	Jan 11, 2016

Logged in as:
Ahmed Ahmed
Account #:
3001020310
LOGOUT

Order Completed

Thank you very much for your order.

This is a License Agreement between Ahmed Ibrahim Ahmed ("You") and Nature Publishing Group ("Nature Publishing Group"). The license consists of your order details, the terms and conditions provided by Nature Publishing Group, and the payment terms and conditions.

Get the printable license.

License Number	3852890224157
License date	Apr 20, 2016
Licensed content publisher	Nature Publishing Group
Licensed content publication	Nature Reviews Materials
Licensed content title	Structurally uniform and atomically precise carbon nanostructures
Licensed content author	Yasutomo Segawa, Hideto Ito, Kenichiro Itami
Licensed content date	Jan 11, 2016
Type of Use	reuse in a dissertation / thesis
Volume number	1
Issue number	1
Requestor type	academic/educational
Format	electronic
Portion	figures/tables/illustrations
Number of figures/tables/illustrations	1
High-res required	no
Figures	Figure 1
Author of this NPG article	no
Your reference number	None
Title of your thesis / dissertation	Study on the properties of organic molecule / nano-carbon conjugates
Expected completion date	Sep 2016
Estimated size (number of pages)	150
Total	0 JPY

ORDER MORE... | CLOSE WINDOW

Copyright Clearance Center RightsLink®

Home | Account Info | Help | Live Chat

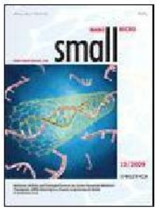

Title: Chemically Functionalized Carbon Nanotubes
Author: Kannan Balasubramanian,Marko Burghard
Publication: Small
Publisher: John Wiley and Sons
Date: Dec 28, 2004

Logged in as:
Ahmed Ahmed

LOGOUT

Order Completed

Thank you for your order.

This Agreement between Ahmed Ibrahim Ahmed ("You") and John Wiley and Sons ("John Wiley and Sons") consists of your license details and the terms and conditions provided by John Wiley and Sons and Copyright Clearance Center.

Your confirmation email will contain your order number for future reference.

Get the printable license.

License Number	3852351076498
License date	Apr 19, 2016
Licensed Content Publisher	John Wiley and Sons
Licensed Content Publication	Small
Licensed Content Title	Chemically Functionalized Carbon Nanotubes
Licensed Content Author	Kannan Balasubramanian,Marko Burghard
Licensed Content Date	Dec 28, 2004
Licensed Content Pages	13
Type of use	Dissertation/Thesis
Requestor type	University/Academic
Format	Electronic
Portion	Figure/table
Number of figures/tables	2
Original Wiley figure/table number(s)	Figure 1 and Figure 2
Will you be translating?	No
Title of your thesis / dissertation	Study on the properties of organic molecule / nano-carbon conjugates
Expected completion date	Sep 2016
Expected size (number of pages)	150
Requestor Location	Ahmed Ibrahim Ahmed Grad. School of Scince Chemistry Department, Ogawa lab Machikaneyamacho 1-1 Toyonakashi, Japan 5600043 Attn: Ahmed Ibrahim Ahmed
Billing Type	Invoice
Billing address	Ahmed Ibrahim Ahmed Grad. School of Scince Chemistry Department, Ogawa lab

Machikaneyamacho 1-1
Toyonakashi, Japan 5600043
Attn: Ahmed Ibrahim Ahmed

Total 0 JPY

Would you like to purchase the full text of this article? If so, please continue on to the content ordering system located here: Purchase PDF

If you click on the buttons below or close this window, you will not be able to return to the content ordering system.

CLOSE WINDOW

Copyright Clearance Center **RightsLink**®

Home | Account Info | Help | Live Chat

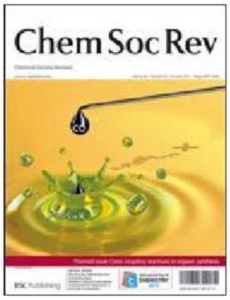

Title: Carbon nanotube catalysts: recent advances in synthesis, characterization and applications

Author: Yibo Yan,Jianwei Miao,Zhihong Yang,Fang-Xing Xiao,Hong Bin Yang,Bin Liu,Yanhui Yang

Publication: Chemical Society Reviews

Publisher: Royal Society of Chemistry

Date: Apr 9, 2015

Logged in as:
Ahmed Ahmed
Account #:
3001020310

LOGOUT

Order Completed

Thank you for your order.

This Agreement between Ahmed Ibrahim Ahmed ("You") and Royal Society of Chemistry ("Royal Society of Chemistry") consists of your license details and the terms and conditions provided by Royal Society of Chemistry and Copyright Clearance Center.

Your confirmation email will contain your order number for future reference.

Get the printable license.

License Number	3863050264293
License date	May 06, 2016
Licensed Content Publisher	Royal Society of Chemistry
Licensed Content Publication	Chemical Society Reviews
Licensed Content Title	Carbon nanotube catalysts: recent advances in synthesis, characterization and applications
Licensed Content Author	Yibo Yan,Jianwei Miao,Zhihong Yang,Fang-Xing Xiao,Hong Bin Yang,Bin Liu,Yanhui Yang
Licensed Content Date	Apr 9, 2015
Licensed Content Volume	44
Licensed Content Issue	10
Type of Use	Thesis/Dissertation
Requestor type	academic/educational
Portion	figures/tables/images
Number of figures/tables/images	1
Distribution quantity	100000
Format	electronic
Will you be translating?	no
Order reference number	None
Title of the thesis/dissertation	Study on the properties of organic molecule / nano-carbon conjugates
Expected completion date	Sep 2016
Estimated size	150
Requestor Location	Ahmed Ibrahim Ahmed Grad. School of Scince Chemistry Department, Ogawa lab Machikaneyamacho 1-1 Toyonakashi, Japan 5600043 Attn: Ahmed Ibrahim Ahmed

Billing Type	Invoice
Billing address	Ahmed Ibrahim Ahmed Grad. School of Scince Chemistry Department, Ogawa lab Machikaneyamacho 1-1 Toyonakashi, Japan 5600043 Attn: Ahmed Ibrahim Ahmed
Total	0 JPY

ORDER MORE CLOSE WINDOW

Copyright Clearance Center RightsLink®

Home | Account Info | Help | Live Chat

Title: Functionalization of Single-Walled Carbon Nanotubes

Author: Andreas Hirsch

Publication: Angewandte Chemie International Edition

Publisher: John Wiley and Sons

Date: May 28, 2002

Logged in as:
Ahmed Ahmed
LOGOUT

Order Completed

Thank you for your order.

This Agreement between Ahmed Ibrahim Ahmed ("You") and John Wiley and Sons ("John Wiley and Sons") consists of your license details and the terms and conditions provided by John Wiley and Sons and Copyright Clearance Center.

Your confirmation email will contain your order number for future reference.

Get the printable license.

License Number	3852350024223
License date	Apr 19, 2016
Licensed Content Publisher	John Wiley and Sons
Licensed Content Publication	Angewandte Chemie International Edition
Licensed Content Title	Functionalization of Single-Walled Carbon Nanotubes
Licensed Content Author	Andreas Hirsch
Licensed Content Date	May 28, 2002
Licensed Content Pages	7
Type of use	Dissertation/Thesis
Requestor type	University/Academic
Format	Electronic
Portion	Figure/table
Number of figures/tables	1
Original Wiley figure/table number(s)	Figure 5
Will you be translating?	No
Title of your thesis / dissertation	Study on the properties of organic molecule / nano-carbon conjugates
Expected completion date	Sep 2016
Expected size (number of pages)	150
Requestor Location	Ahmed Ibrahim Ahmed Grad. School of Scince Chemistry Department, Ogawa lab Machikaneyamacho 1-1 Toyonakashi, Japan 5600043 Attn: Ahmed Ibrahim Ahmed
Billing Type	Invoice
Billing address	Ahmed Ibrahim Ahmed Grad. School of Scince Chemistry Department, Ogawa lab

Machikaneyamacho 1-1
Toyonakashi, Japan 5600043
Attn: Ahmed Ibrahim Ahmed

Total 0 JPY

Would you like to purchase the full text of this article? If so, please continue on to the content ordering system located here: Purchase PDF

If you click on the buttons below or close this window, you will not be able to return to the content ordering system.

CLOSE WINDOW

Chapter II. First Observation of Handedness Chirality of *P*- and *M*-Single-walled Carbon Nanotubes using Scanning Tunneling Microscopic Images

2.1. Introduction

In order to identify the structure of single-walled carbon nanotubes (SWNT); (*n,m*) indices are usually used. Since the cylindrical structure of SWNT can be simply identified as a rolled up graphene sheet, so the structure can be defined by a roll-up vector $\boldsymbol{C_h}$; this vector is given as $\boldsymbol{C_h} = n\boldsymbol{a_1} + m\boldsymbol{a_2}$, where $\boldsymbol{a_1}$ and $\boldsymbol{a_2}$ are the unit vectors of a 2D-graphene sheet, in which *n* and *m* are integers and are referred to the roll-up index (*n,m*) and/or chiral index, whilst $\boldsymbol{C_h}$ is referred to chiral vector. The electronic and optical properties of SWNTs are mainly depend on their (*n,m*) values[1-4]. However, (*n,m*) indices are not sufficient for the identification of SWNT in some structures. That is helicity or handedness chirality; which represents right- and left-handed enantiomers. This type of chirality presents in some biological molecules *i.e*. amino acids, where these molecules can be found in two mirror image structures[5]. SWNTs also can be formed in two ways; either right or left handed helix cylindrical shapes. Except SWNTs whose terminals have armchair and zigzag structures, as they do not have their non-superposable mirror image, all the SWNTs have handedness chirality. ***P*** and ***M*** terminology would be used to define right- and left-handed helical structures of SWNTs[6], respectively (Fig. 1). This can be further explained using tube vector lines; as each SWNT contains these lines which represented using the arrows *I, II* and *III* in Fig. 1. If two of these lines are rotated towards the right however the third one to the left, the chiral SWNT is known as ***P*** type. Similarly, when the SWNT has two lines rotated to the left and the third is to the right, it is termed as ***M***.

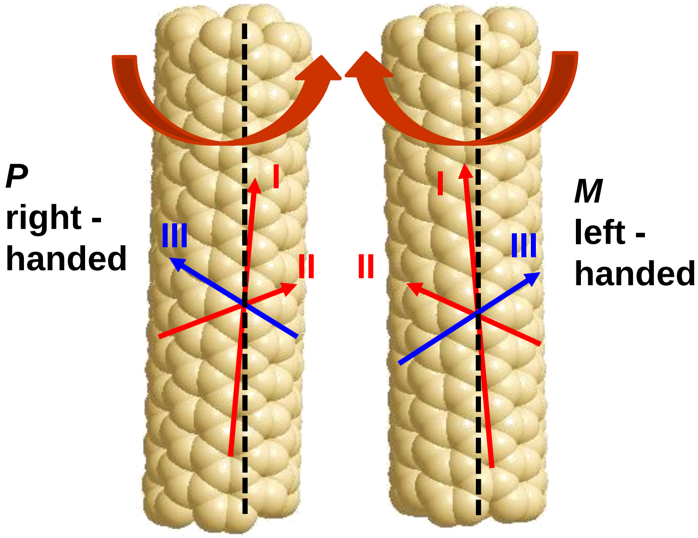

Figure 1. Definition ***P*** and ***M*** stereoisomers of (6,5)-SWNTs. The solid arrows *I, II and III* represented the vector lines, however the black dotted line is the SWNT axis.

Although *(n,m)* indices of SWNTs can be identified using spectroscopic techniques, such as UV-Vis., Raman, and photoluminescence (PL) spectroscopy, the identification of handedness chiralities ***P***, ***M*** of SWNTs is not established yet. This is mainly because of the difficulty of isolation of pure ***P*** and ***M*** handedness chiral SWNTs heretofore. In previous reports, we have succeeded to isolate almost pure ***P*** and ***M*** handedness chiral SWNTs using chiral organic molecules. Their ***P*** and ***M*** handedness chiralities were indirectly determined based on the stability of the SWNT-organic molecule complexes as calculated by using molecular mechanics[7,8].

If the handedness chirality can be observed directly by scanning tunneling microscopy (STM), it can provide conclusive assignment. However it is not easy because the spacial resolution of STM to observe the curved surface of SWNTs is not enough to determine handedness chirality. Another possible way to observe the handedness chirality of SWNTs is utilization of supramolecular structure of organic molecules on the SWNT surface. Since the supramolecular structure of simple organic molecules like n-alkanes on highly oriented pyrolytic graphite (HOPG) can be predicted easily as shown in Figure 6a (Groszek Model)[9], similar rules can be applied for supramolecular structures on SWNTs curved structures. Unfortunately, n-alkanes did not give stable supramolecular structures on the SWNTs we used here. Based on the previous studies using SWNTs / porphyrin polymer system for imaging and electronic property measurements by point-contact current imaging atomic force microscopy (PCI-AFM)[10], as well as fabrication of porphyrin molecular nanodevices wired using SWNTs[11], we consider porphyrin as the anchoring group to make stable supramolecular structure on SWNT curved surface.

In this study, we displayed the handedness chirality dependent supramolecular structures of 5,15-bisdodecylporphyrin (C12P, Figure 2) on mainly ***P***-, ***M***-(6,5) SWNT surfaces in the aim to discuss the handedness chiral structure of these SWNTs. Based on our best knowledge this is the first article describing supramolecular structures of organic molecules on the handedness chiral SWNT surfaces, and discussing their absolute chirality.

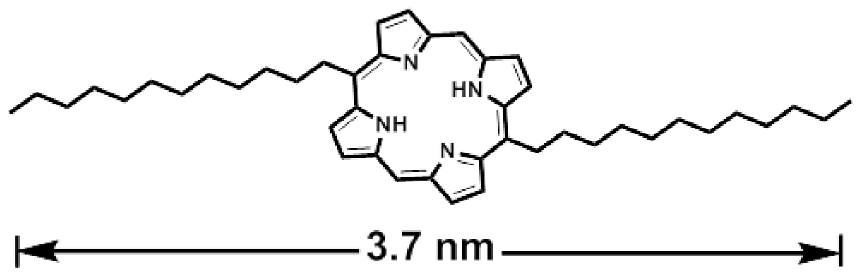

Figure 2. Chemical Structure of 5,15-bisdodecylporphyrins (C12P).

2.2. Experimental

All the reactions were performed in anhydrous solvents under nitrogen atmosphere using well-dried glasswares in an oven at 90 ^{o}C before using. Porphyrin was synthesized under dark conditions. All the solvents i.e. dichloromethane, chloroform and hexane were dried and distilled using molecular sieves 4 Å. Column chromatography was performed using silica-gel (spherical, neutral, 63-200 µm, Kishida Chemicals Co., Ltd.). HOPG was purchased from Alliance Biosystems, Inc. (Spi - 1 Grade 7×7×1 mm). 1- Tetradecane was obtained from Aldrich with a grade (99%) and used as it is. Other chemicals and solvents were of reagent grade and used without any further purification. ^{1}H NMR was carried out on a JEOL 400 and 500 MHz NMR spectrometers. Chemical shifts were given by ppm and all the signals were adjusted using tetramethylsilane (TMS) as an internal standard. Mass spectra were recorded using a Shimadzu AXIMA-CFR MALDI-TOF mass spectrometer. UV/Visible adsorption spectra were recorded on a Shimadzu UV-3150 double-beam spectrophotometer.

SWNT Treatment

Raw Hipco-SWNTs (from Carbon Nanotechnologies Inc. with diameter 0.8-1.2 nm and length around 100-1000 nm) were separated by the reported methods[7]. In which SWNT were dispersed by tip sonication for 40 min. at 20 ^{o}C, followed by centrifugation at 543000 g for 60 min, after that the dispersed SWNTs (to be extracted) were mixed with nanocalipers (R or S) in methanol and bath sonicated at 20 ^{o} C for 36 h followed by centrifugation at 50400 g for 45 h. The resulting supernatant was then concentrated, washed with THF and pyridine to remove nanocalipers to give solid extracted SWNTs (two separated types ***M*** and ***P***) which kept for the reaction with porphyrin derivatives to give the final composites.

STM Measurement

The STM observation was performed using BRUKER multimode 8 scanning probe microscope (SPM) with a special cell for solid – liquid measuments. All the STM images were carried out in a constant current mode under the ambient conditions. The STM tips were mechanically cut and formed from Pt/Ir (80 % / 20 %) wire (0.25 mm in diameter).

To investigate the supramolecular structure of porphyrin molecules on HOPG surface, the compound was dissolved in dry CH_2Cl_2 (~ 0.8 mM). Drops of solution (ca. 5 μL) were casted onto a freshly cleaved HOPG surfaces and fixed in the cell. The substrate was then annealed (without annealing stable supramolecular structure can't be observed) at 60 ^{o}C for 20 - 30 min. and cooled to room temperature. A few drops of 1-Tetradecane were added to the sample, and then the STM tip was immersed in the solution. In order to induce a tunneling current, a bias voltage was applied between the tip and sample, to record images at solid-liquid interface. Whilst the supramolecular structures of porphyrin / SWNT composites samples were prepared using simple drop casting technique and then left to dry at room temperature to be ready for observation. The STM images of graphite surface taken for the lattice parameters calibration were recorded by decreasing the sample bias voltage during imaging of the supramolecular structures. Image calibration (flattening to correct the tilting effect of the substrate, low-pass-filtration to remove high-frequency noise) and unit cell parameter detection were achieved using SPIP (Image Metrology A/S) and NanoScope analysis softwares[12].

Synthesis of Compounds

Dipyrromethane (1)

Dipyrromethane **1** was synthesized using reported procedures[13,14]. In this method, paraformaldehyde (3.46 g, 110 mmol) was mixed with pyrrole (200 mL, 2880 mmol) into a three necked round bottomed-flask. The mixture was degassed and heated at 90 ^{o}C till all the aldehyde perfectly dissolved. To the resulting mixture, using a micro-syringe, trifluoroacetic acid (890 µL) was added. After 15 min. stirring to proceed the reaction, the mixture was treated with aq. solution of NaOH, extracted with ethylacetate (AcOEt) using a separating funnel. The organic layer was then washed with brine solution and the combined extracts were dried over Na_2SO_4. After filtration, the organic solvent and the excess of pyrrole was removed by vacuum distillation at 70 ^{o}C. n-Hexane was added to the tarry residue and stirred at 60 ^{o}C for 10 min. The hot n-Hexane extraction was repeated 5 times. After removing the supernatant liquid by vacuum distillation, the product was purified by recrystallization from EtOH/H_2O (1:1) giving a colorless crystals (8 g, 48 %). ^{1}H NMR

(400 MHz, $CDCl_3$, 25 ^oC, TMS): δ 7.81 (br s, 2H, NH), 6.65 (m, 2H), 6.15 (q, J = 2.8 Hz, 2H), 6.04 (m, 2H), 3.97 ppm (s, 2H, CH_2).

5, 15-bisdodecylporphyrin (C12P) (3)

We synthesized C12P **3** based on our previously reported method[11] with slight modification (Scheme 1). Dipyrromethane (1.0 g, 5 mmol) was dissolved in degassed CH_2Cl_2 (1.1 L) and the flask was shielded from the ambient light. After 20 min from N_2 bubbling, tridecanal (0.7 g, 4.7 mmol) solved in DCM (20 mL) was added dropwise to the solution during 20 min. Trifluoroacetic acid (83 µL) was then added dropwise into the solution after 10 min. The reaction mixture was stirred for 24 h at room temperature, followed by addition of p-chloranil (1.7 g, 7 mmol) with a further stirring for 2 h, 3 mL of Triethylamine (Et_3N) were added to neutralize the solution. Then the product was purified using flash column chromatography (silica gel, Hexane/CH_2Cl_2 = 1:1) and recrystallized from CH_2Cl_2 / excess MeOH to give the target compound as a red purple powder (0.3512 g, 23 %) yield. ^1H NMR (500 MHz, $CDCl_3$, 25 ^oC, TMS): δ 10.16 (s, 2H, *meso*-H), 9.57 (d, J = 4.57 Hz, 4H, β-pyrrole-H), 9.4 (d, J = 4.56 Hz, 4H, β-pyrrole-H), 5.01 (m, 4H, CH_2), 2.55 (m, 4H, CH_2), 1.8 (m, 4H, CH_2), 1.26 (m, 16H, CH_2), 0.87 (t, 6H, CH_3), -2.91 ppm (s, 2H, NH). UV/Vis (CH_2Cl_2): λ_{max}= 410, 504, 535, 577, 632 nm. MS (MALDI-TOF) *m/z* for $C_{44}H_{62}N_4$, [M^+] calcd, 646.50; found, 646.50.

Preparation of C12P / SWNT Composite

The porphyrin/SWNT complex was prepared as follows. After dissolving C12P in dichloromethane, the solution was submitted to ultrasonic bath for 10 min. 0.3 mg of ***P-*** and/or ***M-*** chiral SWNTs were added to porphyrin solution, and sonicated overnight. The resulting suspension was left for sedimentation for 2 h. Then the top 5 % of the supernatant was removed, and the precipitate was filtered by a membrane filter (MILLIPORE) of 0.1 μm mesh. Then rinse with 100 mL CH_2Cl_2 to remove the non-adsorbed porphyrin and dried in a vacuum desiccator until further utilization. For STM measuments, the powder was re-suspended in 10 mL MeOH and drop-casted onto HOPG substrate as illustrated in scheme 2.

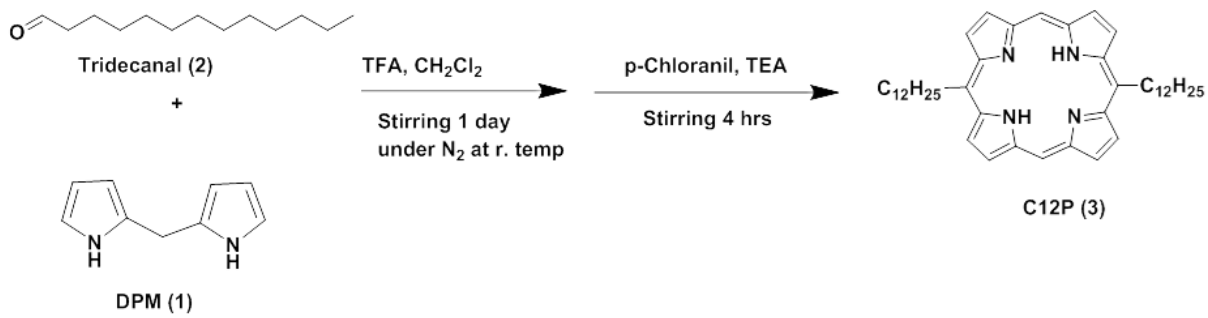

Scheme 1. Procedures for synthesizing 5,15-bisdodecylporphyrins (C12P)**.**

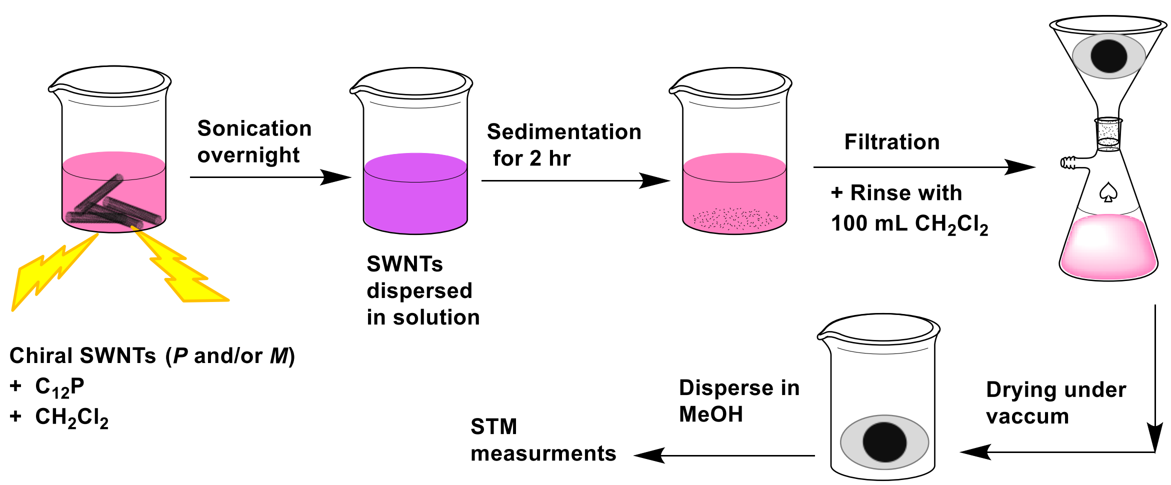

Scheme 2. Procedures to synthesis porphyrin / SWNTs complex.

2.3. Results and discussion

Supramolecular Structures of C12P on *P, M* Handedness Chiral SWNTs Surface observed by STM

Handedness chiral SWNTs were separated by the reported method[7]. In order to investigate how the nanotubes/porphyrin interactions are, and how the porphyrin molecules can be aligned on the CNTs surface especially chiral nanotubes, to afford a well ordered supramolecular structures; we performed the following interaction between C12P molecule and chiral SWNTs. The C12P/SWNTs complex preparation method was duly described in the experimental section (see scheme 2). Prior to STM observation, small portion of the composite samples suspension (ca. 0.06 mg in 0.2 mL of MeOH) was casted on HOPG surface and left to be completely dry and then introduced to the STM machine (Fig. 3).

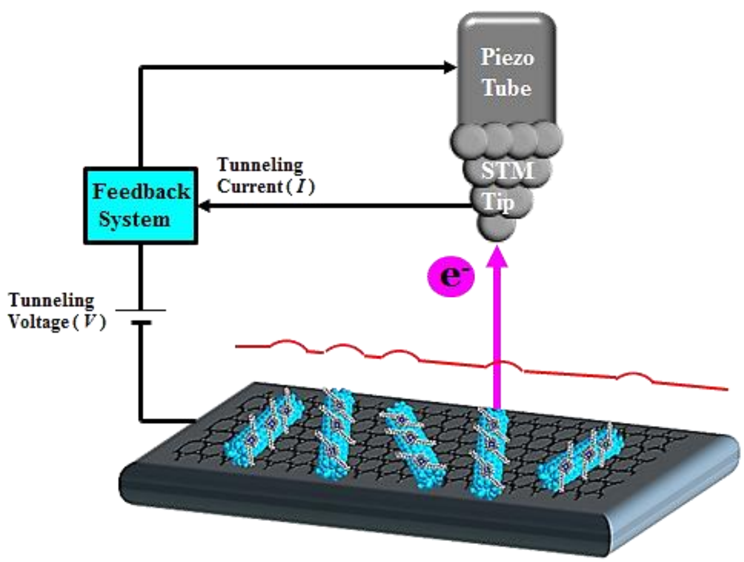

Figure 3. Schematic representation of constant-current mode STM measuments for Porphyrin / SWNTs Complexes.

Interestingly, two opposite supramolecular structures have been found and we assigned them based on CNTs chirality type as follows. As shown in Figure 4, the supramolecular structures made by C12P were strongly dependent on the underlying SWNTs structure. In the STM images of C12P / ***P***- SWNTs complex elucidated in Figure 4a-f, one can see an apparent diagonal orientation of C12P molecules to the right direction can be clearly distinguished. On the other hand, in the case of ***M***-type chiral SWNTs, C12P supramolecular structure aligned on the opposite direction to C12P / ***P***-SWNTs complex, as can be shown in Figure 4g-l. These complexes have been formed due to non-covalent driving forces between CNTs and porphyrin i.e. π-π staking between the two components which possess a high carrier mobility of delocalized π-electrons. Furthermore the C12P / SWNTs complex might be stabilized also due to the alkyl-CNTs interaction (molecular-substrate interactions), or Vander Waals interactions (intermolecular interactions) between alkyl chains or intermolecular interactions between the neighboring porphyrin cores.

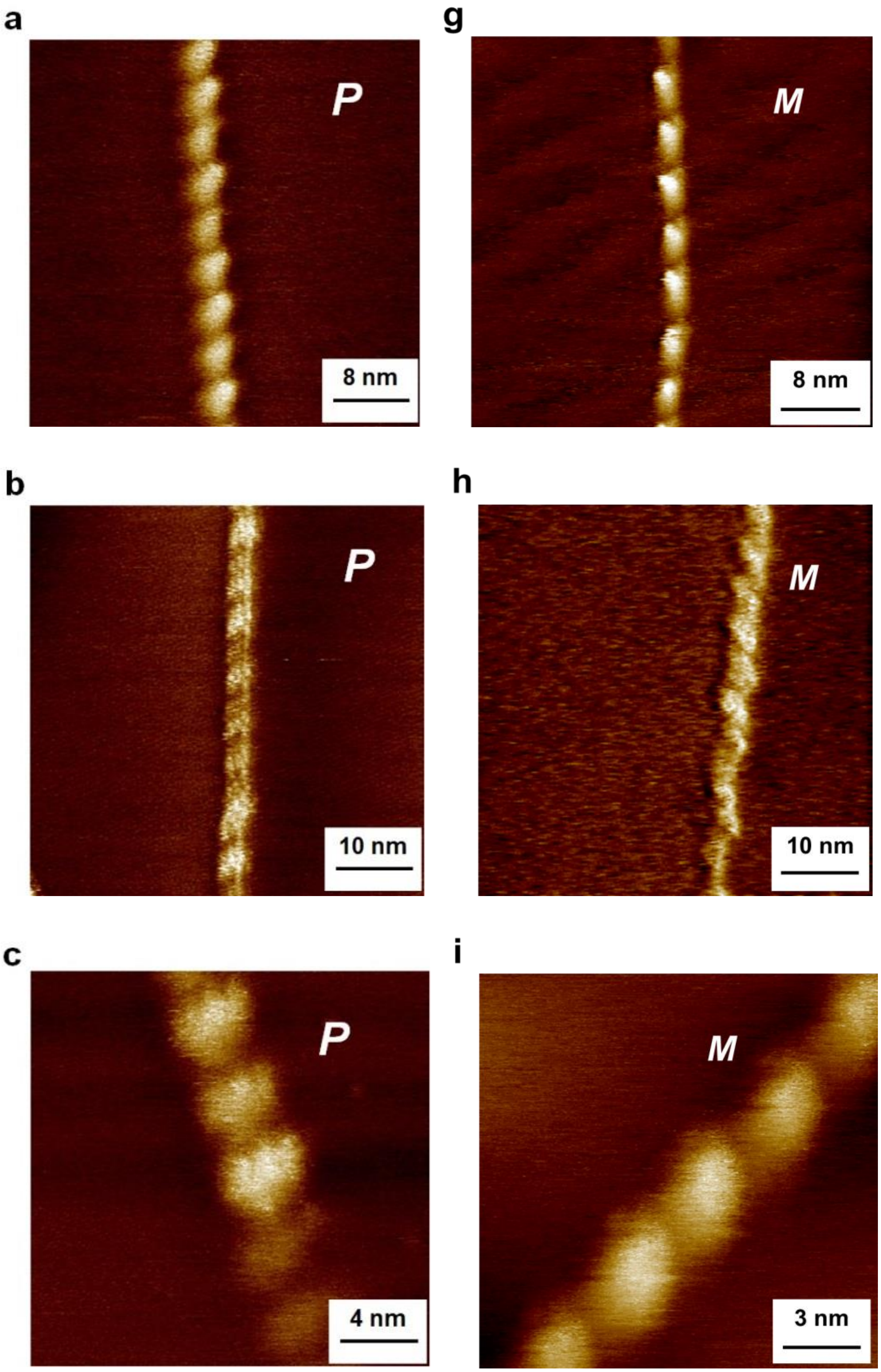
a
P
8 nm
g
M
8 nm
b
P
10 nm
h
M
10 nm
c
P
4 nm
i
M
3 nm

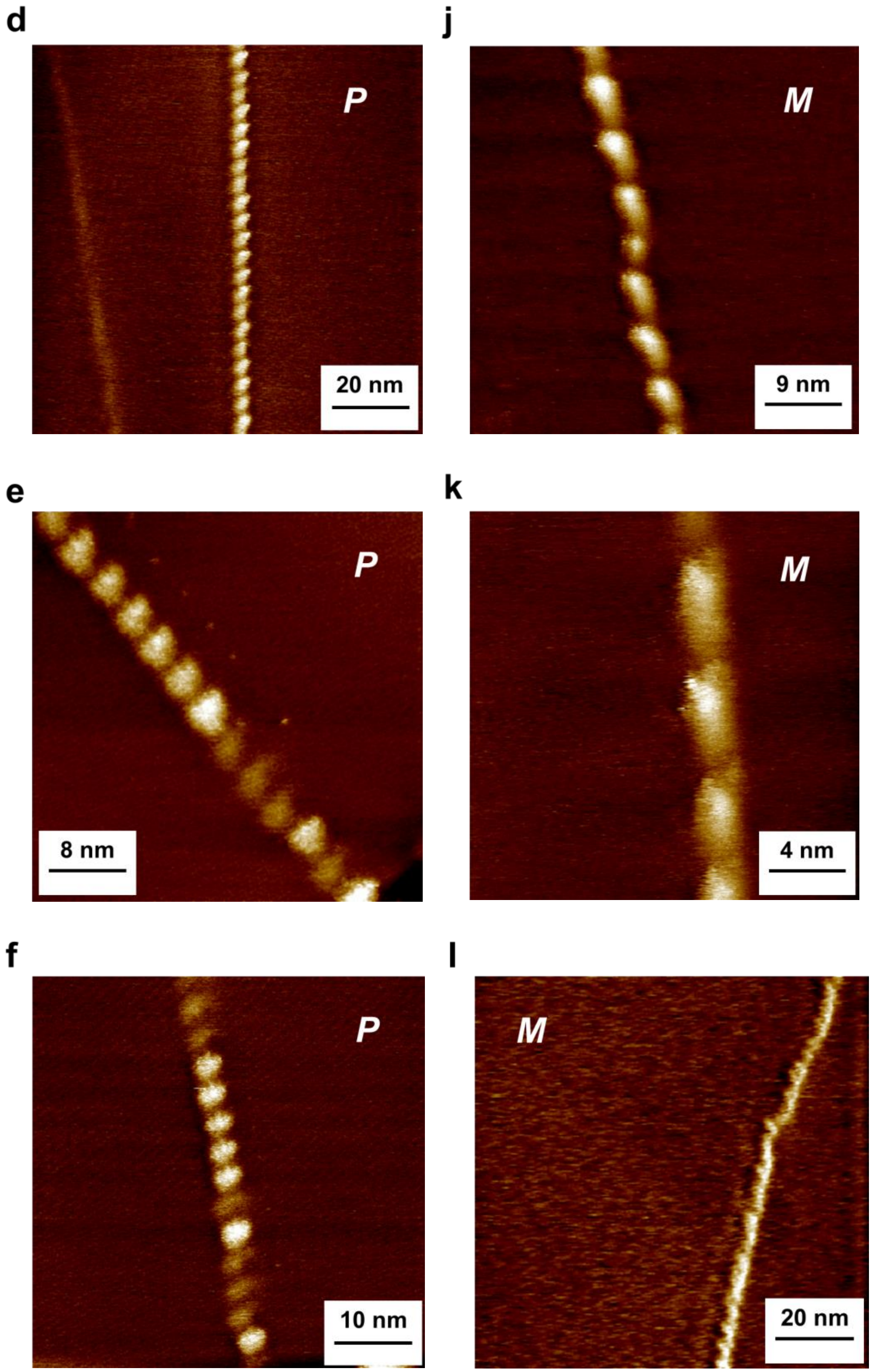
d
P
20 nm
j
M
9 nm
e
P
8 nm
k
M
4 nm
f
P
10 nm
l
M
20 nm

Figure 4. Typical STM images for supramolecular structures of C12P / ***P***- and ***M***- SWNTs complexes on HOPG surface. All images were taken at V_{sample} = 0.100 V and I_t = 0.010 nA. **a**, C12P / ***P***- SWNTs complex (40 nm × 40 nm) **b**, C12P / ***P***- SWNTs complex (50 nm × 50 nm) **c**, C12P / ***P***- SWNTs complex (20 nm × 20 nm) **d**, C12P / ***P***- SWNTs complex (100 nm × 100 nm) **e**, C12P / ***P***- SWNTs complex (40 nm × 40 nm) **f**, C12P / ***P*** - SWNTs complex (50 nm × 50 nm) **g**, C12P / ***M***- SWNTs complex (40 nm × 40 nm) **h**, C12P / ***M***- SWNTs complex (50 nm × 50 nm) **i**, C12P / ***M***- SWNTs complex (15 nm × 15 nm) **j**, C12P / ***M*** - SWNTs complex (45 nm × 45 nm) **k**, C12P / ***M*** - SWNTs complex (20 nm × 20 nm) **l**, C12P / ***M*** - SWNTs complex (100 nm × 100 nm).

In order to discuss the absolute handedness chirality of the SWNTs, further elucidations were made using the supramolecular structure of C12P on HOPG surface, on which better resolution of the molecular structure can be obtained and detailed discussion is possible.

Supramolecular Structures of C12P on HOPG Surface observed by STM.

A highly reproducible ordered pattern of self-assemble monolayer of C12P deposited from 1-tetradecane onto HOPG surface is observed, forming a distinctive lamellar structures with a well-defined pattern of bright and dark domains as shown in Figure 5a-c. The bright areas in the images could be attributed to the porphyrin cores, separated by the alkyl chains which appear in the dark regions as linear features. The two dodecyl chains are closely packed, interacted giving regular geometry[15-17]. The unit cell parameters were $\boldsymbol{a}$ = 1.05 ± 0.01 nm, $\boldsymbol{b}$ = 2.55 ± 0.02 nm, γ = 53 ± 8 °.

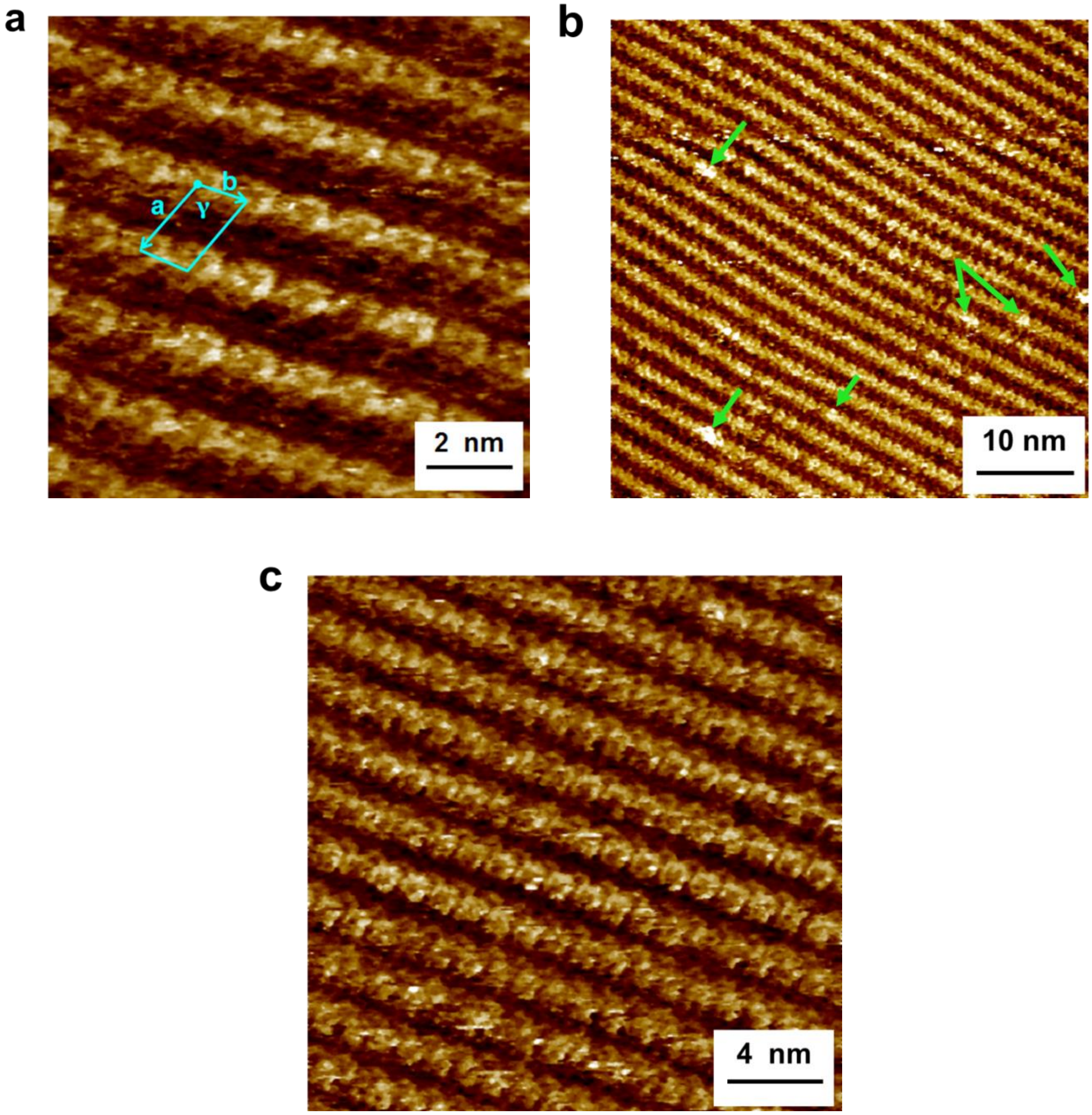

Figure 5. STM image of 2D supramolecular structure of 5,15-bisdodecylporphyrin (C12P) on HOPG-tetradecane interface **a**, V_{sample} = - 1.050 V, I_t = 0.081 nA, with a unit cell parameters, ***a*** = 1.05 ± 0.01 nm, ***b*** = 2.55 ± 0.02 nm, γ = 53 ± 8 °. **b**, V_{sample} = - 1.000 V, I_t = 0.080 nA. The green arrows accentuate the formation of the second layer in some parts in the image. **c**, V_{sample} = - 1.000 V, I_t = 0.080 nA.

The driving forces by which these supramolecular structures may be possibly formed can be classified into two main types. First, molecular-substrate interaction i.e. interaction between porphyrin cores and HOPG substrate and/or interaction between two dodecyl alkyl chains and HOPG surface. The second type of driving forces are intermolecular interactions i.e. Vander Waals interactions between the alkyl chains, the CH-N interactions between the porphyrin cores (Fig. 5a and c). In Fig. 5b, it is clear apparently that there are some sites on which second layer of C12P arrays was formed (marked by green arrows); formation of second layer supramolecular structures of porphyrin derivatives has been reported by many researchers[18,19].

The supramolecular structures of the *n*-alkanes on graphite substrate are usually described by the Groszek model (Fig. 6a)[9,20]. As shown in Figure 6a, the interatomic distance between the two carbon atoms within the repeated three methylene groups (C^*H_2-CH_2-C^*H_2) is ca. 0.25 nm, whilst that in graphite (C*-C-C*) is 0.246 nm. Because of the similarity of the distances, usually *n*-alkanes make stable supramolecular structures along the lattice of the graphite[20-24] which is defined by the vector made by two carbon atoms of the repeated units C*-C-C*.

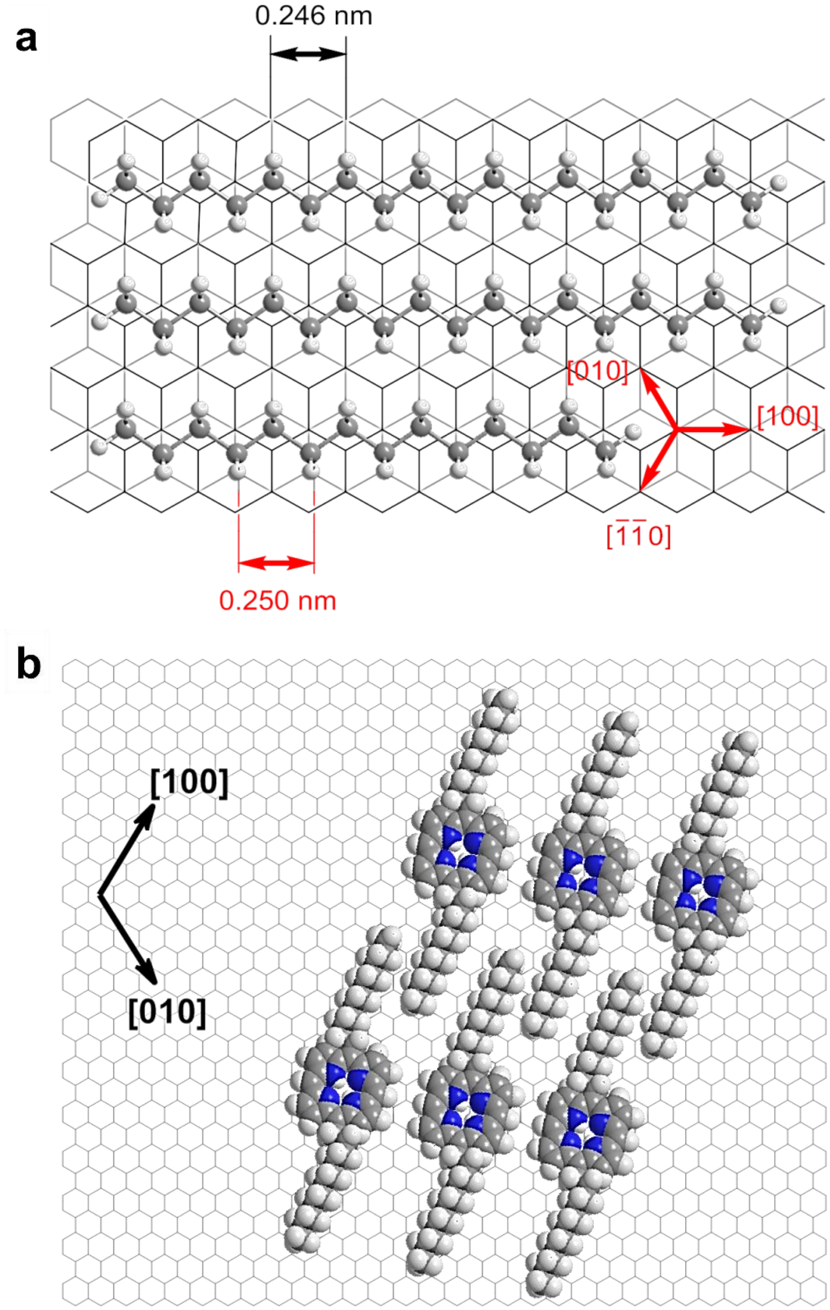

Figure 6. a, Groszek model in which *n*-alkanes can be aligned along the basal plane of graphite to display a close-packed lamellar structure **b,** Proposed model intended to elucidate the geometries of arrays for C12P molecules on HOPG surface in which C12P can be aligned on graphite to display a close-packed lamellar structure.

In order to elucidate C12P molecular alignment on HOPG surface, we made STM images including both the supramolecular structure of C12P and the HOPG surface underlying the molecules. The measurements can be performed by decreasing the sample bias during STM imaging of the supramolecular structures, to move the STM tip towards the HOPG surface, giving images shown in Figure 7a and b. The upper part of the Figure 7 demonstrates C12P molecular layer, whilst the lower part represents the graphite layer lying under the molecules. From this image it is possible to clarify the HOPG hexagons beneath the C12P molecules as it is shown using graphite hexagon models. The white dot lines are parallel to the lattice vectors ***a*** and ***b*** of C12P. The molecular lattice vector ***a*** reconciles the porphyrin cores in the row; while the molecular lattice vector ***b*** corresponds to the porphyrin cores in the period. The lattice directions of the graphite were indicated by the white solid arrows.

As shown in Figure 7, the angle between the molecular lattice vector ***a*** and the lattice direction [**010**] of HOPG is ca. 5 °, that between the molecular lattice vector ***b*** and [**100**] is ca. 4 °, and that between ***b*** and [**110**] equals to 55 °. If the alkyl chains of C12P align on the HOPG surface according to the Groszek model, the angle between ***a*** and one of the HOPG lattices should be 0 °. The observed angle ca. 4 ° means C12P is a little bit deviated from the Groszek model, probably because of the interaction of the porphyrin core with HOPG surface. The schematic model of the observed structure is shown in Figure 7. Similar alignments were observed for free base and zinc-5,10,15,20-*meso*-tetradodecylporphyrin[15,16], in which two dodecyl tails physisorbed along the main axis of

HOPG. The results will be very helpful for understanding the supramolecular structures of C12P on curved surface cases.

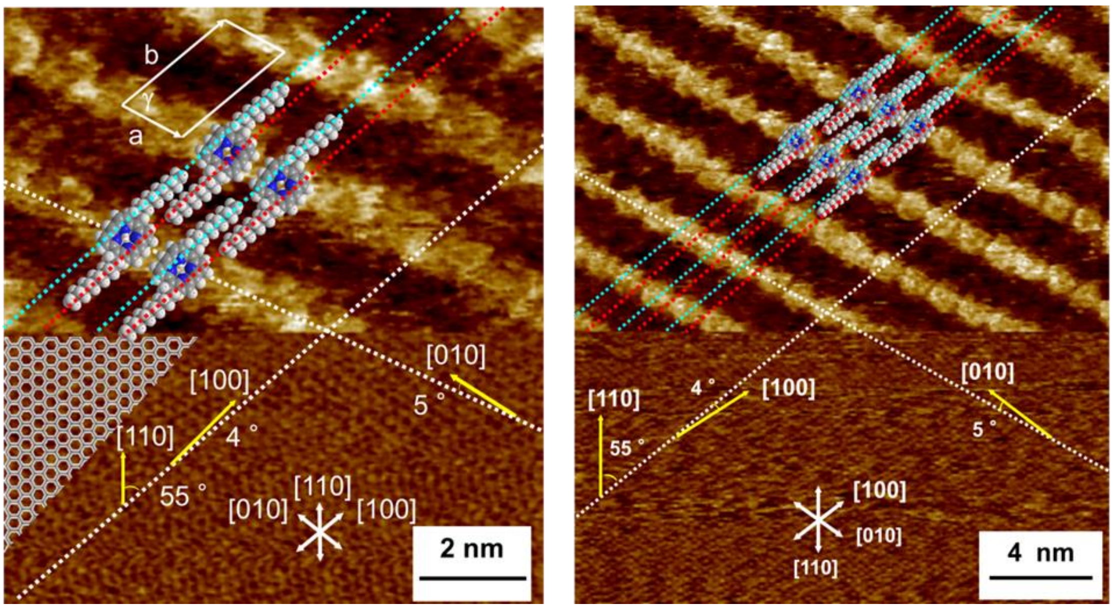

Figure 7. STM images for alignments of C12P on lattice of HOPG substrate (V_{sample} = -1.000 V, I_t = 0.080 nA for the upper image part, and V_{sample} = 0.100 V, I_t = 0.080 nA for the lower image part). The cell parameters are ***a*** = 1.05 ± 0.01 nm, ***b*** = 2.55 ± 0.02 nm, γ = 53 ± 8 °. The lattice directions of the graphite were indicated by the white arrows; schematically models were drawn to elucidate the orientation of C12P molecules.

Molecular Modeling

As an attempting to demonstrate the observed geometries of our molecules on the surface of chiral SWNTs, three proposed models were built using ***P***- and ***M***- (6,5) chiral SWNTs and C12P molecule. The first proposed model (Fig. 8a) in which C12P molecules are aligned linearly on the vector line *I* (Type *I*), the second one (Type *II*) in which the molecules are assembled on the vector line *II* forming short helix arrays (Fig. 8b) and the third model showed that the molecules are aligned in between the vector lines *I* and *II* giving long helix arrays, which illustrated in Fig. 8c and represented by the green arrow *IV* in Fig. 8d (Type *IV*). By measuring mathematically the angles made by the molecular orientations in the directions *I* and *II* with SWNT principle axis (Fig. 8d), they are found equal 3 ° and 63 ° respectively.

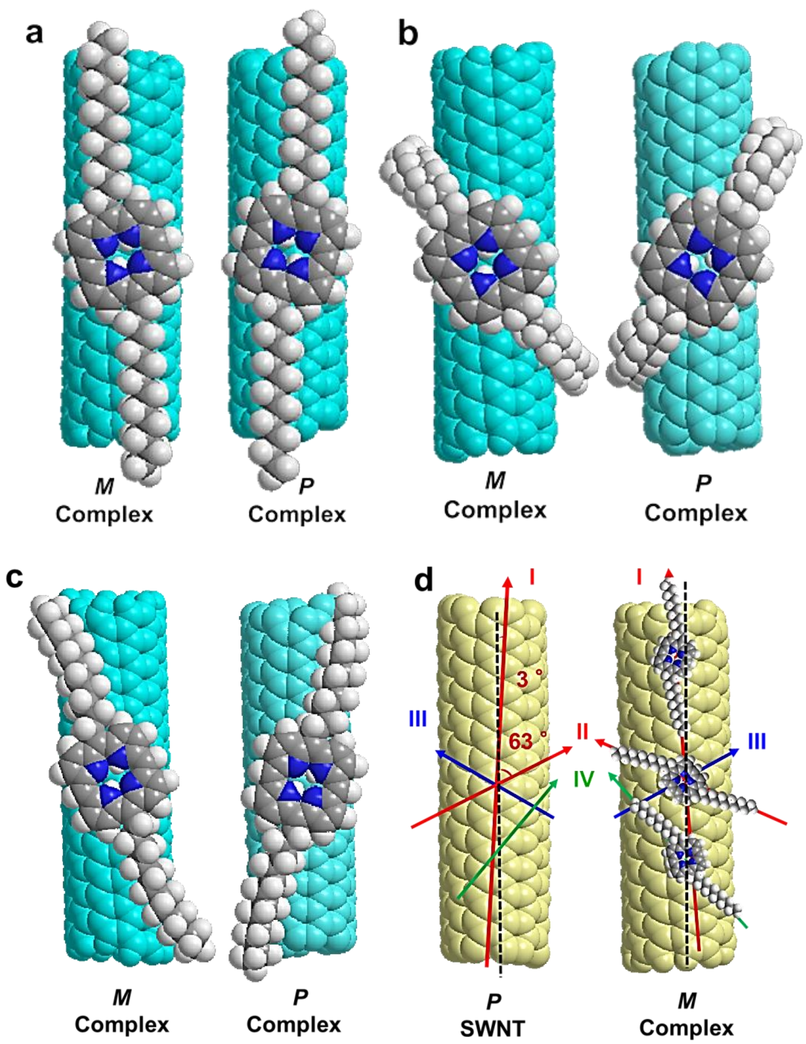

Figure 8. Proposed models intended to elucidate the geometries of arrays observed in C12P / ***M***- and ***P***- SWNTs complexes, based on alignment of porphyrin molecules on which chiral vector line on chiral SWNTs surfaces. **a**, molecules are aligned towards the vector line *I* (Type *I*) **b,** molecules are assembled towards the vector line *II* (Type *II*) **c**, molecules are assembled in between the two vector lines *I* and *II* which represented by the green arrow *IV* (Type *IV*) **d**, angles made by the molecular alignment with SWNT axis in the directions *I* and *II* which equals 3 ° and 63 °, respectively.

Since there are three possible ways for the molecule to be aligned on the tube surface, we performed some theoretical calculations in order to know exactly which one is the most appropriate for the molecule to be aligned on SWNT surface from an energetic point of view and also to provide further understanding into SWNT-C12P interaction mechanism.

DFT Calculations

All the calculations have been employed using density functional theory (DFT) functionals which involved in Gaussian 09 software[25]. Since the main driving forces in SWNT/C12P conjugates are Van der Waals (VdW) and the fundamental interactions are long-range non-covalent interactions, therefore local density approximation (LDA) and the traditional generalized gradient approximation (GGA) functionals can't be used to measure such kind of these long-range interactions[26]. Subsequently for more convenient characterization of the non-local nature of VdW interactions, we performed DFT calculations using long range corrected functionals i.e. the Minnesota functionals (M05-2X and M06-2X)[26,27] with 3-21G basis set.

We used an open ended chiral ***P***- (6,5) SWNT modeling with 2.5 nm length, 0.8 nm in diameter (designed by our group) and composed of 222 carbon atoms and 22 hydrogen atoms; in addition to porphyrin macrocycle ring which consist of 20 carbon atoms, 4 nitrogen atoms and 14 hydrogen atoms. The length of that CNT model is 2.5 nm which is totally enough to host the porphyrin core on its surface. In fact we tried CNT modeling with 10 nm and 5 nm lengths in the calculations but unfortunately the calculations were very difficult to be continued. All the calculations have been done using M05-2X / 3-21G theoretical level. The frontier molecular orbitals (HOMOs and LUMOs) and their absolute energies values in eV of ***P***-(6,5) SWNT, porphyrin molecule and SWNT / Porphyrin complex are demonstrated in table 1.

	SWNT	**Porphyrin**	**SWNT / Porphyrin Complex**
LUMO 3	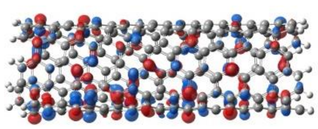 -2.12817 eV	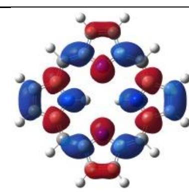 3.844098 eV	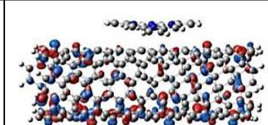 -2.102866 eV
LUMO 2	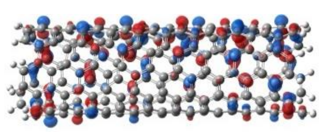 -2.17661 eV	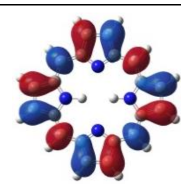 0.61252 eV	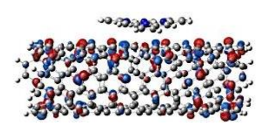 - 2.149941eV

LUMO 1	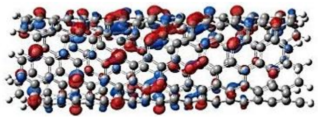 -2.69416 eV	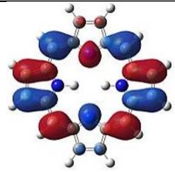 -1.49987 eV	 - 2.666678 eV
LUMO	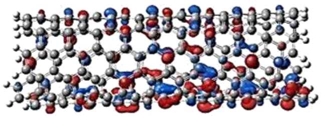 -2.73144 eV	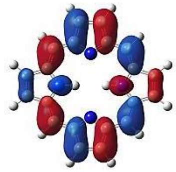 -1.58096 eV	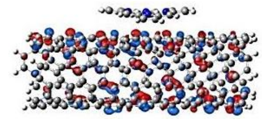 - 2.702869 eV
HOMO	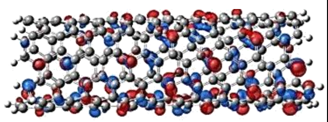 -5.78098 eV	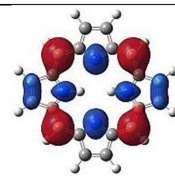 -6.17064 eV	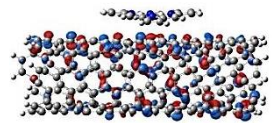 - 5.753494eV
HOMO 1	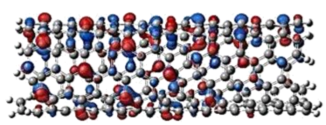 -5.8237 eV	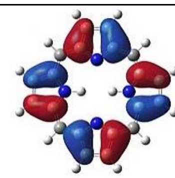 -6.90751 eV	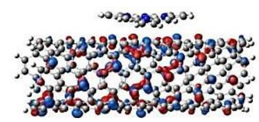 - 5.796215 eV
HOMO 2	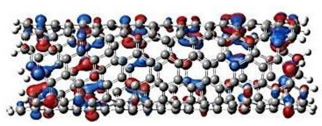 -6.30016 eV	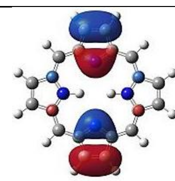 -7.88874 eV	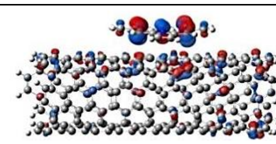 - 6.071863 eV
HOMO 3	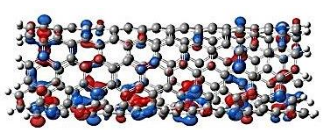 -6.3603 eV	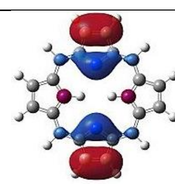 -7.99922 eV	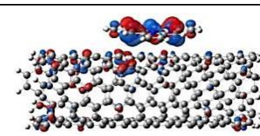 - 6.209006 eV

Table 1. The frontier molecular orbitals (HOMOs and LUMOs) and their absolute energies values in eV of ***P***-(6,5) SWNT, porphyrin molecule and SWNT / porphyrin complex, calculated using M05-2X / 3-21G theoretical level.

Since the energy of formation (binding energy) of the complex ($\Delta E_{complex}$) can be calculated using the following formula[28,29]:

$$\Delta E_{complex} = E_{complex} - (E_{SWNT} + E_{por})$$

where $E_{complex}$, E_{SWNT} and $E_{por.}$ are the corresponding absolute energies of the complex, SWNT and porphyrin molecule, respectively. The energy of formation of the complex, HOMO-LUMO energy gab, the closest intermolecular distance between the porphyrin core and the tube surface ($d_{SWNT/Por.}$), in addition to the angle made by porphyrin molecule with the main axis of the tube, are being summarized in the table 2.

Functional/basis set	**HOMO/LUMO energy gap (eV)**	**Distance $d_{SWNT/Por.}$ (Å)**	**Angle made by por. with the main axis of the tube (°)**	**Energy of Formation $\Delta E_{complex}$ (eV)**
M052X / 321G	3.05	3.1	13	-5.8

Table 2. DFT calculations summary for SWNT / porphyrin complex, including HOMO-LUMO energy gab, the separation distance between porphyrin molecule and SWNT surface, the angle made by porphyrin molecule with the main axis of the tube and the energy of formation of the complex calculated using M05-2X / 3-21G theoretical level.

As demonstrated from table 2, the calculation displayed strong exothermal energy of formation. The intermolecular contact distance is calculated and equals 3.1 Å, which is very similar to the distance obtained for tetraphenylporphyrin (TPP) /C_{60} system[30] which is 3 Å and with TPP/SWNT system[31] which is $3.0 \leq d \leq 3.3$ Å . It is worth to mention that the angle made by porphyrin molecule with respect to the main axis of the tube equals around 13 °, this angle in a quite agreement with the experimentally measured angle of C12P with [100] lattice direction on HOPG surface (Fig. 7) which equals 4 °.

Figure 9 represents the frontier molecular orbitals of the nanotube, porphyrin core and SWNT / porphyrin conjugates in which one can see that the frontier orbitals of the complex are mainly located on the tube surface because the HOMO and LUMO energy levels of the complex are close to the HOMO and LUMO energies of the nanotube models.

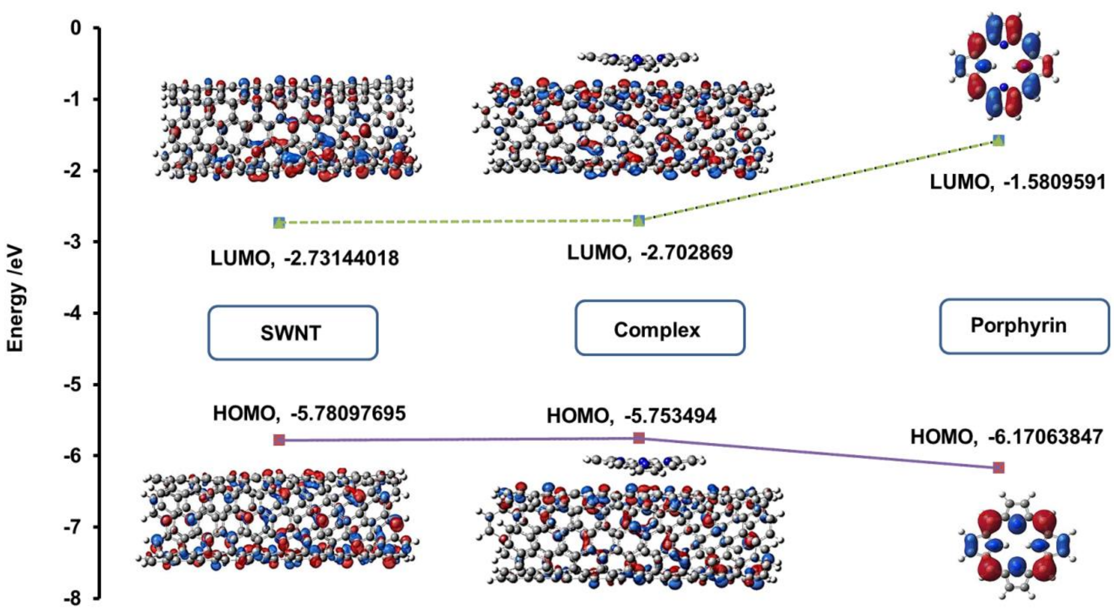

Figure 9. The HOMO-LUMO plot and the frontier orbital shapes of ***P***-(6,5) SWNT, porphyrin molecule and SWNT / porphyrin complex, calculated using M05-2X functional with 3-21G basis set.

Very magnificent findings have been interestingly obtained through the calculations which were depicted in Figure 10. After structure optimization the main axis of the tube has become x-axis instead of z-axis, on the other hand the porphyrin ring is aligned on y-axis, tilted towards the right direction, with angle equal 13 ° with the main axis of the tube indicating that porphyrin alignment on the tube surface has been affected by the handedness chirality of SWNT as demonstrated in Fig. 10b. Additionally the porphyrin molecule was bent towards the tube surface (with intermolecular distance $d_{\mathbf{SWNT/Por.}}$ = 0.3 nm) taking chips shaped like structure or saddle structure (Fig. 10a).

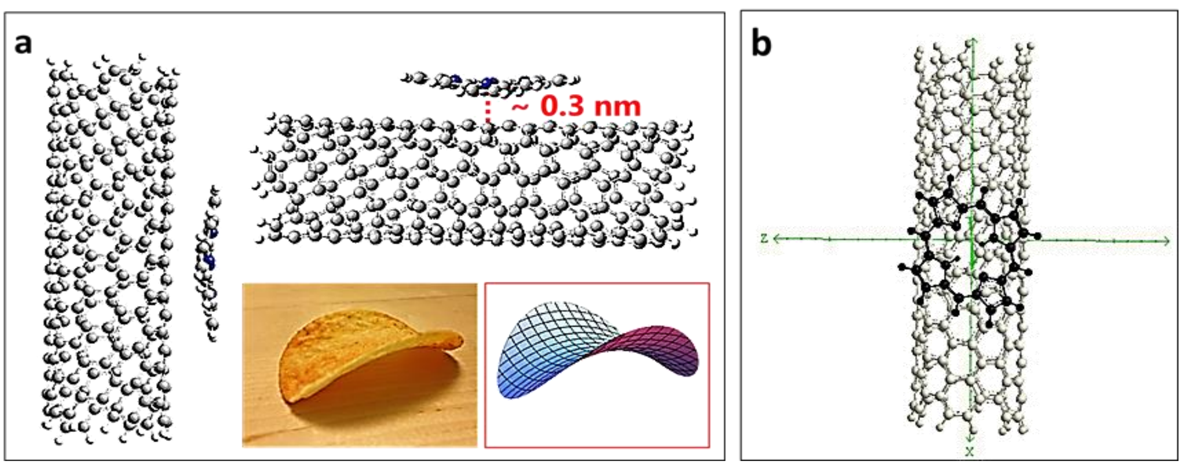

Figure 10. Optimized geometric structure obtained for the non-covalent interaction of ***P***-(6,5) SWNT / porphyrin complex. **a**, The porphyrin molecule was bent towards the tube surface (with intermolecular distance $d_{SWNT/Por.}$ = 0.3 nm) taking chips shaped like structure.

b, After structure optimization the main axis of the tube has become x-axis instead of z-axis, and the porphyrin ring was tilted by angle equal 13 ° towards the right direction, with the main axis of the tube.

For consideration which model (Type *I*, *II* or *III*) is the most appropriate for C12P molecule to be aligned on SWNT surface and also to clarify SWNT/C12P interaction mechanism, we deducted that C12P molecules should be aligned near to the lattice vector *I* (Type *I*) presented in Fig. 8a as they are some evidences for that i.e. firstly in this model (Type *I*) C12P molecules with its alkyl chains are lying flatly and typically oriented towards the right and left directions showing the substantial SWNTs handedness chirality effect which almost matching with experimental results. Secondly there is a quite agreement between the calculated angle (mathematically) in between the main axis of the tube and [100] lattice direction (lattice vector *I*) which equals 3 ° (Fig. 8d) and the calculated angle (from DFT calculations) made with the principle axis of the CNTs, by which porphyrin molecules are aligned on the tube surface which equals around 13 ° (Fig. 10b), and the experimentally measured angle of C12P with [100] lattice direction on HOPG surface (Fig. 7) which equals 4 °, consequently C12P molecules probably can be aligned near to [100] direction on SWNT surface obeying to Groszek model (Fig. 6 and 7) with a little bit deviation due to the interaction between the porphyrin cores and the SWNT curved surface.

Therefore once the alkyl chains are physisorbed and hence closely packed linearly and flatly on the basal plane of graphite or SWNT surfaces, leading to that all the inner methylene (CH_2) groups face each other in order to maximize the interdigitation of the alkyl chains, this is will be very helpful in their lateral interaction in order to improve the structure stabilization. Accordingly, C12P molecules can form a well-ordered supramolecular structure on the basal plane of SWNT surfaces that minutely maintains the Grozsek geometry with a little bit deviation.

2.4. Conclusion

In conclusion by using STM imaging technique and DFT calculations; the handedness chirality of single-walled carbon nanotubes (SWNT) has been successfully investigated for the first time. This is can be achieved using the supramolecular chemistry of some porphyrin derivatives i.e. 5,15-bisdodecylporphyrin (C12P) on the tube surface. Surprisingly, by using two different types of chiral SWNTs (right handed ***P*** or plus SWNT and left handed ***M*** or minus SWNT); two opposite supramolecular structures have been observed showing the marvelous effect of SWNT handedness chirality on the alignment of organic molecules on its surfaces. Based on our results, it has been found that alkyl chain substituted porphyrins can form a well-ordered supramolecular structure on the basal plane of SWNT surfaces that minutely maintains the Grozsek geometry with a little bit deviation. This vital finding explicate that SWNTs handedness chirality plays a crucial role for the molecular orientation of organic molecules on its surface. Moreover, this gorgeous finding effectively will identify directly the absolute handedness chirality of SWNT, and being as key point for further understanding and building new supramolecular architectures on curved nanocarbon surfaces, as well as can be used for designing and fabricating novel molecular architectonics of porphyrin / SWNTs based devices.

References

1 Wilder, J. W., Venema, L. C., Rinzler, A. G., Smalley, R. E. & Dekker, C. Electronic structure of atomically resolved carbon nanotubes. *Nature* **391**, 59-62 (1998).

2 Saito, R., Fujita, M., Dresselhaus, G. & Dresselhaus, u. M. Electronic structure of chiral graphene tubules. *Applied physics letters* **60**, 2204-2206 (1992).

3 Kataura, H. *et al.* Optical properties of single-wall carbon nanotubes. *Synthetic metals* **103**, 2555-2558 (1999).

4 Nanot, S., Hároz, E. H., Kim, J. H., Hauge, R. H. & Kono, J. Optoelectronic Properties of Single- Wall Carbon Nanotubes. *Advanced Materials* **24**, 4977-4994 (2012).

5 Barlow, S. M. & Raval, R. Complex organic molecules at metal surfaces: bonding, organisation and chirality. *Surface Science Reports* **50**, 201-341 (2003).

6 Komatsu, N. Stereochemistry of carbon nanotubes. *Japanese Journal of Applied Physics* **49**, 02BC01 (2010).

7 Liu, G. *et al.* Simultaneous discrimination of diameter, handedness, and metallicity of single-walled carbon nanotubes with chiral diporphyrin nanocalipers. *Journal of the American Chemical Society* **135**, 4805-4814 (2013).

8 Wang, F., Matsuda, K., Rahman, A. M., Kimura, T. & Komatsu, N. Improved selectivity in discriminating handedness and diameter of single-walled carbon nanotubes with N-substituted 3, 6-carbazolylene-bridged chiral diporphyrin nanotweezers. *Nanoscale* **3**, 4117-4124 (2011).

9 Groszek, A. in *Proceedings of the Royal Society of London A: Mathematical, Physical and Engineering Sciences.* 473-498 (The Royal Society).

10 Tanaka, H., Yajima, T., Kawao, M. & Ogawa, T. Electronic properties of a single-walled carbon nanotube/150mer-porphyrin system measured by point-contact current imaging atomic force microscopy. *Journal of nanoscience and nanotechnology* **6**, 1644-1648 (2006).

11 Tanaka, H., Yajima, T., Matsumoto, T., Otsuka, Y. & Ogawa, T. Porphyrin Molecular Nanodevices Wired Using Single- Walled Carbon Nanotubes. *Advanced Materials* **18**, 1411-1415 (2006).

12 Fitzgerald, C. NanoScope Command Reference Manual, version 5.12, revision B; Digital Instruments/Veeco Metrology Group, Inc.: Santa Barbara, CA. 2001. 52.

13 Handayani, M., Gohda, S., Tanaka, D. & Ogawa, T. Design and Synthesis of Perpendicularly Connected Metal Porphyrin–Imide Dyads for Two- Terminal Wired Single Molecular Diodes. *Chemistry–A European Journal* **20**, 7655-7664 (2014).

14 Littler, B. J. *et al.* Refined synthesis of 5-substituted dipyrromethanes. *The Journal of Organic Chemistry* **64**, 1391-1396 (1999).

15 Katsonis, N. *et al.* Self-Organized Monolayer of m eso-Tetradodecylporphyrin Coordinated to Au (111). *Journal of the American Chemical Society* **128**, 15537-15541 (2006).

16 Visser, J., Katsonis, N., Vicario, J. & Feringa, B. L. Two-dimensional molecular patterning by surface-enhanced zn-porphyrin coordination. *Langmuir* **25**, 5980-5985 (2009).
17 Plamont, R. *et al.* Nanoscopic Imaging of meso- Tetraalkylporphyrins Prepared in High Yields Enabled by Montmorrilonite K10 and 3 Å Molecular Sieves. *Chemistry–A European Journal* **19**, 11293-11300 (2013).
18 Li, M. *et al.* Conformation-Dependent Stacking Behavior of Porphyrin Assemblies Observed by Using Scanning Tunneling Microscopy. *The Journal of Physical Chemistry C* **114**, 1881-1884 (2010).
19 Buchner, F. *et al.* Chemical fingerprints of large organic molecules in scanning tunneling microscopy: imaging adsorbate− substrate coupling of metalloporphyrins. *The Journal of Physical Chemistry C* **113**, 16450-16457 (2009).
20 Rabe, J. P. & Buchholz, S. Commensurability and mobility in two-dimensional molecular patterns on graphite. *Science* **253**, 424-427 (1991).
21 Bléger, D. *et al.* An optimized alkyl chain-based binding motif for 2D self-assembly: a comprehensive crystallographic approach. *Nanoscale* **5**, 1452-1455 (2013).
22 Rabe, J. P. & Buchholz, S. Direct observation of molecular structure and dynamics at the interface between a solid wall and an organic solution by scanning tunneling microscopy. *Physical review letters* **66**, 2096 (1991).
23 Buchholz, S. & Rabe, J. P. Molecular imaging of alkanol monolayers on graphite. *Angewandte Chemie International Edition in English* **31**, 189-191 (1992).
24 Claypool, C. L., Faglioni, F., Goddard, W. A. & Lewis, N. S. Tunneling Mechanism Implications from an STM Study of H3C (CH2) 15HC C CH (CH2) 15CH3 on Graphite and C14H29OH on MoS2. *The Journal of Physical Chemistry B* **103**, 7077-7080 (1999).
25 Gaussian09, R. A. 1, MJ Frisch, GW Trucks, HB Schlegel, GE Scuseria, MA Robb, JR Cheeseman, G. Scalmani, V. Barone, B. Mennucci, GA Petersson et al., Gaussian. *Inc., Wallingford CT* (2009).
26 Rodríguez-Galván, A., Amelines-Sarria, O., Rivera, M., Carreón-Castro, M. d. P. & Basiuk, V. A. Adsorption and Self-assembly of Anticancer Antibiotic Doxorubicin on Single-Walled Carbon Nanotubes. *NANO* (2015).
27 Zhao, Y., Schultz, N. E. & Truhlar, D. G. Design of density functionals by combining the method of constraint satisfaction with parametrization for thermochemistry, thermochemical kinetics, and noncovalent interactions. *Journal of Chemical Theory and Computation* **2**, 364-382 (2006).
28 Basiuk, E. V., Basiuk, V. A., Santiago, P. & Puente-Lee, I. Noncovalent functionalization of carbon nanotubes with porphyrins: meso-tetraphenylporphine and its transition metal complexes. *Journal of nanoscience and nanotechnology* **7**, 1530-1538 (2007).
29 Basiuk, V. A. & Bassiouk, M. Nanoassembly of meso-tetraphenylporphines on surfaces of carbon materials: initial steps as studied by molecular mechanics and scanning tunneling microscopy. *Journal of nanoscience and nanotechnology* **8**, 259-267 (2008).

30 Basiuk, V. A., Kolokoltsev, Y. & Amelines-Sarria, O. Noncovalent interaction of meso-tetraphenylporphine with C60 fullerene as studied by several DFT methods. *Journal of nanoscience and nanotechnology* **11**, 5519-5525 (2011).

31 Orellana, W. & Correa, J. D. Noncovalent functionalization of carbon nanotubes and graphene with tetraphenylporphyrins: stability and optical properties from ab initio calculations. *Journal of Materials Science* **50**, 898-905 (2015).

Chapter III. Supramolecular Structure of Different Metal Center Porphyrins on Single Walled Carbon Nanotube (SWNT) Surface.

3.1. Introduction

The term molecular electronics is describing the field in which single molecules, small group of molecules or nanoscale objects can be utilized to perform electronic functions as the main active components in the electronic devices[1,2]. There is a wide variety of molecular building blocks , which can be used for the fabrication of electronic components .i.e. molecules, nanoparticles, nanotubes and nanowires to form new devices and circuit architectures[3]. These molecular building blocks can be designed and/or assembled in such a way that they have properties which resemble traditional electronic components i.e. wire, transistor, rectifier, memory and switch. By emerging the properties inherent in single molecule components for fabricating a functional device; this will offer unlimited possibilities for technological development because the potentially diverse electronic functions of the component molecules[4].

Accordingly since Aviram and Ratner's proposal, the molecular electronics field (occasionally also referred as moletronics[5]) has significantly expanded and attracted interest of many researchers[6-11]. Consequently numerous models of single molecule electronic devices have been actively designed and developed with a wide range of characteristic functions including diodes[12-15], memories[16-18], switches[19-23], logic gates[24-27], negative differential resistance[28], transistors[29-31] and wires[32].

Since the main subject-matter in molecular electronics is the concept of size decreasing offered by molecular level control of properties even by individual molecules or by the use of small ensembles as functional building blocks in electronic device; it is well known that solid-state devices are fabricated from the "top-down" approach which utilizes an assortment of sophisticated lithographic techniques in order to pattern a substrate and this approach has become increasingly challenging as feature size decreases. On the other hand, the molecules are synthesized and designed from "bottom-up" approach that emerges small structures from the atomic, molecular, or single device level which offers a very precise design of atoms and molecules with specific and significant functionalities.

When compared to the traditional inorganic materials i.e. silicon; organic semiconductors molecules (like π-conjugated organic molecules and polymers) have a very unique advantages and properties such as their low cost, low-temperature processing on flexible substrates, high-speed fabrication and tunable electronic properties. Furthermore, single molecules provide ideal systems to investigate charge transport on the molecular scale. In addition by using the chemical synthesis, very interesting devices and promising collections can be obtained such as nanocarbon materials / molecular junctions. Moreover, by using the physical and electronic properties of organic molecules designed by synthetic methods, chemical engineering can bring a novel dimensions in design flexibility that doesn't existent in typical inorganic electronic materials. Finally, the amalgamation of molecules and other nanoscale structures has led to a number of demonstrations of new and potentially useful applications. All of these aspects render single molecules a promising candidate for the next generation of electronics, so this is where the richness of molecular electronics emerges[1,4,33].

Since porphyrins can show promising physical and optoelectronic properties; so they can be utilized in many fantastic applications i.e. enzymes simulation, catalysis, solar cells fabrication and energy conversion, light harvesting and molecular electronics applications. Focusing on the latter type of applications; as porphyrins have a characteristic, reversible and rich redox chemistry which enhances employ as switches, wires, junctions, transistors and photodiodes. The physical and electronic properties of porphyrins are controlled by the substituents which can bind to β - and/or *meso*- positions, and also by the type of metal ions which can be incorporated inside the porphyrin macrocycle. As divalent ligands, porphyrins can be coordinated with almost every metal in the periodic table, which leads to further modification and enhancement the optoelectronic properties of porphyrins[34,35].

As they possess adaptable photonic properties, high stability, and synthesis availability, porphyrins and its related materials are highly recommended to be used as main components of organic light emitting devices, sensors, solar cells, and photocatalysts. There are two common ways through which porphyrins can be organized onto material surfaces; the first one in which the porphyrin active molecules can be covalently attached to the surface via well-established surface chemistries, this way is known as self-assembled monolayers (SAMs). In the second way porphyrins can be self-organized giving two dimensional arrays and/or layers via non-covalent adsorption onto surfaces. In the two cases, the molecular structure, surface chemistry and energetics are playing essential roles in the fabrication and organization of the final photonic materials[34,35].

Due to their adorable and remarkable properties i.e. high surface area, chemical stability, unique electronic and physical properties, high electrical and thermal conductivity, carbon nanotubes (CNTs) are being used in a wide potential applications in many fields for instance, nano-electronics, micro-electronics, molecular electronics, optoelectronics, sensors, energy storage materials, gas storage materials, catalysis, polymer reinforcements, composite materials, nano-biotechnology, and nano-medicine. Consequently, they become one of the most attractive materials in the field of nanotechnology[36-39].

CNTs can be functionalized mainly by two broad approaches, covalent and non-covalent (supramolecular chemistry) (Fig. 13 in chapter 1). Although, covalent functionalization of CNTs has been widely investigated and yield a wide variety of modified nanotube structures conjugated with both small molecules and polymers, but some covalently modified-SWNTs aren't suitable to be used in some applications which based on the high conductivity or mechanical strength of SWNTs. This is because the covalent functionalization strategy significantly disorganizes the conjugated pi-system of the CNT; consequently, result in spectacular alternations in its electronic and structural properties. On the other hand, the non-covalent functionalization includes molecular adsorption on the tube surface via pi-stacking or Van der Waals interactions with pi-conjugated sidewall of the tube. As a result, this strategy can maintain both the electronic and structural impartiality of SWNTs, allowing the employ of both conductivity and strength properties in definitive application, and this is the richness and power of supramolecular approach[40].

However, supramolecular structure assembles of porphyrins on flat nanocarbon surfaces like HOPG[41-46] or on other metallic surfaces[47-52] have attracted much more attentions; but supramolecular structures on curved surfaces like carbon nanotubes are still challenging to predict or to understand; although many research groups have focused on porphyrin / SWNTs complex even covalently[53-55], noncovalently[40,56-68], assembling of ordered protonated porphyrin driven by SWNTs[69], forming nanohybrid for detecting volatile organic compounds[70] as well as dispersion and solubilization of SWNTs[40,58].

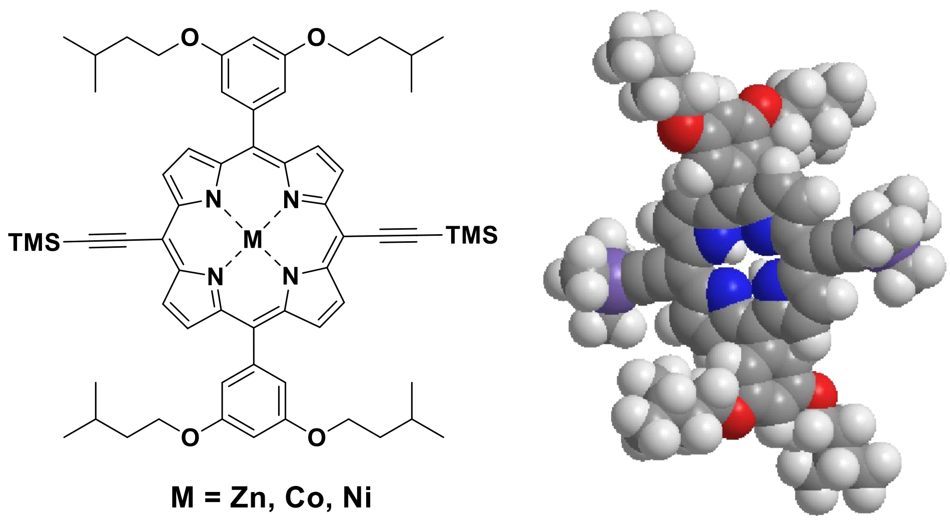

Figure 1. Chemical Structure of 5,15-bis(3,5-bis(isopentyloxyphenyl)-10,20-bistrimethylsilylethynylporphinato] with different metal centers i.e. Zn, Co, and Ni.

In this chapter we synthesized some porphyrins with different central metals i.e. Zn, Co and Ni (Figure 1) with the aim to observe their supramolecular structures on SWNTs (curved nanocarbon) surface using STM measuments, as well as display the effect of different metal centers on the supramolecular structures of porphyrins on SWNT surface. The porphyrin / SWNT complexes have been characterized using UV-Visible spectroscopy, high resolution transmission electron microscopy (HR-TEM) and DFT theoretical calculations.

3.2. Experimental

All the reactions were performed in anhydrous solvents under nitrogen atmosphere using well-dried glasswares in an oven at 90 ^{o}C before using. All the metal porphyrin were synthesized under dark conditions. All the solvents i.e. dichloromethane, chloroform and hexane were dried and distilled using molecular sieves 4 Å. Column chromatography was performed using silica-gel (spherical, neutral, 63-200 µm, Kishida Chemicals Co., Ltd.). HOPG was purchased from Alliance Biosystems, Inc. (Spi - 1 Grade 7×7×1 mm). 1-Tetradecane was obtained from Aldrich with a grade (99%) and used as it is. Other chemicals and solvents were of reagent grade and used without any further purification. ^{1}H NMR was carried out on a JEOL 400 and 500 MHz NMR spectrometers. Chemical shifts were given by ppm and all the signals were adjusted using tetramethylsilane (TMS) as an internal standard. Mass spectra were recorded using a Shimadzu AXIMA-CFR MALDI-TOF mass spectrometer. UV/Visible adsorption spectra were recorded on a Shimadzu UV-3150 double-beam spectrophotometer.

STM observation has been done using BRUKER multimode 8 SPM with a special cell for solid - liquid measuments has been used. All the STM images were carried out in a constant current mode under the ambient conditions. The STM tips were mechanically cut and formed from Pt / Ir (80 / 20 %) wire (0.25 mm in diameter). Supramolecular structures of metal porphyrin / SWNT composite samples were prepared using simple drop casting technique and then left to dry at room temperature to be ready for observation. Image calibration (flattening to correct the tilting effect of the substrate, low-pass-filtration to remove high-frequency noise) and unit cell parameter detection were achieved using NanoScope analysis softwares[71].

Synthesis of Compounds

The target molecules have been synthesized using our previously reported scheme[72] with slight modification, which displayed in scheme 1.

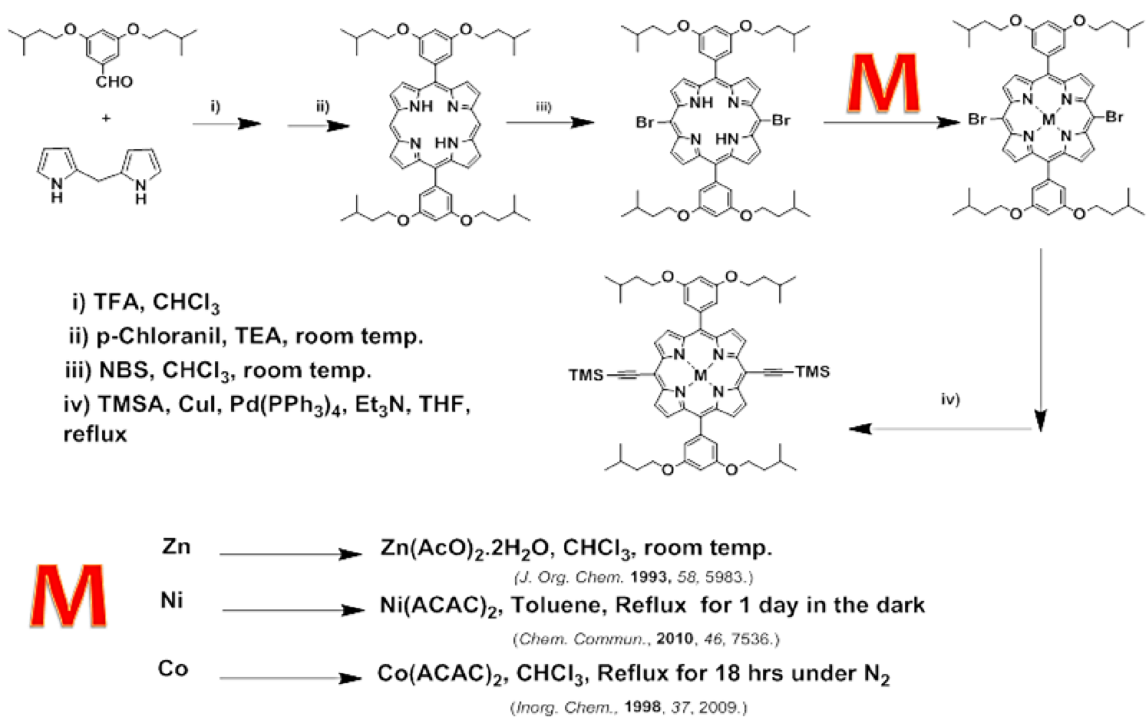

Scheme 1. Procedures for synthesizing 5,15-bis(3,5-bis(isopentyloxyphenyl)-10,20 bistrimethylsilylethynylporphinato] with different central metals i.e. Zn, Ni and Co.

5,15-bis(3,5-bis(isopentyloxy)phenyl)porphyrin (1)

Porphyrin **1** has been synthesized by acid-catalyzed condensation of benzaldehyde, by dissolving 3,5-bis(isopentyloxy)benzaldehyde (1.0934 g, 3.928 mmol) and dipyrromethane

(0.5746 g, 3.931 mmol) in dry $CHCl_3$ (570 mL), then the mixture has been stirred under N_2 gas at room temperature for 24 h in dark conditions. Afterward the resulting solution was quenched with triethylamine (0.5 mL), following by adding (0.5587 g, 2.272 mmol) of *p*-chloranil as an oxidizing agent and continuing stirring for additional 3 h under the same conditions. The solution was concentrated via evaporating the solvent under vacuum and the residue was purified using column chromatography (silica gel, $CHCl_3$: hexane = 70 : 30). After evaporating the solvent, solid purple compound was obtained and purified again using recrystallization with $CHCl_3$/excess MeOH, giving pure red purple powder (0.491 g, 31 %) yield. ^1H NMR (500 MHz, $CDCl_3$, 25 ^oC, TMS): δ 10.30 (s, 2H, *meso*-H), 9.38 (d, 4H, β-pyrrole-H), 9.19 (d, 4H, β-pyrrole-H), 7.43 (s, 4H, benzene CH), 6.92 (s, 2H, benzene CH), 4.19 (t, 8H, CH_2), 1.89 (m, 4H, CH_2), 1.79 (q, 8H, CH), 0.99 (d, 24H, CH_3), -3.15 ppm (s, 2H, NH). UV/Vis. ($CHCl_3$): λ_{max}= 410, 504, 535, 577, 632 nm. MS (MALDI-TOF) *m/z* for $C_{52}H_{62}N_4O_4$, $[M^+]$ calcd, 807.09; found $[M^+ + H^+]$, 808.1

5,15-bis(3,5-bis(isopentyloxyphenyl)-10,20-dibromoporphyrin (2)

N-Bromosuccinimide (0.044 g, 0.247 mmol) was dissolved in $CHCl_3$ (200 mL) and the solution was added dropwise to 5,15-bis(3,5-bis(isopentyloxy)phenyl)porphyrin **1** solution (0.1003 g, 0.124 mmol) in $CHCl_3$, then the mixture was stirred at room temperature for 1 h in dark conditions. After evaporating the solvent, the residue was purified using column chromatography (silica gel, $CHCl_3$: hexane = 60 : 40) followed by recrystallization with $CHCl_3$/excess MeOH, giving pure red purple powder (0.100 g, 84 %) yield. ^1H NMR (500 MHz, $CDCl_3$, 25 ^oC, TMS): δ 9.60 (d, 4H, β-pyrrole-H), 8.98 (d, 4H, β-pyrrole-H), 7.36 (s, 4H, benzene CH), 6.93 (s, 2H, benzene CH), 4.20 (t, 8H, CH_2), 1.90 (m, 4H, CH_2), 1.80 (q, 8H, CH), 1.01 (d, 24H, CH_3), -2.72 ppm (s, 2H, NH). UV/Vis. ($CHCl_3$): λ_{max}= 425, 520, 558, 601, 661 nm. MS (MALDI-TOF) *m/z* for $C_{52}H_{60}N_4O_4Br_2$, [M^+] calcd, 964.88; found [$M^+ + H^+$], 965.5

[5,15-bis(3,5-bis(isopentyloxyphenyl)-10,20-dibromo-porphinato]zinc(II) (3)

Zinc porphyrin **3** has been synthesized using reported method[73] in which $Zn(OAc)_2.2H_2O$ (1.9639 g, 8.9443 mmol) was dissolved in MeOH (100 mL) and the solution was added dropwise to 5,15-bis(3,5-bis(isopentyloxyphenyl)-10,20-dibromoporphyrin **2** solution (0.4325 g, 0.4482 mmol) in $CHCl_3$, then the mixture was stirred at room temperature for 4 h in dark conditions. The resulting solution was washed three times with water and brine solution. The crude solid has been obtained after removing the solvent under vacuum, and purified using column chromatography (silica gel, $CHCl_3$: hexane = 70 : 30) followed by recrystallization with $CHCl_3$/excess MeOH, giving pure red purple powder (0.4046 g, 88 %) yield. ^1H NMR (500 MHz, $CDCl_3$, 25 ^oC, TMS): δ 9.67 (d, 4H, β-pyrrole-H), 9.04 (d, 4H, β-pyrrole-H), 7.28 (s, 4H, benzene CH), 6.89 (s, 2H, benzene CH), 4.16 (t, 8H, CH_2), 1.87 (m, 4H, CH_2), 1.75 (q, 8H, CH), 0.94 (d, 24H, CH_3). UV/Vis. ($CHCl_3$): λ_{max}= 428, 563, 605 nm. MS (MALDI-TOF) *m/z* for $C_{52}H_{58}N_4O_4Br_2Zn$, [M^+] calcd, 1028.25; found [$M^+ + H^+$], 1029.8

5,15-bis(3,5-bis(isopentyloxyphenyl)-10,20-bistrimethylsilylethynylporphinato]zinc(II) (4)

A mixture of [5,15-bis(3,5-bis(isopentyloxyphenyl)-10,20-dibromo-porphinato]zinc (II) **3** (0.3443 g, 0.3348 mmol), CuI (0.186 g) and $Pd(PPh_3)_4$ (0.186 g) were dissolved in THF (45 mL). Then trimethylsilylacetylene (0.75 mL) and triethylamine (15 mL) were added to the solution and the reaction mixture was stirred for 24 h at 45 °C under N_2 gas in dark conditions. The solution was concentrated via evaporating the solvent under vacuum and the residue was purified using column chromatography (silica gel, $CHCl_3$: hexane = 70 : 30) giving pure blue purple powder (0.3537 g, ~100 %) yield. ^1H NMR (500 MHz, $CDCl_3$, 25 °C, TMS): δ 9.66 (d, 4H, β-pyrrole-H), 9.02 (d, 4H, β-pyrrole-H), 7.32 (s, 4H, benzene CH), 6.89 (s, 2H, benzene CH), 4.17 (t, 8H, CH_2), 1.86 (m, 4H, CH_2), 1.76 (q, 8H, CH), 0.98 (d, 24H, CH_3), 0.61 (s, 18H, CH_3). UV/Vis. ($CHCl_3$): λ_{max}= 440, 580, 632 nm. MS (MALDI-TOF) *m/z* for $C_{62}H_{76}N_4O_4Si_2Zn$, [M^+] calcd, 1062.86; found [$M^+ \pm 2H^+$], 1064.4, 1060.86

[5,15-bis(3,5-bis(isopentyloxyphenyl)-10,20-dibromo-porphinato]nickel(II) (5)

Nickel metalized porphyrin **5** was synthesized using previously reported method[74] in which a solution of 5,15-bis(3,5-bis(isopentyloxyphenyl)-10,20-dibromoporphyrin **2** (0.2945 g, 0.305 mmol) in toluene (50 mL) was refluxed with $Ni(acac)_2.2H_2O$ (0.11 g, 0.414 mmol) at 120 ° C for 1 day in dark conditions. The reaction mixture was then quenched with water (100 mL) and extracted with $CHCl_3$; the organic layer was washed three times with water, brine and dried over Na_2SO_4. After removing the solvent, the crude solid was purified by recrystallization with $CHCl_3$/ MeOH, giving pure red purple crystals (0.2870 g, yield 92 %). ^1H NMR (500 MHz, $CDCl_3$, 25 °C, TMS): δ 9.44(d, 4H, β-pyrrole-H), 8.82 (d, 4H, β-pyrrole-H), 7.09 (s, 4H, benzene CH), 6.3 (s, 2H, benzene CH), 4.11 (t, 8H, CH_2), 1.86 (m, 4H, CH_2), 1.76 (q, 8H, CH), 0.96 (d, 24H, CH_3). UV/Vis. ($CHCl_3$): λ_{max}= 432, 553, 592 nm. MS (MALDI-TOF) *m/z* for $C_{52}H_{58}N_4O_4Br_2Ni$, [M^+] calcd, 1021.56; found [$M^+ - H^+$], 1020.1

5,15-bis(3,5-bis(isopentyloxyphenyl)-10,20-bistrimethylsilylethynylporphinato] nickel(II) (6)

A mixture of [5,15-bis(3,5-bis(isopentyloxyphenyl)-10,20-dibromo-porphinato]nickel (II) **5** (0.2870 g, 0.2809 mmol), CuI (0.166 g) and $Pd(PPh_3)_4$ (0.166 g) were dissolved in THF (40 mL). Then trimethylsilylacetylene (0.62 mL) and triethylamine (11 mL) were added to the solution and the reaction mixture was stirred for 24 h at 45 °C under N_2 gas in dark conditions. The solution was concentrated via evaporating the solvent under vacuum and the residue was purified using column chromatography (silica gel, $CHCl_3$: hexane = 70 : 30) giving pure purple crystals (0.2598 g, 88 %) yield. ^{1}H NMR (500 MHz, $CDCl_3$, 25 ^{o} C, TMS): δ 9.40 (d, 4H, β-pyrrole-H), 8.84 (d, 4H, β-pyrrole-H), 7.51 (s, 4H, benzene CH), 7.12 (s, 2H, benzene CH), 4.07 (t, 8H, CH_2), 1.86 (m, 4H, CH_2), 1.73 (q, 8H, CH), 0.98 (d, 24H, CH_3), 0.50 (s, 18H, CH_3). UV/Vis. ($CHCl_3$): λ_{max}= 432, 552, 592 nm. MS (MALDI-TOF) *m/z* for $C_{62}H_{76}N_4O_4Si_2Ni$, [M^+] calcd, 1056.18; found [M^+ - $2H^+$], 1054.6

[5,15-bis(3,5-bis(isopentyloxyphenyl)-10,20-dibromo-porphinato]cobalt(II) (7)

We synthesized cobalt metalized porphyrin **7** using previously reported method[75], in which a solution of 5,15-bis(3,5-bis(isopentyloxyphenyl)-10,20-dibromoporphyrin **2** (0.2614 g, 0.271 mmol) in $CHCl_3$ (70 mL) was refluxed with $Co(acac)_2$ (1.01 g, 3.92 mmol) at 70 ° C for 20 h under N_2 gas in dark conditions. After removing the solvent, the crude solid was purified column chromatography (silica gel, CH_2Cl_2) followed by recrystallization with MeOH (few drops), giving pure red purple crystals (0.2546 g, yield 92 %). ^{1}H NMR (500 MHz, $CDCl_3$, 25 ^{o} C, TMS): δ 16.23 (*broad* d, 4H, β-pyrrole-H), 15.38 (*broad* d, 4H, β-pyrrole-H), 11.88 (*broad* s, 4H, benzene CH), 8.68 (s, 2H, benzene

CH), 5.26 (t, 8H, CH_2), 3.44 (m, 4H, CH_2), 2.31 (q, 8H, CH), 1.12 (d, 24H, CH_3). UV/Vis. ($CHCl_3$): λ_{max}= 416, 535 nm. MS (MALDI-TOF) *m/z* for $C_{52}H_{58}N_4O_4Br_2Co$, [M^+] calcd, 1021.80; found [$M^+ \pm H^+$], 1020.9, 1022.9

5,15-bis(3,5-bis(isopentyloxyphenyl)-10,20-bistrimethylsilylethynylporphinato] cobalt(II) (8)

A mixture of [5,15-bis(3,5-bis(isopentyloxyphenyl)-10,20-dibromo-porphinato]cobalt (II) **7** (0.2546 g, 0.2491 mmol), CuI (0.15 g) and $Pd(PPh_3)_4$ (0.15 g) were dissolved in THF (40 mL). Then trimethylsilylacetylene (0.56 mL) and triethylamine (10 mL) were added to the solution and the reaction mixture was stirred for 24 h at 45 °C under N_2 gas in dark conditions. The solution was concentrated via evaporating the solvent under vacuum and the residue was purified using column chromatography (silica gel, $CHCl_3$: hexane = 70 : 30) followed by recrystallization with MeOH (few drops), giving pure purple crystals (0.2518 g, 96 %) yield. ^1H NMR (500 MHz, $CDCl_3$, 25 °C, TMS): δ 16.47 (*broad* d, 4H, β-pyrrole-H), 15.88 (*broad* d, 4H, β-pyrrole-H), 12.21 (*broad* s, 4H, benzene CH), 8.81 (s, 2H, benzene CH), 5.28 (t, 8H, CH_2), 2.39 (m, 4H, CH_2), 2.19 (q, 8H, CH), 1.55 (d, 24H, CH_3), 1.18 (s, 18H, CH_3). UV/Vis. ($CHCl_3$): λ_{max}= 430, 552, 592 nm. MS (MALDI-TOF) *m/z* for $C_{62}H_{76}N_4O_4Si_2Co$, [M^+] calcd, 1056.42; found [M^+], 1056

Purification of SWNT

Since we used in this chapter raw SWNT (HiPCO™, Carbon Nanotechnologies), so we purified it using some reported procedures which have described elsewhere[68,76] with slight modification, which depicted in scheme 2. In this method, SWNTs firstly have been heated at 200 °C (for removing the amorphous carbons), sonicated in concentrated hydrochloric acid for a few minutes followed by refluxing with conc. HCl at 105 °C for 1 h in order to remove the metal catalysts i.e. Fe. The tubes were then collected using filter membrane and washed with aqueous solution of $NaHCO_3$ to neutralize it (pH was being checked during the washing process). Finally SWNTs were dried at 50 °C overnight giving purified SWNTs (p-SWNTs).

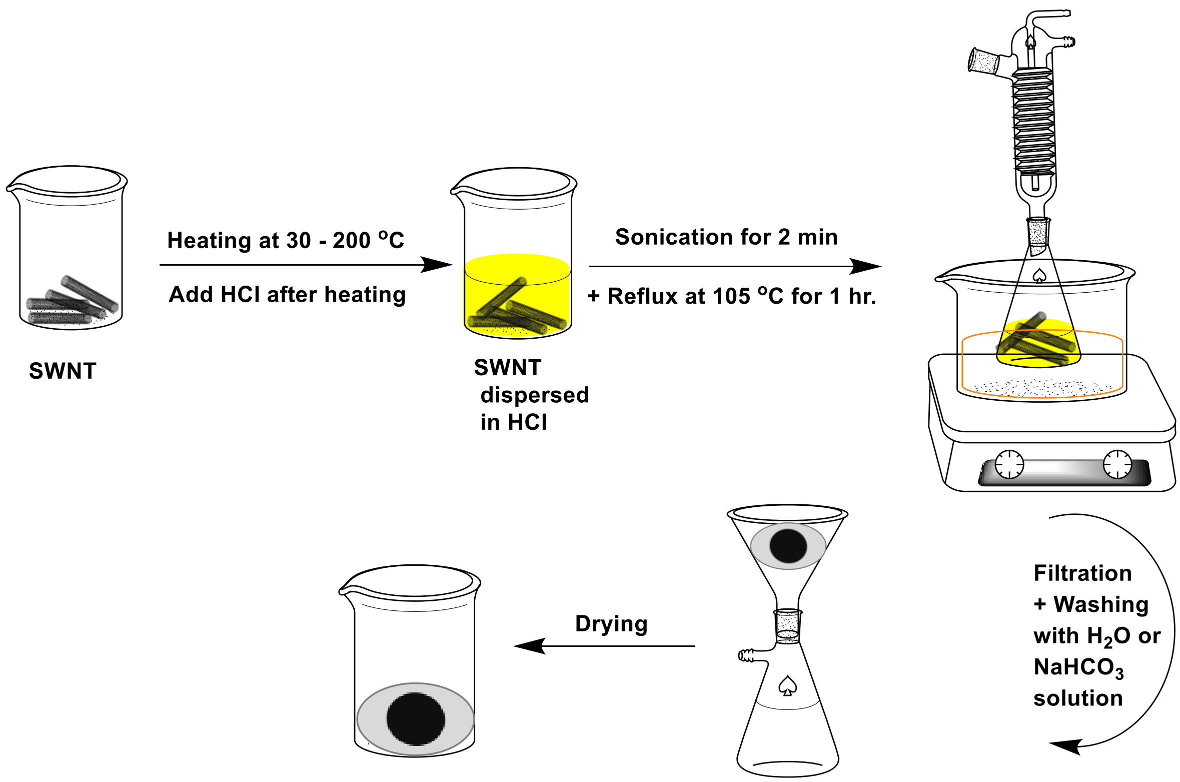

Scheme 2. HiPCO SWNTs purification

Preparation of metal porphyrins / SWNTs Complexes

The metal porphyrin/SWNT complexes were fabricated as follows. After dissolving porphyrin in chloroform, the solution was submitted to ultrasonic bath for 10 min. 5 mg of HiPCO SWNTs were added to porphyrin solution and sonicated overnight. The resulting suspension was left for sedimentation for 2 h. Then the top 5 % of the supernatant was removed, and the precipitate was filtered by a membrane filter (MILLIPORE) of 0.1 μm mesh. Then rinse with 100 mL $CHCl_3$ to remove the non-adsorbed porphyrin and dried in a vacuum desiccator until further utilization, as described in scheme 2 the experimental section of chapter 2.

3.3. Results and discussion

UV-Visible Spectroscopic measuments

UV-Visible spectroscopy has been measured in order to confirm that the non-covalent interactions between the metal porphyrins and SWNTs surface have been successfully done and the complexes have been successfully prepared. Figure 2 illustrates UV-Visible spectra of pristine SWNT, ZnPor, CoPor, NiPor, ZnPor / SWNT complex, CoPor / SWNT complex and NiPor / SWNT complex.

As it is clearly shown in Fig. 2, the spectra of ZnPor / SWNT complex, CoPor / SWNT complex and NiPor / SWNT complex were shifted either for longer or shorter wavelengths, as an evidence that SWNT has been successfully functionalized by the different metal center porphyrins. Additionally one can see that the complexes spectra are including the peaks of both SWNTs and porphyrins. For ZnPor / SWNT and NiPor / SWNT, the spectra are blue shifted however the spectrum of CoPor / SWNT is red shifted; this may be attributed to formation of H-aggregates in the case of ZnPor and NiPor complexes, however CoPor formed J-aggregates on SWNTs surface therefore CoPor / SWNT spectrum is red shifted towards longer wavelength.

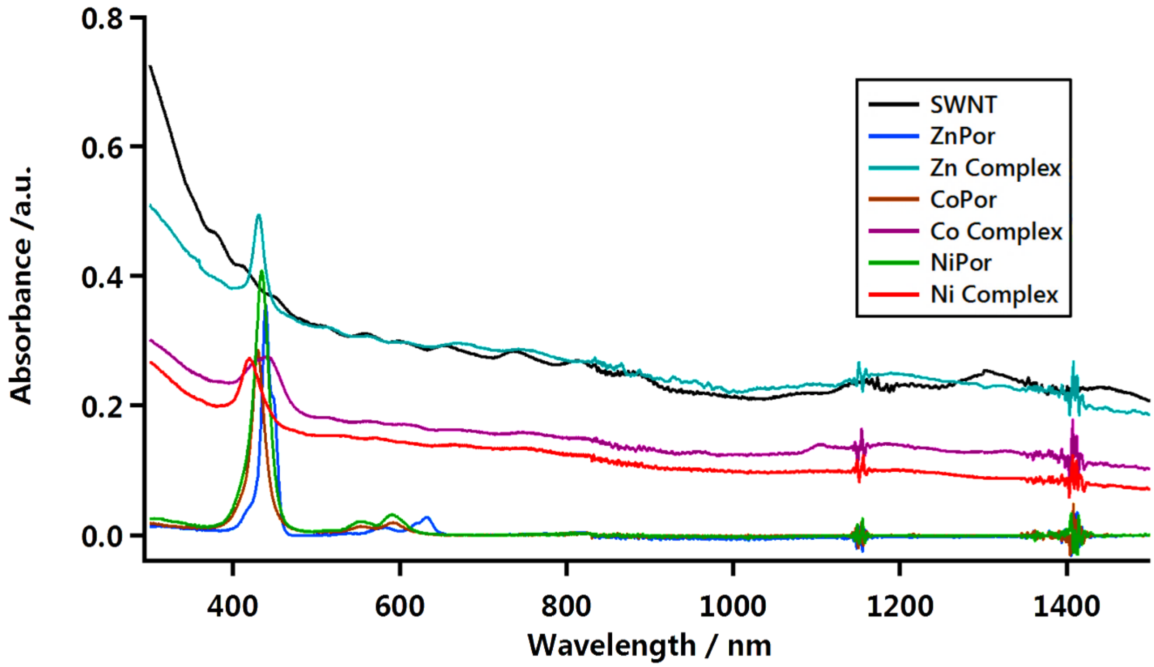

Figure 2. UV-Visible spectra of pristine SWNTs, ZnPor, CoPor, NiPor, ZnPor / SWNT complex, CoPor / SWNT complex and NiPor / SWNT complex, in $CHCl_3$.

High Resolution Transmission Electron Microscopic (HR-TEM) measuments

The HR-TEM images results of pristine SWNTs, CoPor / SWNT complex, NiPor / SWNT complex and ZnPor / SWNT complex are shown in Fig. 3. It is clearly seen in pristine SWNTs image (Fig. 3a) that they are recognized as bundles with smooth surfaces, additionally the sidewalls of the pristine SWNTs can be typically distinguished. However in Fig. 3b-d which representing CoPor, NiPor and ZnPor / SWNT complexes, respectively; the SWNTs seem apparently covered with the adsorbed porphyrin molecules which preventing the clear appearance of the tubes sidewalls. Consequently, the bundles of the complexes appear slightly denser than the pristine ones due to the accumulation of the porphyrin molecules on SWNTs surfaces via stacking interactions which led to additional agglomeration of the nanotubes. On the other hand there are also some notable debundling effects in the complex samples in Fig. 3b-d which attributed to the adsorption of porphyrin on SWNTs surface leading to more dispersed SWNTs within the same samples. Our TEM results are in a good agreement with which have been found elsewhere[77] however they used tetraphenylporphyrin (TPP).

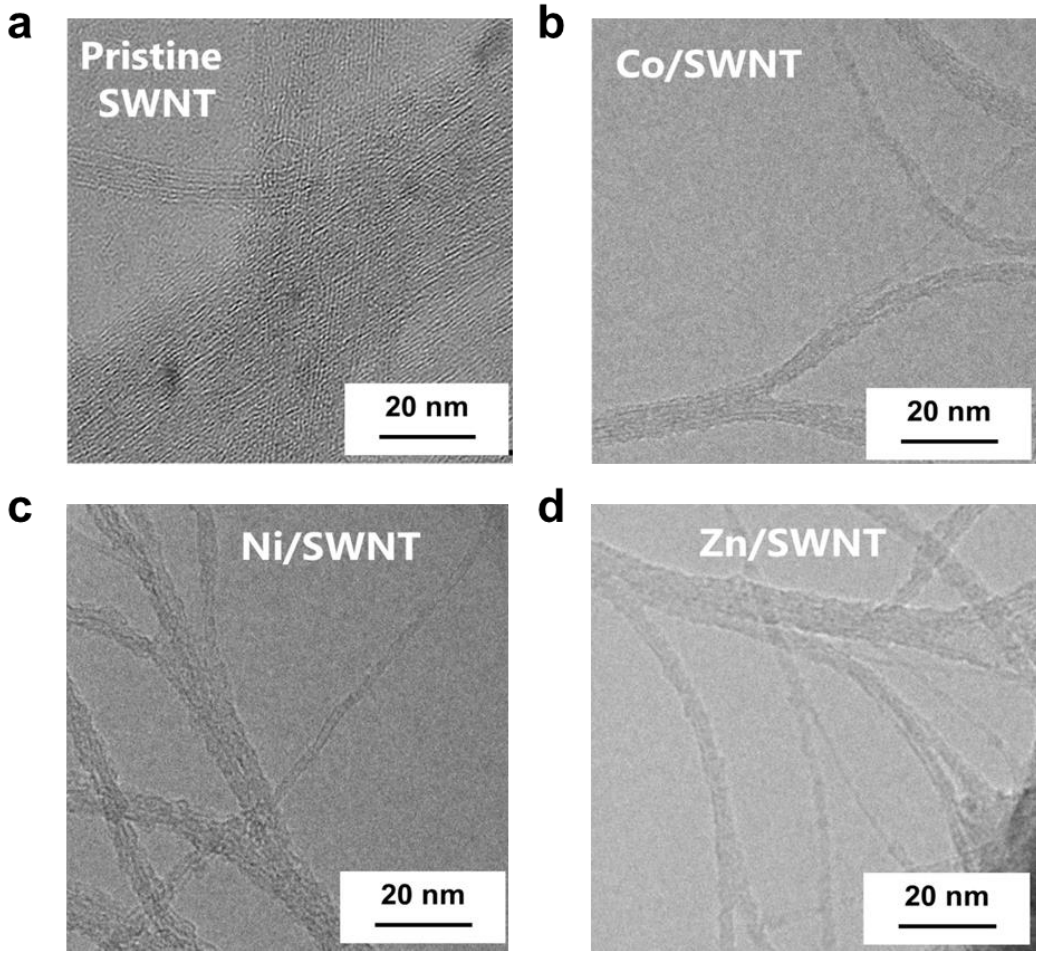

Figure 3. HR-TEM images of **a**, pristine SWNTs **b**, CoPor / SWNT complex **c**, NiPor / SWNT complex and **d**, ZnPor / SWNT complex. All images were taken at 200 KV.

Supramolecular structures of different central metal porphyrins on SWNT surface observed by STM

The supramolecular structure of porphyrin molecules have been investigated on SWNT surface using STM measuments. Prior to STM observation, small portion of the complex samples suspension was simply drop casted onto a freshly cleaved HOPG surface and left to completely dry and then introduced to the STM machine to be measured under the ambient conditions. In order to induce a tunneling current, a bias voltage was applied between the tip and sample to record images at solid-gas interface.

Since SWNT can be functionalized either covalently or non-covalently; ZnPor, CoPor and NiPor complexes with SWNTs have been formed mainly via non-covalent interactions between metalized porphyrins and SWNTs for instance π-π staking between the complex components due to the high carrier mobility of delocalized π-electrons, in addition to molecular-substrate interactions, intermolecular interactions and Vander Waals interactions i.e. porphyrin-porphyrin interaction, and alkyl chain-alkyl chain interaction.

The representative STM images which showing the supramolecular structures of ZnPor / SWNT complex, CoPor / SWNT complex and NiPor / SWNT complex are displayed in Fig. 4, in which one can see apparently that porphyrin molecules are adsorbed evidently onto SWNT surface in all the SWNT / porphyrin complexes (Fig. 4a-i).

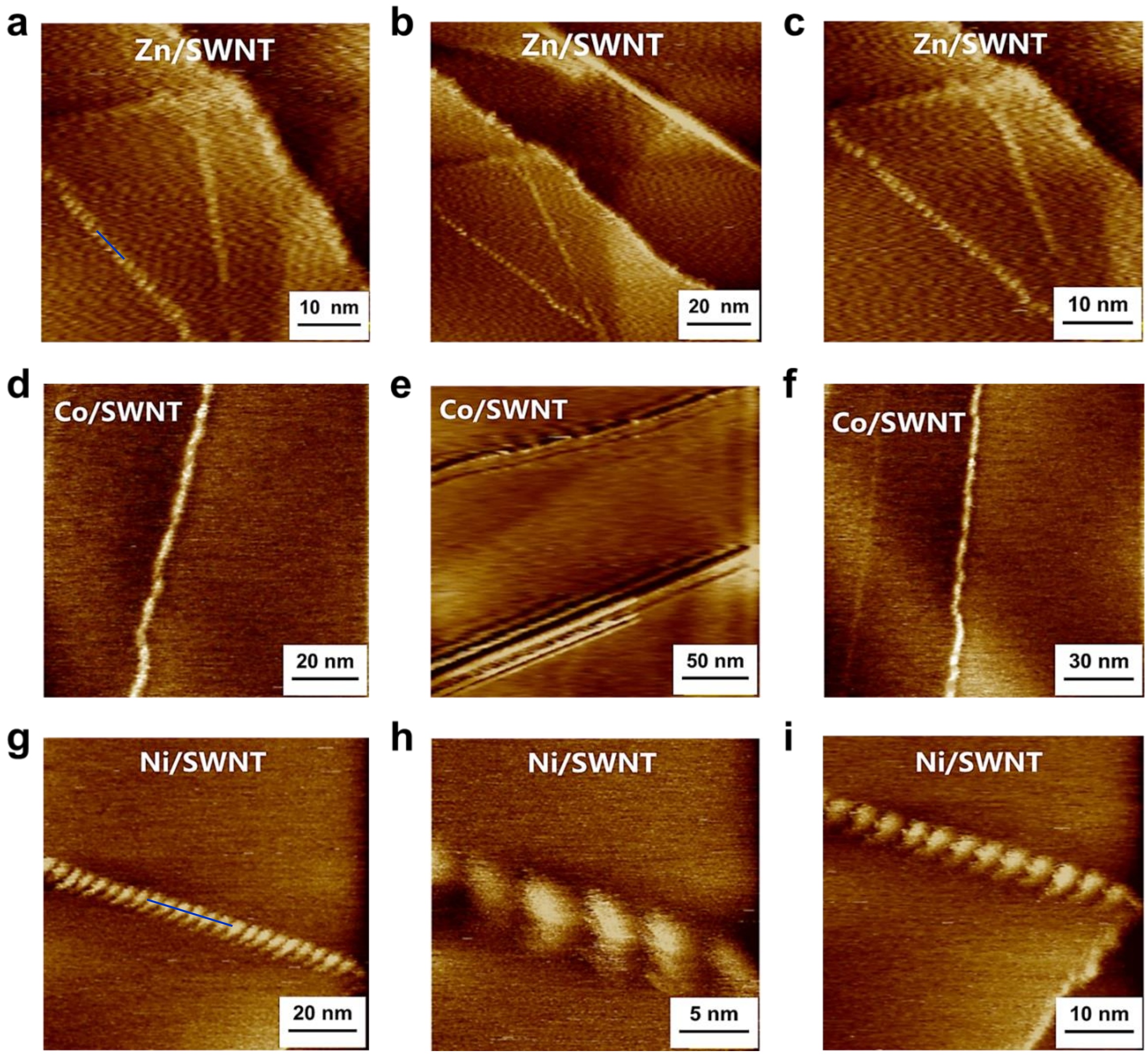

Figure 4. Typical STM images for supramolecular structures of ZnPor, CoPor and NiPor / SWNTs complexes on HOPG surface. All images were taken at V_{sample} = 0.100 V and I_t = 0.010 nA. **a**, ZnPor / SWNT complex (50 nm × 50 nm) **b**, ZnPor / SWNT complex (100 nm × 100 nm) **c**, ZnPor / SWNT complex (50 nm × 50 nm) **d**, CoPor / SWNT complex (100 nm × 100 nm) **e**, CoPor / SWNT complex (250 nm × 250 nm) **f**, CoPor / SWNT complex (150 nm × 150 nm) **g**, NiPor / SWNT complex (100 nm × 100 nm) **h**, NiPor / SWNT complex (25 nm × 25 nm) **i**, NiPor / SWNT complex (50 nm × 50 nm).

From all the STM images it is clearly shown a significant debundling effect of SWNTs due to interaction with the adsorbed porphyrins which led to highly dispersed SWNTs which are almost fully covered with the porphyrin molecules. Therefore STM imaging suggests the strong interactions between metalized porphyrins and SWNTs which expressed not only through the debundling effect, but also through the SWNTs surface full coverage.

There are different possible molecular arrangements have been observed for the metalized porphyrins on SWNTs surface, for instance in the case of ZnPor (Fig. 4a-c) the porphyrins molecules are aligned on the tube surface forming a supramolecular regular arrays interacting to each other, with a center to center distances of about 2.2 ± 0.2 nm, as it can be seen from the topographic profile in Fig. 5a which reveal the periodicity of neighboring porphyrin molecules along the axis of the tube. According to the topographic profile, the small center to center distances suggest also formation of short helix-shaped arrays.

On the other hand a notably diagonal orientation of NiPor molecules can be clearly distinguished on the tube surface (elucidated in Fig. 4g-i), with center to center distance equals about 3.8 ± 0.3 nm (Fig. 5b) which is larger than ZnPor case. This suggests that NiPor molecules formed well-ordered long helix-shaped arrays with a regular periodicity on SWNT surface stabilized with non-covalent and π-staking interactions within the neighboring porphyrin molecules. It is worth to mention that among the three metal porphyrin samples (ZnPor, NiPor and CoPor); the best STM resolution images have been observed in the case of NiPor, probably this is due to the electronegativity effect; as Ni has higher electronegative compared to Zn and Co (Zn (1.65) < Co (1.88) < Ni (1.91), Pauling scale[78]) which increases the electro-positivity of the porphyrin ring and hence increases its ability to interact with the electron rich identities i.e. CNT, therefore making the interaction stronger.

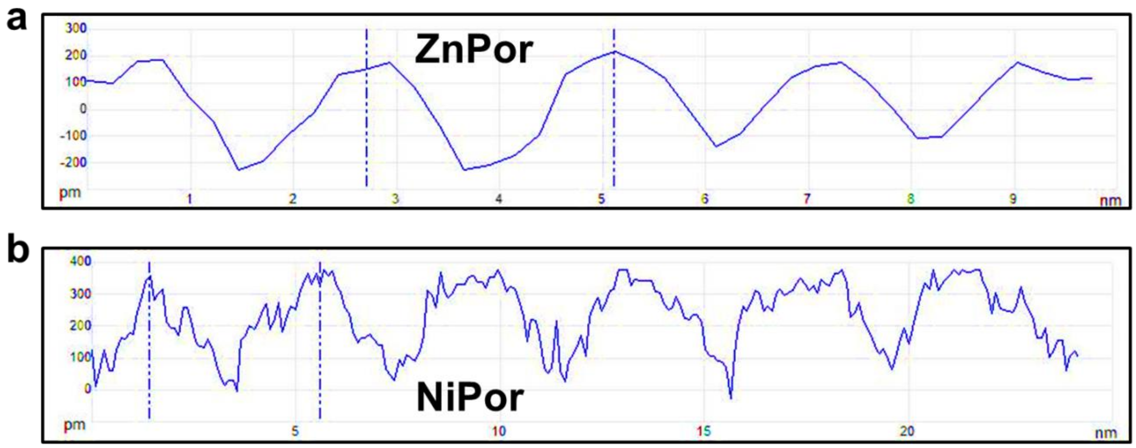

Figure 5. Topographic profiles representing the center to center distances (marking with the blue lines in Fig. 4a and 4g) for **a**, ZnPor molecules (equals about 2.2 ± 0.2 nm) and **b**, NiPor molecules (equals about 3.8 ± 0.3 nm) on SWNTs surface.

Although one can see apparently some helical structures formed by CoPor molecules on SWNTs surface (Fig. 4d and 4f), but generally CoPor molecules didn’t show regular supramolecular structures on the tube surface as in the other metal porphyrin cases (Fig. 4d-f). Furthermore an interesting extra debundling effect has been observed for CoPor molecules (Fig. 4e) which attributed not only to strong interaction with SWNTs but also because CoPor molecules are able to intercalate and considerably disperse SWNT bundles and hence adsorb onto the surface of individual SWNTs[77].

Density Functional Theory (DFT) calculations

With the purpose for identifying the effect of metalation on the supramolecular structures of porphyrins on SWNT surface from an energetic point of view, in addition to establish the stability of the formed metalized porphyrin /SWNT complexes; we performed some DFT calculations using long-range corrected functionals which involved in Gaussian 09 software[79] for instance the Minnesota functionals (M05-2X)[80,81] with 3-21G basis set which can be used in the characterization of the non-local nature of VdW interactions.

All the initial setup of these calculations has been explained in details in chapter 2 in which we used an open ended chiral ***P***- (6,5) SWNT modeling with 2.5 nm length, 0.8 nm in diameter (designed by our group) and composed of 222 carbon atoms and 22 hydrogen atoms; however for the metalized porphyrins we used porphyrin macrocycle ring which consist of 20 carbon atoms, 4 nitrogen atoms, 12 hydrogen atoms , incorporating with different metal centers i.e. Ni atom, Co atom and Zn atom, respectively.

Prior to complexes structures optimization, at first we succeed to optimize the structures of the individual components i.e. SWNT, NiPor, ZnPor and CoPor. Consequently these optimized structures have been used in the structure optimization of the porphyrins / SWNT complexes. All the calculations have been done using M05-2X / 3-21G theoretical level. The frontier molecular orbitals (HOMOs and LUMOs) and their absolute energies values in eV of ***P***-(6,5) SWNT, Ni-porphyrin, Co-porphyrin (α-shape) and Zn-porphyrin molecules are demonstrated in table 1.

	SWNT	NiPor.	CoPor. (α-shape)	ZnPor.
LUMO 3	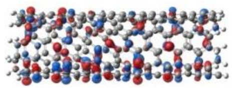 -2.12817 eV	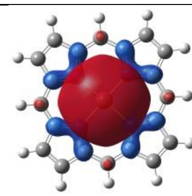 0.641907 eV	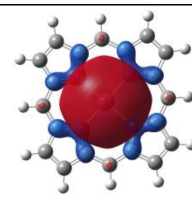 2.359466 eV	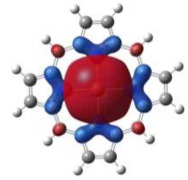 2.072118 eV
LUMO 2	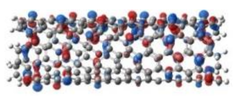 -2.17661 eV	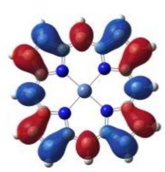 2.455249 eV	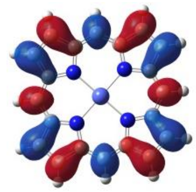 0.637554 eV	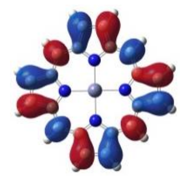 0.575241 eV
LUMO 1	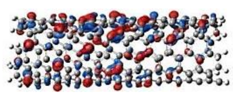 -2.69416 eV	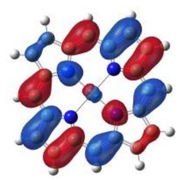 0.641907 eV	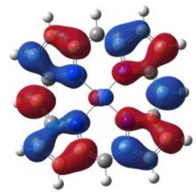 -1.44246 eV	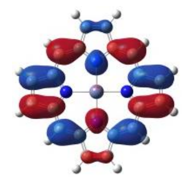 -1.5181 eV
LUMO	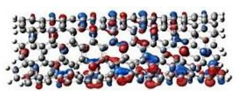 -2.73144 eV	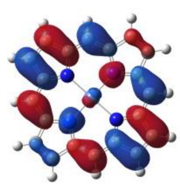 -1.46558 eV	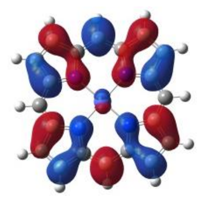 -1.44273 eV	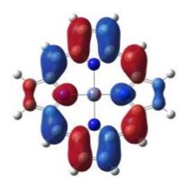 -1.51837 eV
HOMO	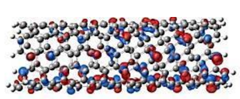 -5.78098 eV	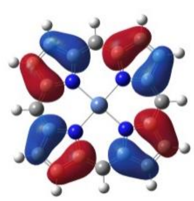 -6.27159 eV	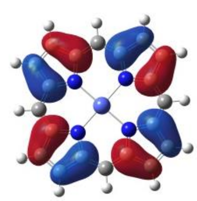 -6.25227 eV	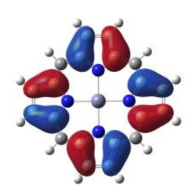 -6.26941 eV

HOMO 1	 -5.8237 eV	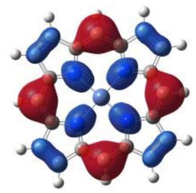 -6.47023 eV	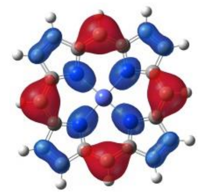 -6.4237 eV	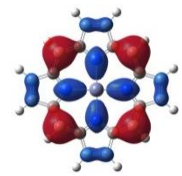 -6.37227 eV
HOMO 2	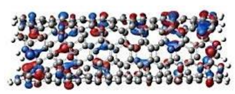 -6.30016 eV	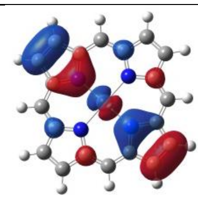 -7.7867 eV	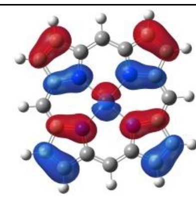 -7.63296 eV	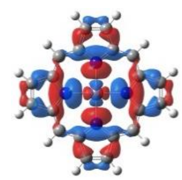 -7.63867 eV
HOMO 3	 -6.3603 eV	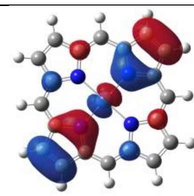 -7.78697 eV	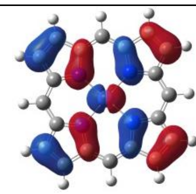 -7.63323 eV	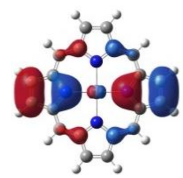 -8.26398 eV

Table 1. The frontier molecular orbitals (HOMOs and LUMOs) and their absolute energies values in eV (calculated using M05-2X/3-21G theoretical level) of ***P***-(6,5) SWNT, Ni-porphyrin, Co-porphyrin (α-shape) and Zn-porphyrin molecules, respectively.

By using the optimized structures of the individual components i.e. SWNT and metal porphyrins; the structures of their complexes have been successfully optimized. The energies of formation ($\Delta E_{complex}$) of the complexes, the HOMOs and LUMOs energies, the HOMO / LUMO gap energies and the closest distances between the metal porphyrins and SWNT surface are summarized in table 2 .

Complex	E_{HOMO} (eV)	E_{LUMO} (eV)	HOMO/LUMO energy gap (eV)	Energy of formation $\Delta E_{complex}$ (eV)	Distance between Por. and SWNT ($d_{SWNT/Por.}$) (Å)
ZnPor / SWNT	-5.66	-2.75	2.91	-1.49	3
NiPor / SWNT	-5.63	-2.69	2.94	-1.36	3.1
CoPor / SWNT	-5.66	-2.71	2.95	-1.58	3

Table 2. DFT calculations summary for ZnPor / SWNT, NiPor / SWNT and CoPor / SWNT complexes calculated using M05-2X / 321G theoretical level, including the energies of formation, HOMOs-LUMOs energies, HOMO / LUMO energies gap, the separation distance between metal porphyrin molecules and SWNT surface.

The energies of formation (binding energies) of the complexes ($\Delta E_{complex}$) were calculated using the following formula[82,83]:

$$\Delta E_{complex} = E_{complex} - (E_{SWNT} + E_{M\text{-}por})$$

where $E_{complex,}$ E_{SWNT} and E_{Mpor} are the corresponding absolute energies of the complex, SWNT and metal-porphyrin molecule, respectively. As demonstrated from the table, all the complexes displaying strong exothermal binding energies ($\Delta E_{complex}$) equal to -1.58 eV, -1.49 eV and -1.36 eV for CoPor / SWNT complex, ZnPor / SWNT complex and NiPor / SWNT complex, respectively. Among the three metal porphyrin complexes, CoPor has the lowest binding energy, which means the strongest interaction with SWNT; therefore the most stable structure can be produced. In other word, from an energetic point of view the stability of these metal porphyrins complexes with the following order Ni < Zn < Co.

Similar results have been found elsewhere[77] in which they stated that among Co, Zn and Ni-TPP; CoTPP gave the strongest interaction with SWNT as it can not only adsorbed on the tube surface but also intercalate producing very stable complex.

It worth to mention that all the complexes gave almost the same intermolecular contact distance between the porphyrin and SWNT surface which equal around 3.1 Å, which is very similar to the distance obtained for tetraphenylporphyrin (TPP) /C_{60} system[84] which is 3 Å and with TPP/SWNT system[85] which is $3.0 \leq d \leq 3.3$ Å. Furthermore, the porphyrin ring was bent towards the tube surface taking chips shaped like structure or saddle structure (Fig. 6)

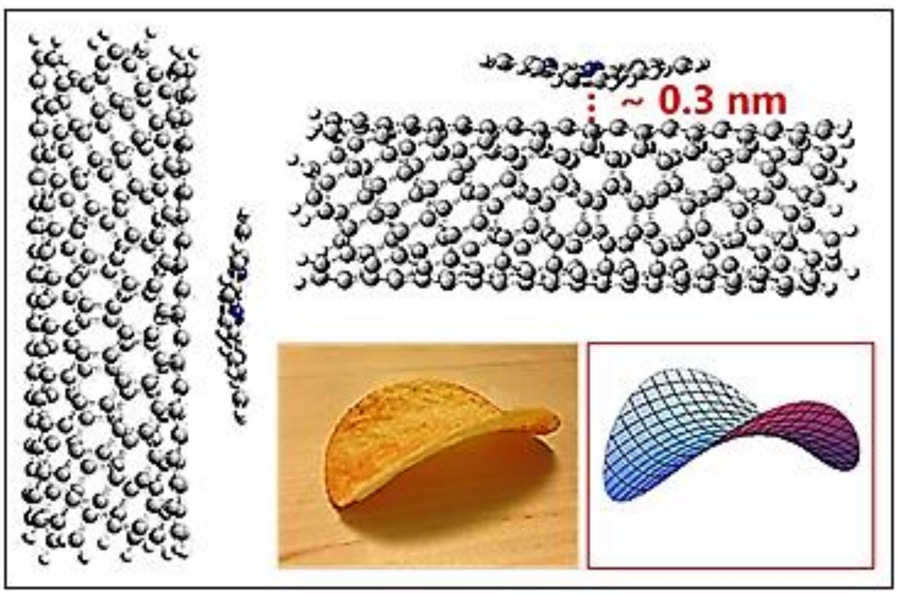

Figure 6. Optimized geometric structure obtained using M05-2X functional with 3-21G basis set for the non-covalent interaction of ***P***-(6,5) SWNT / Zn, Co and Ni-Por complexes in which the porphyrin ring was bent towards the tube surface (with intermolecular distance $d_{SWNT/Por.}$ = 0.3nm) taking chips shaped like structure or saddle structure.

The frontier molecular orbitals (HOMOs and LUMOs) of the complexes and their absolute energies values in eV are represented in Fig. 7. The frontier orbitals of the nanotube, porphyrin core and SWNT / porphyrin conjugates resulting by using M05-2X functional with 3-21G basis set, from which it is obvious that the HOMO - LUMO energies gap are almost same. Additionally the frontier orbitals of the complexes are located on both the tube surface and the molecules.

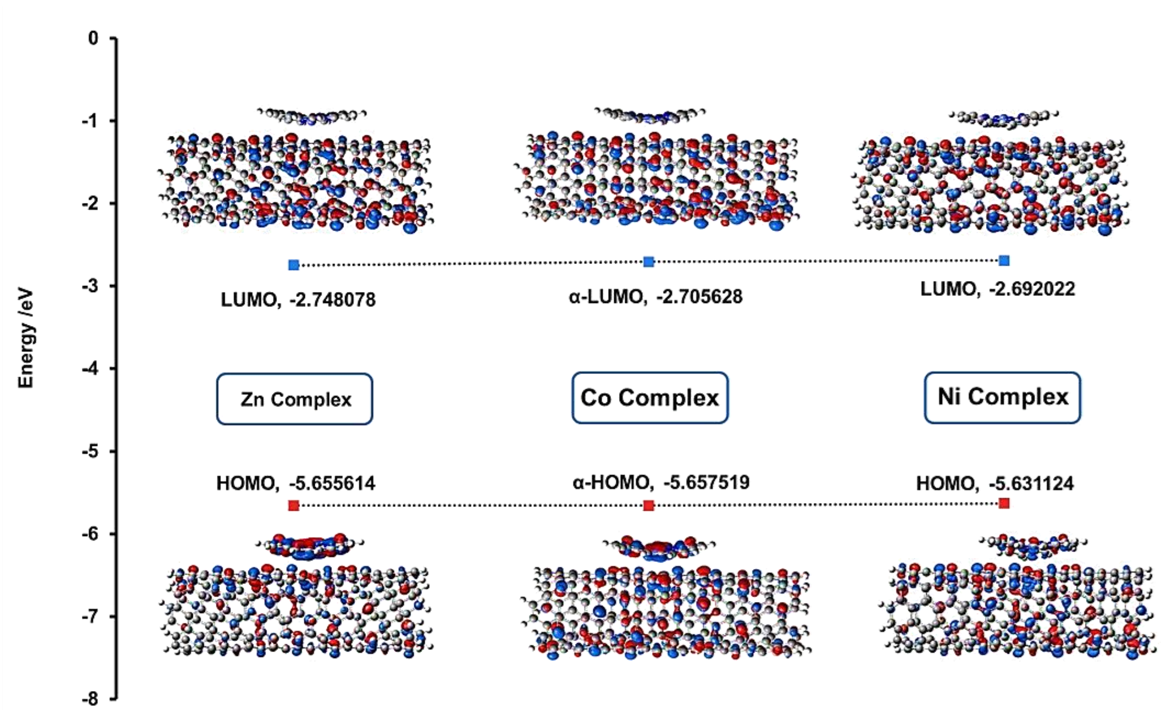

Figure 7. The HOMO-LUMO plot and the frontier orbital shapes of SWNT / metal porphyrin complexes and their energies (in eV), calculated using M05-2X functional with 3-21G basis set.

3.4. Conclusion

With the purpose for identifying the effect of metalation on the supramolecular structures of porphyrins on SWNT surface; supramolecular structures of different central metal porphyrins i.e. ZnPor, NiPor and CoPor were successfully observed on SWNT (HiPCO raw) surface by using STM imaging technique and further characterized via HR-TEM and UV - Visible spectroscopy. All the metal porphyrins can be adsorbed effectively on the tube surface leading to well-ordered supramolecular structures (especially in the cases of NiPor and ZnPor) on SWNT surface, as well as strong debundling effect (especially in CoPor case) for the nanotubes. Among the three metal porphyrins; NiPor produced the best STM resolution images. From an energetic point of view, DFT results displayed that the stability of these metal porphyrins complexes with the following order Ni < Zn < Co, additionally all the metal porphyrins complexes took chips shaped like structure or saddle structure with almost the same intermolecular contact distance between the porphyrin and SWNT surface which equal around 3 Å. Consequently by changing the central metal incorporated inside the porphyrin ring; different supramolecular structures can be observed on SWNT surface, which displaying the marvelous effect of different metal centers on the supramolecular structure of porphyrins on SWNT surface. This substantial finding will be very helpful as key point for further understanding and building new supramolecular architectures on curved nanocarbon surfaces as well as can be used for designing and fabricating novel molecular architectonics of porphyrin / SWNTs based devices.

References

1 Heath, J. R. Molecular electronics. *Annual Review of Materials Research* **39**, 1-23 (2009).

2 Carroll, R. L. & Gorman, C. B. The genesis of molecular electronics. *Angewandte Chemie International Edition* **41**, 4378-4400 (2002).

3 Vuillaume, D. Molecular nanoelectronics. *Proceedings of the IEEE* **98**, 2111-2123 (2010).

4 Song, H., Reed, M. A. & Lee, T. Single molecule electronic devices. *Advanced Materials* **23**, 1583-1608 (2011).

5 Lent, C. S. Bypassing the transistor paradigm. *Science* **288**, 1597 (2000).

6 Andrews, D. Q., Solomon, G. C., Van Duyne, R. P. & Ratner, M. A. Single molecule electronics: increasing dynamic range and switching speed using cross-conjugated species. *J. the American Chemical Society* **130**, 17309-17319 (2008).

7 Moth-Poulsen, K. & Bjørnholm, T. Molecular electronics with single molecules in solid-state devices. *Nature nanotechnology* **4**, 551-556 (2009).

8 Kaneko, S. *et al.* Site selection in single-molecule junction for highly reproducible molecular electronics. *Journal of the American Chemical Society* (2016).

9 Huang, Z., Chen, F., Bennett, P. A. & Tao, N. Single molecule junctions formed via Au-thiol contact: Stability and breakdown mechanism. *Journal of the American Chemical Society* **129**, 13225-13231 (2007).

10 Heath, J. R. & Ratner, M. A. Molecular electronics. (2003).

11 Tour, J. M. Molecular electronics. Synthesis and testing of components. *Accounts of Chemical Research* **33**, 791-804 (2000).

12 Metzger, R. M. *et al.* Unimolecular electrical rectification in hexadecylquinolinium tricyanoquinodimethanide. *Journal of the American Chemical Society* **119**, 10455-10466 (1997).

13 Metzger, R. M. Unimolecular electrical rectifiers. *Chemical reviews* **103**, 3803-3834 (2003).

14 Elbing, M. *et al.* A single-molecule diode. *Proceedings of the National Academy of Sciences of the United States of America* **102**, 8815-8820 (2005).

15 Hihath, J. *et al.* Inelastic transport and low-bias rectification in a single-molecule diode. *ACS nano* **5**, 8331-8339 (2011).

16 Flood, A. H., Stoddart, J. F., Steuerman, D. W. & Heath, J. R. Whence molecular electronics? *Science* **306**, 2055-2056 (2004).

17 Waser, R. & Aono, M. Nanoionics-based resistive switching memories. *Nature materials* **6**, 833-840 (2007).

18 Liu, Z., Yasseri, A. A., Lindsey, J. S. & Bocian, D. F. Molecular memories that survive silicon device processing and real-world operation. *Science* **302**, 1543-1545 (2003).

19 Liljeroth, P., Repp, J. & Meyer, G. Current-induced hydrogen tautomerization and conductance switching of naphthalocyanine molecules. *Science* **317**, 1203-1206 (2007).

20 Koumura, N., Zijlstra, R. W., van Delden, R. A., Harada, N. & Feringa, B. L. Light-driven monodirectional molecular rotor. *Nature* **401**, 152-155 (1999).
21 Browne, W. R. & Feringa, B. L. Making molecular machines work. *Nature nanotechnology* **1**, 25-35 (2006).
22 Dulić, D. *et al.* One-way optoelectronic switching of photochromic molecules on gold. *Physical review letters* **91**, 207402 (2003).
23 Auwärter, W. *et al.* A surface-anchored molecular four-level conductance switch based on single proton transfer. *Nature nanotechnology* **7**, 41-46 (2012).
24 Okawa, Y. *et al.* Chemical wiring and soldering toward all-molecule electronic circuitry. *Journal of the American Chemical Society* **133**, 8227-8233 (2011).
25 Collier, C. *et al.* Electronically configurable molecular-based logic gates. *Science* **285**, 391-394 (1999).
26 Kompa, K. & Levine, R. A molecular logic gate. *Proceedings of the National Academy of Sciences* **98**, 410-414 (2001).
27 Joachim, C., Renaud, N. & Hliwa, M. The different designs of molecule logic gates. *Advanced Materials* **24**, 312-317 (2012).
28 Lam, H. Y. & Natelson, D. Transport in single-molecule transistors: Kondo physics and negative differential resistance. *Nanotechnology* **15**, S517 (2004).
29 Kubatkin, S. *et al.* Single-electron transistor of a single organic molecule with access to several redox states. *Nature* **425**, 698-701 (2003).
30 van der Zant, H. S. *et al.* Molecular three-terminal devices: fabrication and measurements. *Faraday discussions* **131**, 347-356 (2006).
31 Liang, W., Shores, M. P., Bockrath, M., Long, J. R. & Park, H. Kondo resonance in a single-molecule transistor. *Nature* **417**, 725-729 (2002).
32 Staykov, A., Areephong, J., R. Browne, W., L. Feringa, B. & Yoshizawa, K. Electrochemical and photochemical cyclization and cycloreversion of diarylethenes and diarylethene-capped sexithiophene wires. *ACS nano* **5**, 1165-1178 (2011).
33 Ratner, M. A. *et al.* Molecular wires: Charge transport, mechanisms, and control. *Annals of the New York Academy of Sciences* **852**, 22-37 (1998).
34 Jurow, M., Schuckman, A. E., Batteas, J. D. & Drain, C. M. Porphyrins as molecular electronic components of functional devices. *Coordination chemistry reviews* **254**, 2297-2310 (2010).
35 Smith, K. M. & Falk, J. E. *Porphyrins and metalloporphyrins*. (Elsevier Amsterdam, 1975).
36 Yan, Y. *et al.* Carbon nanotube catalysts: recent advances in synthesis, characterization and applications. *Chemical Society Reviews* **44**, 3295-3346 (2015).
37 Singh, P. *et al.* Organic functionalisation and characterisation of single-walled carbon nanotubes. *Chemical Society Reviews* **38**, 2214-2230 (2009).
38 Gao, C., Guo, Z., Liu, J.-H. & Huang, X.-J. The new age of carbon nanotubes: an updated review of functionalized carbon nanotubes in electrochemical sensors. *Nanoscale* **4**, 1948-1963 (2012).
39 Paul Holister, T. E. H. a. C. R. V. Nanotubes. *CMP-Científica*, 1-13. (2003).

40 Cheng, F. & Adronov, A. Noncovalent functionalization and solubilization of carbon nanotubes by using a conjugated Zn–porphyrin polymer. *Chemistry–A European Journal* **12**, 5053-5059 (2006).

41 Zhang, X. *et al.* Solvent dependent supramolecular self-assembly and surface reversal of a modified porphyrin. *Physical Chemistry Chemical Physics* **15**, 12510-12515 (2013).

42 Oncel, N. & Bernasek, S. L. The effect of molecule-molecule and molecule-substrate interaction in the formation of Pt-octaethyl porphyrin self-assembled monolayers. *Applied Physics Letters* **92**, 133305 (2008).

43 Ikeda, T. *et al.* STM observation of alkyl-chain-assisted self-assembled monolayers of pyridine-coordinated porphyrin rhodium chlorides. *Langmuir* **20**, 5454-5459 (2004).

44 Ikeda, T., Asakawa, M., Miyake, K., Goto, M. & Shimizu, T. Scanning tunneling microscopy observation of self-assembled monolayers of strapped porphyrins. *Langmuir* **24**, 12877-12882 (2008).

45 Ogunrinde, A., Hipps, K. & Scudiero, L. A scanning tunneling microscopy study of self-assembled nickel (II) octaethylporphyrin deposited from solutions on HOPG. *Langmuir* **22**, 5697-5701 (2006).

46 Shen, Y. *et al.* Self-assembling in fabrication of ordered porphyrins and phthalocyanines hybrid nano-arrays on HOPG. *CrystEngComm* **15**, 5526-5531 (2013).

47 Teugels, L. G., Avila-Bront, L. G. & Sibener, S. Chiral domains achieved by surface adsorption of achiral nickel tetraphenyl-or octaethylporphyrin on smooth and locally kinked Au (111). *The Journal of Physical Chemistry C* **115**, 2826-2834 (2011).

48 Murphy, B. *et al.* Growth and ordering of Ni (II) diphenylporphyrin monolayers on Ag (111) and Ag/Si (111) studied by STM and LEED. *Journal of Physics: Condensed Matter* **24**, 045005 (2012).

49 Haq, S. *et al.* Versatile bottom-up construction of diverse macromolecules on a surface observed by scanning tunneling microscopy. *ACS nano* **8**, 8856-8870 (2014).

50 Yoshimoto, S. & Itaya, K. Advances in supramolecularly assembled nanostructures of fullerenes and porphyrins at surfaces. *Journal of Porphyrins and Phthalocyanines* **11**, 313-333 (2007).

51 Phan, T. H., Kosmala, T. & Wandelt, K. Potential dependence of self-assembled porphyrin layers on a Cu (111) electrode surface: In-situ STM study. *Surface Science* **631**, 207-212 (2015).

52 Phan, T. H. & Wandelt, K. Self-assembly of metal free porphyrin layers at copper-electrolyte interfaces: Dependence on substrate symmetry. *Surface Science* **607**, 82-91 (2013).

53 Guo, Z. *et al.* Covalently porphyrin-functionalized single-walled carbon nanotubes: a novel photoactive and optical limiting donor–acceptor nanohybrid. *Journal of Materials Chemistry* **16**, 3021-3030 (2006).

54 Baskaran, D., Mays, J. W., Zhang, X. P. & Bratcher, M. S. Carbon nanotubes with covalently linked porphyrin antennae: photoinduced electron transfer. *Journal of the American Chemical Society* **127**, 6916-6917 (2005).

55 Liu, Z. B. *et al.* Enhanced Optical Limiting Effects in Porphyrin‐Covalently Functionalized Single‐Walled Carbon Nanotubes. *Advanced materials* **20**, 511-515 (2008).

56 Sáfar, G. d. A. M. *et al.* Interactions of porphyrins and single walled carbon nanotubes: A fine duet. *Synthetic Metals* **193**, 64-70 (2014).

57 Sprafke, J. K., Stranks, S. D., Warner, J. H., Nicholas, R. J. & Anderson, H. L. Noncovalent binding of carbon nanotubes by porphyrin oligomers. *Angewandte Chemie International Edition* **50**, 2313-2316 (2011).

58 Cheng, F., Zhang, S., Adronov, A., Echegoyen, L. & Diederich, F. Triply Fused ZnII–Porphyrin Oligomers: Synthesis, Properties, and Supramolecular Interactions with Single‐Walled Carbon Nanotubes (SWNTs). *Chemistry–A European Journal* **12**, 6062-6070 (2006).

59 AminuráRahman, G. Electronically interacting single wall carbon nanotube–porphyrin nanohybrids. *Journal of Materials Chemistry* **16**, 62-65 (2006).

60 Tuncel, D. Non-covalent interactions between carbon nanotubes and conjugated polymers. *Nanoscale* **3**, 3545-3554 (2011).

61 Bilalis, P., Katsigiannopoulos, D., Avgeropoulos, A. & Sakellariou, G. Non-covalent functionalization of carbon nanotubes with polymers. *RSC Advances* **4**, 2911-2934 (2014).

62 Guldi, D. M. *et al.* Functional single-wall carbon nanotube nanohybrids associating SWNTs with water-soluble enzyme model systems. *Journal of the American Chemical Society* **127**, 9830-9838 (2005).

63 Satake, A., Miyajima, Y. & Kobuke, Y. Porphyrin-carbon nanotube composites formed by noncovalent polymer wrapping. *Chemistry of materials* **17**, 716-724 (2005).

64 Chen, J. & Collier, C. P. Noncovalent functionalization of single-walled carbon nanotubes with water-soluble porphyrins. *The Journal of Physical Chemistry B* **109**, 7605-7609 (2005).

65 Chitta, R. *et al.* Donor-acceptor nanohybrids of zinc naphthalocyanine or zinc porphyrin noncovalently linked to single-wall carbon nanotubes for photoinduced electron transfer. *The Journal of Physical Chemistry C* **111**, 6947-6955 (2007).

66 Roquelet, C. *et al.* Light harvesting with non covalent carbon nanotube/porphyrin compounds. *Chemical Physics* **413**, 45-54 (2013).

67 Zhong, Q. *et al.* Fused Porphyrin–Single-Walled Carbon Nanotube Hybrids: Efficient Formation and Photophysical Characterization. *ACS nano* **7**, 3466-3475 (2013).

68 Murakami, H., Nomura, T. & Nakashima, N. Noncovalent porphyrin-functionalized single-walled carbon nanotubes in solution and the formation of porphyrin–nanotube nanocomposites. *Chemical Physics Letters* **378**, 481-485 (2003).

69 Hasobe, T., Fukuzumi, S. & Kamat, P. V. Ordered assembly of protonated porphyrin driven by single-wall carbon nanotubes. j-and h-aggregates to nanorods. *Journal of the American Chemical Society* **127**, 11884-11885 (2005).

70 Sarkar, T., Srinives, S., Sarkar, S., Haddon, R. C. & Mulchandani, A. Single-Walled Carbon Nanotube–Poly (porphyrin) Hybrid for Volatile Organic Compounds Detection. *The Journal of Physical Chemistry C* **118**, 1602-1610 (2014).

71 Fitzgerald, C. NanoScope Command Reference Manual, version 5.12, revision B; Digital Instruments/Veeco Metrology Group, Inc.: Santa Barbara, CA. 2001. 52.

72 Kawao, M., Ozawa, H., Tanaka, H. & Ogawa, T. Synthesis and self-assembly of novel porphyrin molecular wires. *Thin Solid Films* **499**, 23-28 (2006).

73 DiMagno, S. G., Lin, V. S. & Therien, M. J. Facile elaboration of porphyrins via metal-mediated cross-coupling. *The Journal of Organic Chemistry* **58**, 5983-5993 (1993).

74 He, C. *et al.* Turn on fluorescence sensing of vapor phase electron donating amines via tetraphenylporphyrin or metallophenylporphrin doped polyfluorene. *Chemical Communications* **46**, 7536-7538 (2010).

75 Song, X.-Z. *et al.* Metal dependence of the contributions of low-frequency normal coordinates to the sterically induced distortions of meso-dialkyl-substituted porphyrins. *Inorganic Chemistry* **37**, 2009-2019 (1998).

76 Nakashima, N., Tomonari, Y. & Murakami, H. Water-Soluble Single-Walled Carbon Nanotubes via Noncovalent Sidewall-Functionalization with a Pyrene-Carrying Ammonium Ion. *Chemistry Letters*, 638-639 (2002).

77 Bassiouk, M. *et al.* Noncovalent functionalization of single-walled carbon nanotubes with porphyrins. *Applied Surface Science* **275**, 168-177 (2013).

78 Pauling, L. The nature of the chemical bond. IV. The energy of single bonds and the relative electronegativity of atoms. *Journal of the American Chemical Society* **54**, 3570-3582 (1932).

79 Gaussian09, R. A. 1, MJ Frisch, GW Trucks, HB Schlegel, GE Scuseria, MA Robb, JR Cheeseman, G. Scalmani, V. Barone, B. Mennucci, GA Petersson et al., Gaussian. *Inc., Wallingford CT* (2009).

80 Zhao, Y., Schultz, N. E. & Truhlar, D. G. Design of density functionals by combining the method of constraint satisfaction with parametrization for thermochemistry, thermochemical kinetics, and noncovalent interactions. *Journal of Chemical Theory and Computation* **2**, 364-382 (2006).

81 Rodríguez-Galván, A., Amelines-Sarria, O., Rivera, M., Carreón-Castro, M. d. P. & Basiuk, V. A. Adsorption and Self-assembly of Anticancer Antibiotic Doxorubicin on Single-Walled Carbon Nanotubes. *NANO* (2015).

82 Basiuk, E. V., Basiuk, V. A., Santiago, P. & Puente-Lee, I. Noncovalent functionalization of carbon nanotubes with porphyrins: meso-tetraphenylporphine and its transition metal complexes. *Journal of nanoscience and nanotechnology* **7**, 1530-1538 (2007).

83 Basiuk, V. A. & Bassiouk, M. Nanoassembly of meso-tetraphenylporphines on surfaces of carbon materials: initial steps as studied by molecular mechanics and

scanning tunneling microscopy. *Journal of nanoscience and nanotechnology* **8**, 259-267 (2008).

84 Basiuk, V. A., Kolokoltsev, Y. & Amelines-Sarria, O. Noncovalent interaction of meso-tetraphenylporphine with C60 fullerene as studied by several DFT methods. *Journal of nanoscience and nanotechnology* **11**, 5519-5525 (2011).

85 Orellana, W. & Correa, J. D. Noncovalent functionalization of carbon nanotubes and graphene with tetraphenylporphyrins: stability and optical properties from ab initio calculations. *Journal of Materials Science* **50**, 898-905 (2015).

Chapter IV. Confirmation of SWNT Handedness Chirality Identification with Metalized Porphyrins using STM imaging Technique.

4.1. Introduction

Since Aviram and Ratner's proposal[1], the molecular electronics field as significantly expanded and numerous models of single molecule electronic devices have been actively designed and developed with a wide range of characteristic functions including diodes, memories, switches, logic gates, transistors and wires[2-7].

There is a wide variety of molecular building blocks, which can be used for the fabrication of electronic components .i.e. molecules, nanoparticles, nanotubes and nanowires to form new devices and circuit architectures[8] These molecular building blocks can be designed and/or assembled in such a way that they have properties which resemble traditional electronic components i.e. wire, transistor, rectifier, memory and switch. By emerging the properties inherent in single molecule components for fabricating a functional device; this will offer unlimited possibilities for technological development because the potentially diverse electronic functions of the component molecules[9].

Another approach to fabricate molecular electronic devices can be attained by using supramolecular chemistry techniques and/or self-assembly of organic molecules, carbon nanotubes, proteins and others. Self-assembly is a phenomenon in which atoms, molecules or groups of molecules can be arranged spontaneously into regular patterns without interference from outside[10,11].

Due to their magnificent properties i.e. optoelectronic, physical and chemical; porphyrins and related compounds have attracted great attention and have been studied[12]. In addition to their ease of synthesis including very wide variations of substituents, they are not only important as natural photo-catalysts but also they can be used as substantial candidates in many other fields for instance, material science, physics and as well as building blocks in molecular electronic devices[12-17]. Additionally they have a large π-electronic system, and numerous metals can be inserted within their macrocycle giving metalloporphyrins. In fact the optoelectronic properties of porphyrins can be easily altered by insertion of metal center within the molecular ring[18].

In order to get well-ordered nanostructures, self-assembly of organic molecules on metallic or nanocarbon material surfaces is being a promising approach. Interactions of porphyrins and/or related tetraazamacrocyclic compounds with nanocarbon materials i.e. single-walled carbon nanotubes (SWNTs)[19-24], highly oriented pyrolytic graphite (HOPG)[25-30] and graphene[31] have been extensively studied. By combining the unique optical, electronic and magnetic properties of both porphyrins and nanocarbon materials; the overall properties of the novel designed hybrid nanosystems will be enhanced, giving a wide range of applications i.e. catalysts, sensors, electronic, photonic and spintronic devices as a key step for the future development of molecular electronics field[32-34].

However, supramolecular structure assembles of porphyrins on flat nanocarbon surfaces like HOPG[25-30] or on other metallic surfaces[35-40] have attracted much more attentions; but supramolecular structures on curved surfaces like carbon nanotubes are still challenging to predict or to understand; although many research groups have focused on porphyrin / SWNTs complex even covalently[41-43], noncovalently[44-57], assembling of ordered protonated porphyrin driven by SWNTs[58], forming nanohybrid for detecting volatile organic compounds[59] as well as dispersion and solubilization of SWNTs[46,47].

In previous studies, our group has investigated electronic properties of SWNTs / 150mer-Porphyrin system using point-contact current imaging atomic force microscopy (PCI-AFM)[60] as well as fabrication of porphyrin molecular nanodevices wired using SWNTs[61]. Moreover, we assigned the two-dimensional supramolecular structures of a series of N, N`-bis(n-alkyl)-naphthalenediimides (NDIs), whose chain lengths span from C3 to C18, at a liquid - HOPG surface interface, using STM and FM-AFM, with the help of molecular dynamics / molecular mechanics calculations[62].

In this chapter with the aim to confirm determination of the absolute handedness chirality of SWNTs (which has been investigated in chapter 2) using different molecular structure of porphyrin derivatives; we studied the supramolecular structures of 5,15-bisdodecylporphyrin-Ni (Fig. 1) (Ni-C12P) on chiral-SWNTs surface using scanning tunneling microscopy (STM), for the purpose firstly to emphasize the identification of handedness chirality of SWNT and its effect on the supramolecular structure of the organic molecules on SWNT surface, in addition to consider whether porphyrin metalation would have effect on the handedness chirality of SWNT or not.

Again (as in chapter 2) two types of chiral-SWNTs have been used in this study, right handed helix ***P*** (or plus) type and left handed helix ***M*** (or Minus) type[63-66]. Interestingly two opposite supramolecular structures of Ni-C12P molecule on chiral SWNT surface have been observed STM microscopic images, in which Ni-C12P molecules are aligned towards the right direction (assigned as ***P***-type) and to the left direction (assigned as ***M***-type). These results are in agreement with those have been obtained in chapter 2 by using free base porphyrin C12P, which could be indicate that even by changing the molecular structure of the porphyrin i.e. by incorporating metal center; the handedness chirality of SWNT would have the same effect on the orientation and supramolecular structure of organic molecules on its surface. Therefore the handedness chirality of SWNT can be successfully identified using STM imaging technique, via supramolecular structure of organic molecules on the tube surface.

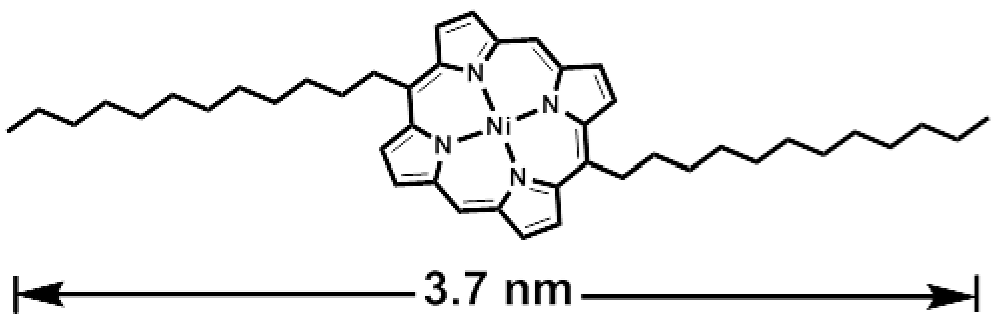

Figure 1. Chemical Structure of 5,15-bisdodecylporphyrin-Ni (Ni-C12P)

4.2. Experimental

All the reactions were performed in anhydrous solvents under nitrogen atmosphere using well-dried glasswares in an oven at 90 ^{o} C before using. Nickel porphyrin was synthesized under dark conditions. All the solvents i.e. dichloromethane, chloroform and hexane were dried and distilled using molecular sieves 4 Å. Column chromatography was performed using silica-gel (spherical, neutral, 63-200 µm, Kishida Chemicals Co., Ltd.). HOPG was purchased from Alliance Biosystems, Inc. (Spi - 1 Grade 7×7×1 mm). 1-Tetradecane was obtained from Aldrich with a grade (99%) and used as it is. Other chemicals and solvents were of reagent grade and used without any further purification. ^{1}H NMR was carried out on a JEOL 400 and 500 MHz NMR spectrometers. Chemical shifts were given by ppm and all the signals were adjusted using tetramethylsilane (TMS) as an internal standard. Mass spectra were recorded using a Shimadzu AXIMA-CFR MALDI-TOF mass spectrometer. UV/Visible adsorption spectra were recorded on a Shimadzu UV-3150 double-beam spectrophotometer.

SWNT treatment, STM measurements on both HOPG and SWNT surfaces have been explained in details in the experimental section of chapter 2. STM observation of Ni-C12P on HOPG surface was performed using JEOL scanning probe microscope (JSPM-5200) with a special hand-made cell for solid – liquid measuments, however to observe Ni-C12P on SWNT surface; BRUKER multimode 8 SPM with a special cell for solid – liquid measuments has been used. All the STM images were carried out in a constant current mode under the ambient conditions. The STM tips were mechanically cut and formed from Pt/Ir (80 % / 20 %) wire (0.25 mm in diameter).

Synthesis of Compounds

We synthesized Ni-C12P **4** based on our previously reported method[61] with slight modification which shown in scheme 1. The synthesis of dipyrromethane **1** and 5, 15-bisdodecylporphyrin (C12P) **3** have been explained in details in the experimental section of chapter 2; however tridecanal **2** has been purchased and used as received.

5, 15-bisdodecylporphyrin-Ni (Ni-C12P) 4

We synthesized C12P-Ni **4** using previously reported method[67], in which C12P (0.3157 g, 0.488 mmol) and Ni (acac)$_2$ (0.17g, 0.659 mmol) were refluxed in toluene (50 mL) at

120 °C for 1 day in dark. The complete metalation was checked by TLC, after that the reaction mixture was poured with 100 mL water and extracted with $CHCl_3$. After collecting the organic layer, it was washed 3 times with water and brine and dried over Na_2SO_4. By removing the solvent under vacuum then recrystallize the residue with $CHCl_3$ / excess MeOH, red purple powder was obtained (0.3 g, 86 % yield). ^{1}H NMR (500 MHz, $CDCl_3$, 25 °C, TMS): δ 9.80 (s, 2H, *meso*-H), 9.60 (d, J = 4.8 Hz, 4H, β-pyrrole-H), 9.34 (d, J = 4.8 Hz, 4H, β-pyrrole-H), 4.95 (m, 4H, CH_2), 2.48 (m, 4H, CH_2), 1.80 (m, 4H, CH_2), 1.63 (m, 16H, CH_2),1.11(t, 6H, CH_3). UV/Vis (CH_2Cl_2): λ_{max}= 403, 517, 550 nm. MS (MALDI-TOF) *m/z* for $C_{44}H_{60}N_4$ Ni, $[M + H]^+$ calcd, 703.6; found, 703.1

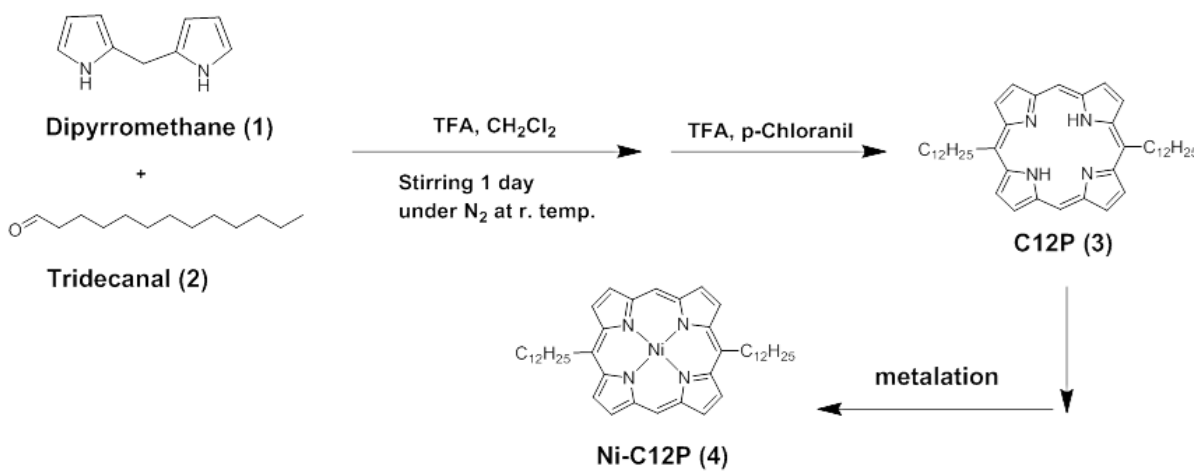

Scheme 1. Procedures for synthesizing 5,15-bisdodecylporphyrins-Ni (Ni-C12P)**.**

Preparation of Ni-C12P / SWNTs Complex

The porphyrin / SWNT complex was prepared as follows. After dissolving Ni-C12P in dichloromethane, the solution was submitted to ultrasonic bath for 10 min. 0.3 mg of ***P-*** and/or ***M-*** chiral SWNTs were added to porphyrin solution, and sonicated overnight. The resulting suspension was left for sedimentation for 2 h. Then the top 5 % of the supernatant was removed, and the precipitate was filtered by a membrane filter (MILLIPORE) of 0.1 μm mesh. Then rinse with 100 mL CH_2Cl_2 to remove the non-adsorbed porphyrin and dried in a vacuum desiccator until further utilization, as illustrated in scheme 2 the experimental section of chapter 2.

4.3. Results and discussion

Supramolecular Structures of Ni-C12P on *P-*, *M-* Handedness Chiral SWNTs Surface observed by STM

After separation using the reported method[63]; handedness chiral SWNTs ***P*** and/or ***M*** have been mixed together with Ni-C12P solution, filtered, dried (as explained in details in the experimental section of this chapter) and the complex powder was re-suspended in 10 mL MeOH, simply drop-casted onto HOPG substrate and left to be completely dry, finally the sample has been introduced to the STM machine to be measured using constant current mode STM imaging technique under ambient conditions.

Surprisingly two converse supramolecular structures of Ni-C12P molecules have been observed on the tube surface; the first one in which Ni-C12P molecules are aligned diagonally to the right direction (this type has been assigned as Ni-C12P / ***P-*** SWNTs complex) which elucidated in Figure 2a-e, however in the second observed supramolecular structure Ni-C12P molecules are being aligned towards to the left direction (we assigned this one as Ni-C12P / ***M***- SWNTs complex) which can be shown in Figure 2f-j. From that dandy finding, one can see clearly the effect of the handedness chirality of SWMT on the alignment of Ni-C12P molecules on its surface; as well as the supramolecular structures made by Ni-C12P were strongly dependent on the underlying SWNTs structure, which in a perfect agreement with the results which have been formed using free base porphyrin C12P in chapter 2. This should indicate that even though by changing the molecular structure of the porphyrin molecule (i.e. by metalation), the SWNT handedness chirality effect can be clearly distinguished using STM microscopic imaging.

Since SWNT can be functionalized either covalently or non-covalently; Ni-C12P / SWNT complexes have been formed mainly via non-covalent interactions between Ni-C12P and SWNT for instance π-π staking between the complex components (Ni-C12P and SWNT) due to the high carrier mobility of delocalized π-electrons, in addition to molecular-substrate interactions, intermolecular interactions and Vander Waals interactions i.e. alkyl-CNTs interaction, porphyrin-porphyrin interaction, and alkyl chain-alkyl chain interaction.

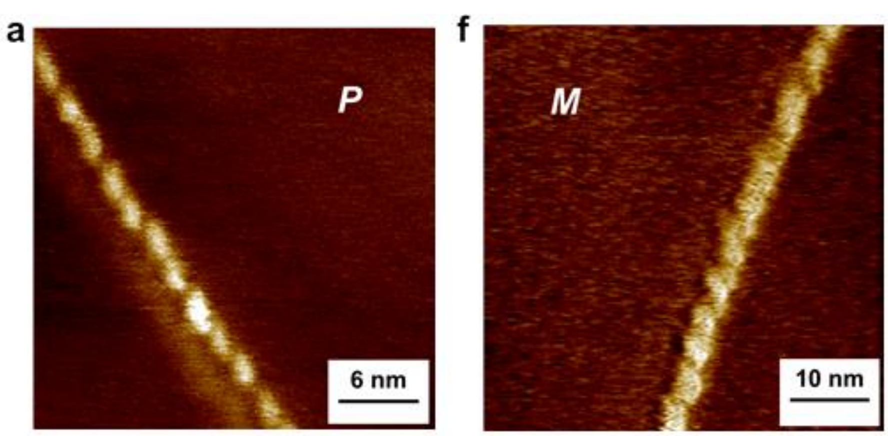

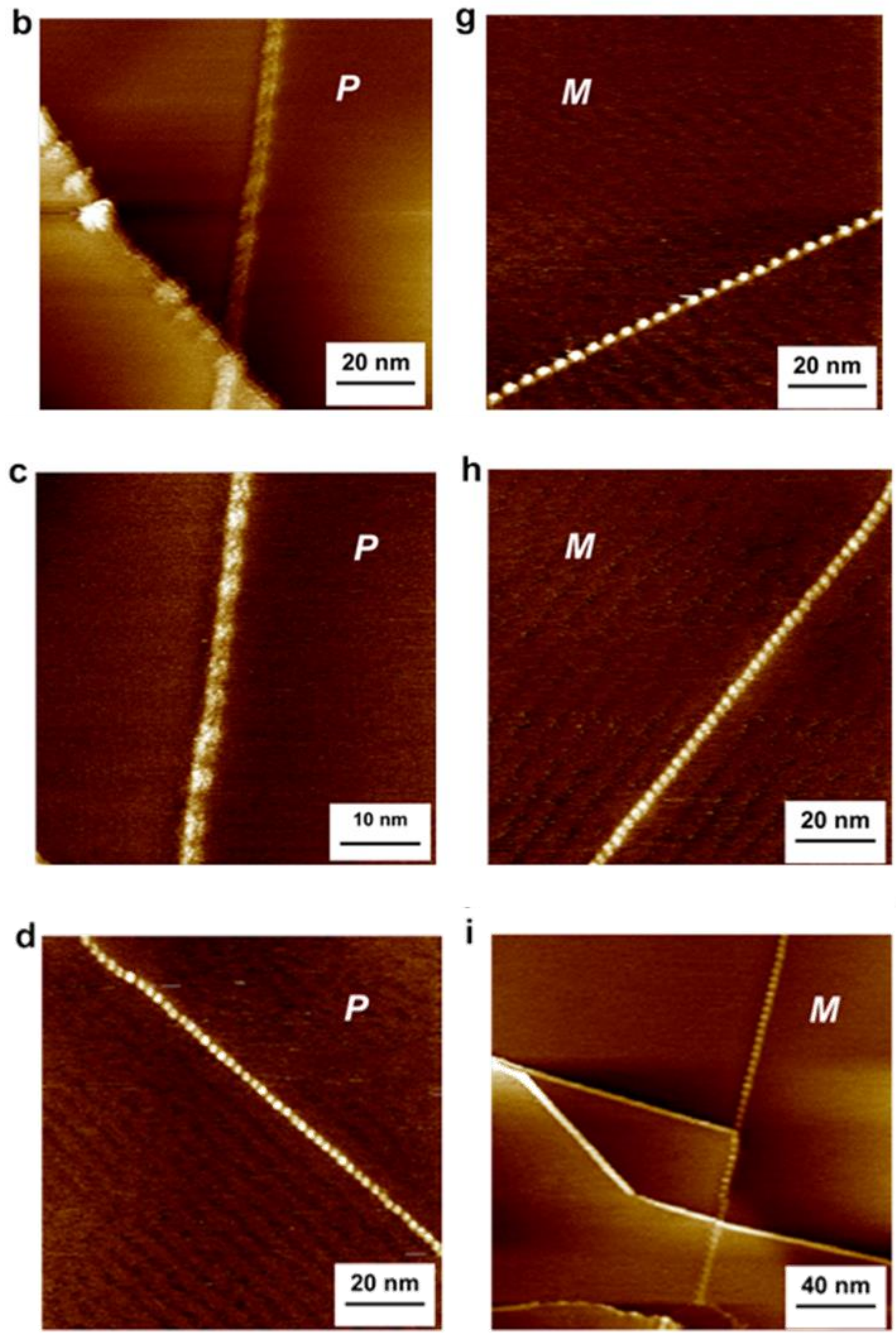

b
P
20 nm
g
M
20 nm
c
P
10 nm
h
M
20 nm
d
P
20 nm
i
M
40 nm

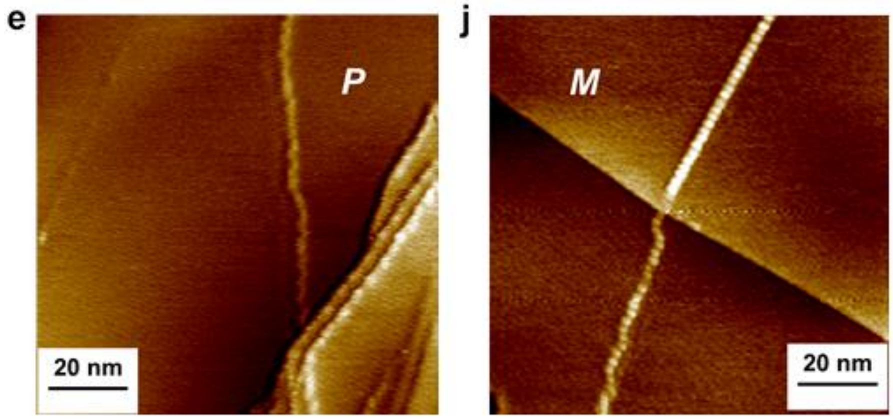

Figure 2. Typical STM images for supramolecular structures of Ni-C12P / ***P***- and ***M***-SWNTs complexes on HOPG surface. All images were taken at V_{sample} = 0.100 V and I_t = 0.010 nA **a**, Ni-C12P / ***P***- SWNTs complex (30 nm × 30 nm) **b**, Ni-C12P / ***P***- SWNTs complex (100 nm × 100 nm) **c**, Ni-C12P / ***P***- SWNTs complex (50 nm × 50 nm) **d**, Ni-C12P / ***P***- SWNTs complex (100 nm × 100 nm) **e**, Ni-C12P / ***P***- SWNTs complex (100 nm × 100 nm) **f**, Ni-C12P / ***M***- SWNTs complex (50 nm × 50 nm) **g**, Ni-C12P / ***M***- SWNTs complex (100 nm × 100 nm) **h**, Ni-C12P / ***M***- SWNTs complex (100 nm × 100 nm) **i**, Ni-C12P / ***M***- SWNTs complex (200 nm × 200 nm) **j**, Ni-C12P / ***M*** - SWNTs complex (100 nm × 100 nm).

The supramolecular structure of Ni-C12P molecules on HOPG surface as a flat nano-carbon substrate has been also studied with the aim to know how the Ni-C12P molecules can be aligned on HOPG surface, additionally better resolution of the molecular structure can be obtained and detailed discussion is possible. Therefore this will be very helpful in the identification of the handedness chirality of SWNT too.

Supramolecular Structures of Ni-C12P on HOPG Surface observed by STM.

The supramolecular structure of Ni-C12P molecule has been investigated on HOPG surface with almost the same protocol which done with C12P molecule (in chapter 2), in which a few drops (ca. 5 µL) of Ni-C12P solution with concentration (~ 0.8 mM) have been simply casted onto a freshly cleaved HOPG surfaces and fixed in the cell. Afterward the substrate was annealed at 60 ^{o} C for 20 - 30 min. and cooled to room temperature, basically without annealing, stable supramolecular structure can't be observed. After adding a few drops of 1- Tetradecane were added to the sample, the sample has been introduced to the STM machine. In order to induce a tunneling current, a bias voltage was applied between the tip and sample to record images at solid-liquid interface.

We succeed to observe a highly reproducible ordered pattern of self-assemble monolayer of Ni-C12P deposited from 1-tetradecane onto HOPG surface, in which Ni-C12P molecule forms a distinctive lamellar structures composed of well-defined pattern of two kinds of domains; bright and dark domains as shown in Fig. 3a-d. The bright domains in the STM images could be attributed to the Ni-porphyrin cores, separated by the alkyl chains which appear in the dark regions as linear features, where the two dodecyl chains are closely packed, interacted altogether giving regular geometry[68-70]. The unit cell parameters were $\boldsymbol{a}$ = 1.15 ± 0.01 nm, $\boldsymbol{b}$ = 2.68 ± 0.02 nm, γ = 58 ± 8 °.

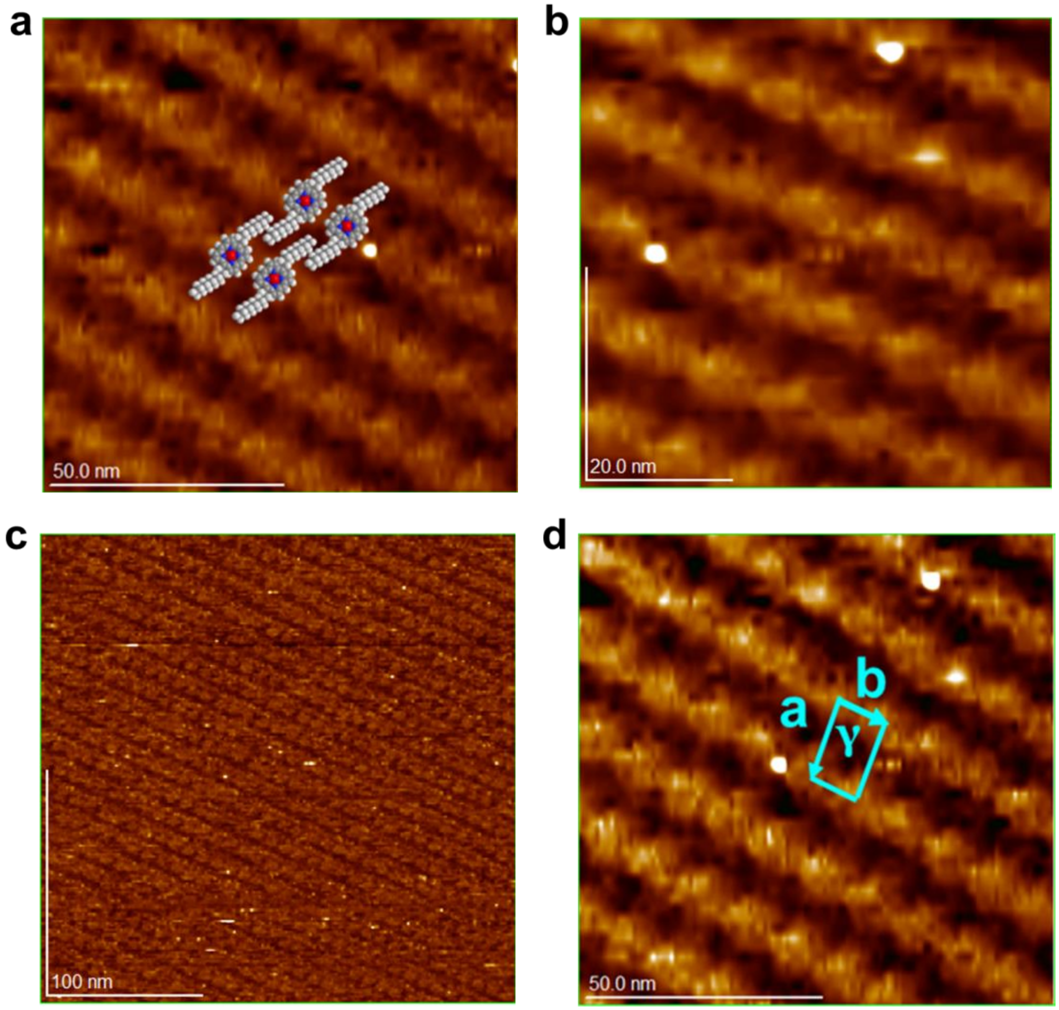

Figure 3. STM image of 2D supramolecular structure of 5,15-bisdodecylporphyrin-Ni (Ni-C12P) on HOPG-tetradecane interface. All images were taken at V_{sample} = - 1.000 V and I_t = 0.056 nA. **a**, 100 nm × 100 nm image, with schematic models drawn to elucidate the orientation of Ni-C12P molecules **b**, 60 nm × 60 nm **c**, 300 nm × 300 nm **d**, 100 nm × 100 nm with a unit cell parameters, ***a*** = 1.15 ± 0.01 nm, ***b*** = 2.68 ± 0.02 nm, γ = 58 ± 8 °.

The driving forces by which the supramolecular structure of the Ni-C12P may be possibly formed are molecular-substrate interaction i.e. interaction between porphyrin cores and HOPG substrate and/or interaction between two dodecyl alkyl chains and HOPG surface, and intermolecular interactions i.e. Vander Waals interactions.

Molecular Modeling

For better understanding regarding how Ni-C12P molecules can be aligned on both HOPG and SWNT surfaces as an endeavor to demonstrate the observed geometries of Ni-C12P molecules on chiral SWNT and HOPG surfaces; a number of proposed models have been built using ***P***- and ***M***- (6,5) chiral SWNTs, HOPG and Ni-C12P molecule. As shown in Fig. 4 there are three possible ways through them Ni-C12P can be aligned on the tube surface where in the first model the molecule can be aligned linearly on the vector line *I* (Type *I*) as in Fig. 4a, the second one (Type *II*) in which the molecules are assembled on the vector line *II* forming short helix arrays (Fig. 4b) and the third model showed that the molecules are aligned in between the vector lines *I* and *II* giving long helix arrays, which illustrated in Fig. 4c and represented by the green arrow *IV* in Fig. 4d.

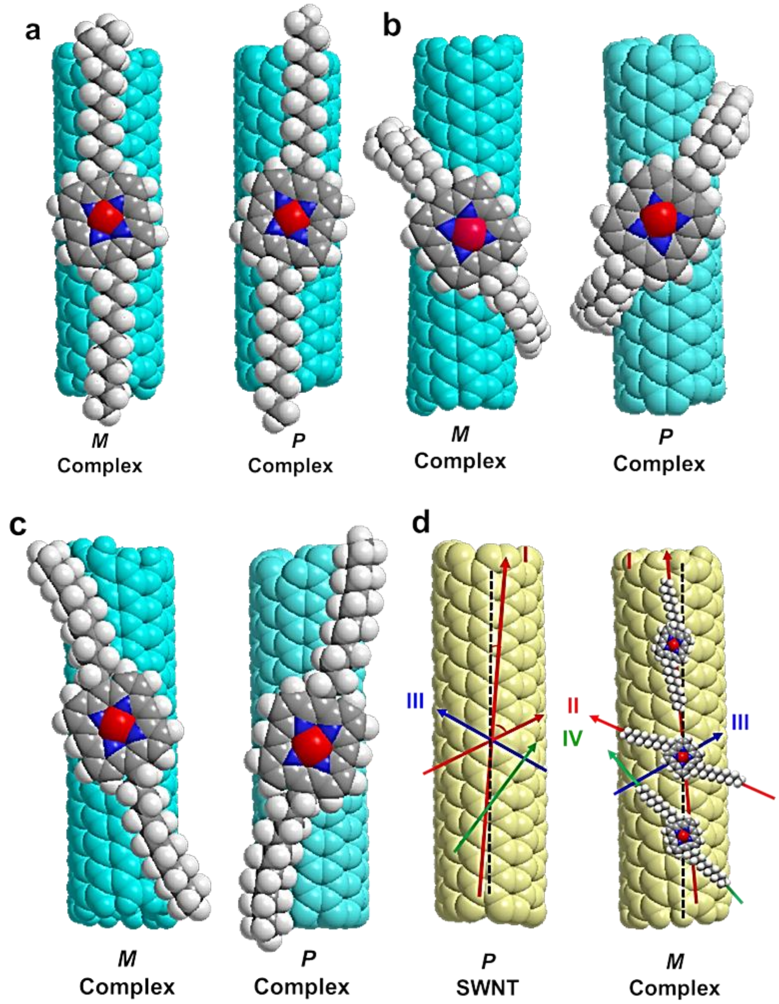

Figure 4. Proposed models intended to elucidate the geometries of arrays observed in Ni-C12P / ***M***- and ***P***- SWNTs complexes, based on alignment of porphyrin molecules on which chiral vector line on chiral SWNTs surfaces. **a**, molecules are aligned towards the vector line *I* (Type *I*) **b,** molecules are assembled towards the vector line *II* (Type *II*) **c**, molecules are assembled in between the two vector lines *I* and *II* which represented by the green arrow *IV* (Type *IV*) **d.** Schematic representation showing the three possible approaches for Ni-C12P molecule to be aligned on chiral SWNT surface altogether.

Figure 5 shows the schematic proposed model which build to elucidate the geometries of Ni-C12P arrays on HOPG surface in which Ni-C12P can be aligned on graphite to display a close-packed lamellar structure. Similar alignments were observed for free base and zinc-5,10,15,20-*meso*-tetradodecylporphyrins[68,69], in which two dodecyl tails physisorbed along HOPG surface.

The geometric structures of the metalized porphyrin for instance Ni-C12P formed on the nano-carbon materials surfaces (chiral SWNT and HOPG) seem in agreement with those which formed by the free base porphyrin C12P (chapter 2). This is an indication that, even though by changing the molecular structure i.e. insertion a metals center to the porphyrin ring; the handedness chirality of SWNT still can be identified using the supramolecular structures of these organic molecules formed on the tube surface.

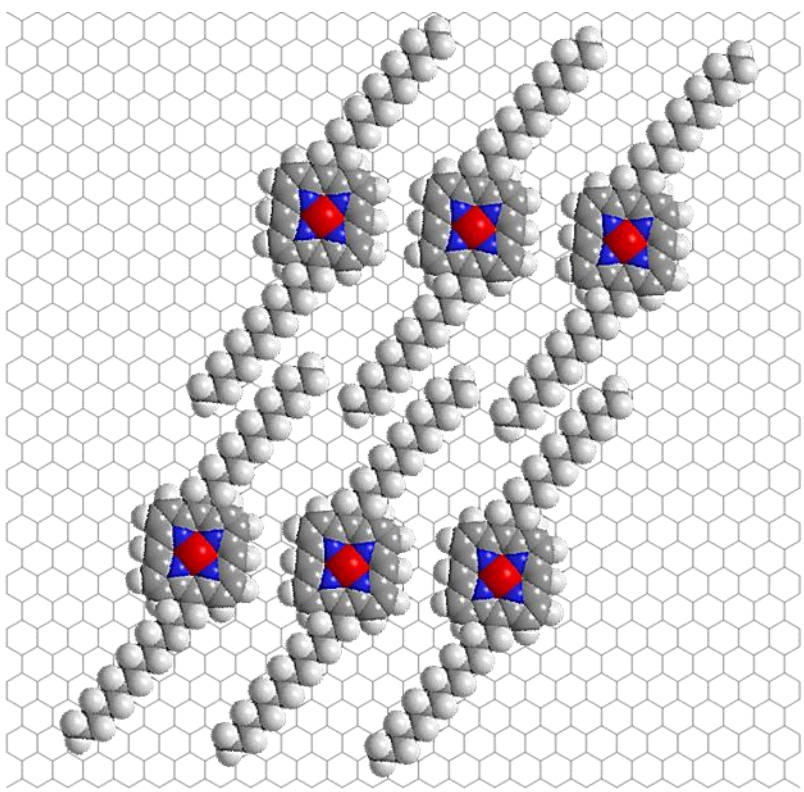

Figure 5. Proposed model intended to elucidate the geometries of Ni-C12P arrays on HOPG surface in which Ni-C12P molecules are aligned on graphite to display a close-packed lamellar structure.

DFT Calculations

In order to establish the most favorable energetic structure of Ni-C12P / SWNT complex; we performed some DFT calculations using long range corrected functionals which involved in Gaussian 09 software[71] for instance Minnesota functionals (M05-2X)[72,73] with 3-21G basis set which can be used in the characterization of the non-local nature of VdW interactions.

The complete set up of these calculations has been explained in details in chapter 2 in which we used an open ended chiral ***P***- (6,5) SWNT modeling with 2.5 nm length, 0.8 nm in diameter (designed by our group) and composed of 222 carbon atoms and 22 hydrogen atoms; in addition to Ni-porphyrin macrocycle ring which consist of 20 carbon atoms, 4 nitrogen atoms, 12 hydrogen atoms and one Ni atom.

All the calculations have been done using M05-2X / 3-21G theoretical level. The frontier molecular orbitals (HOMOs and LUMOs) and their absolute energies values in eV of ***P***-(6,5) SWNT, Ni-Porphyrin molecule and SWNT / Ni-Porphyrin complex are demonstrated in table 1.

	SWNT	Ni- Porphyrin	SWNT / Ni-Porphyrin Complex
LUMO 3	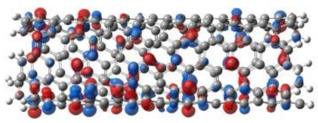 -2.12817 eV	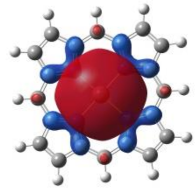 0.641907 eV	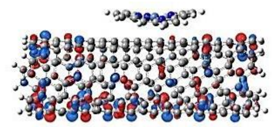 -2.10153 eV
LUMO 2	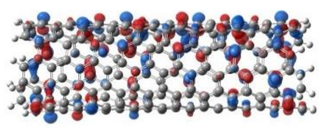 -2.17661 eV	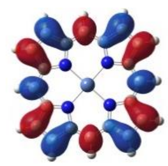 2.455249 eV	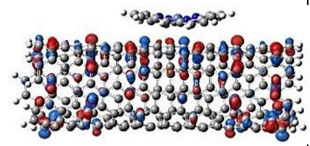 - 2.14861 eV
LUMO 1	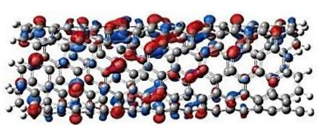 -2.69416 eV	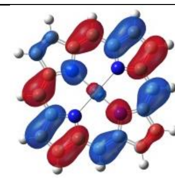 0.641907 eV	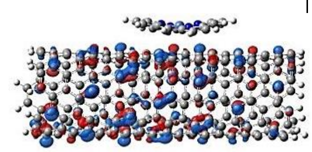 - 2.65011 eV
LUMO	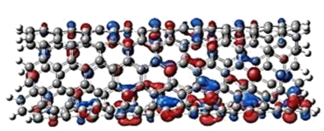 -2.73144 eV	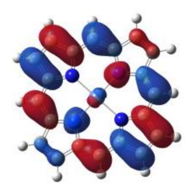 -1.46558 eV	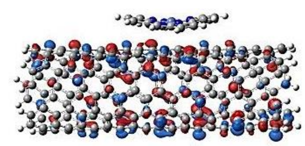 - 2.67732 eV
HOMO	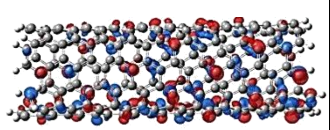 -5.78098 eV	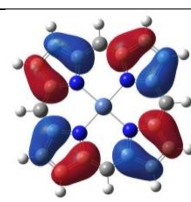 -6.27159 eV	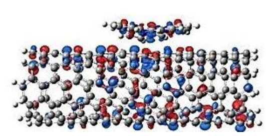 - 5.63112 eV

HOMO 1	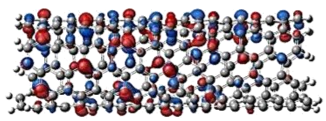 -5.8237 eV	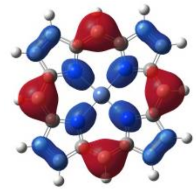 -6.47023 eV	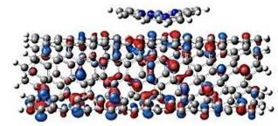 - 5.72663 eV
HOMO 2	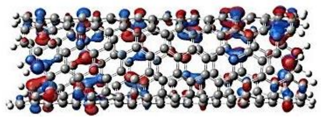 -6.30016 eV	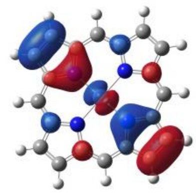 -7.7867 eV	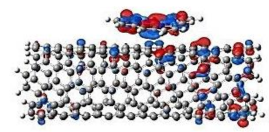 - 6.07031 eV
HOMO 3	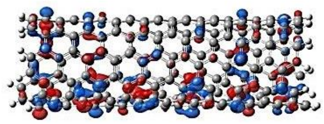 -6.3603 eV	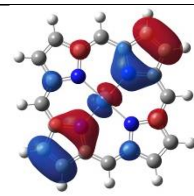 -7.78697 eV	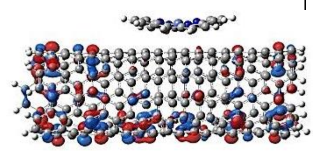 - 6.27277 eV

Table 1. The frontier molecular orbitals (HOMOs and LUMOs) and their absolute energies values in eV of ***P***-(6,5) SWNT, Ni-Porphyrin molecule and SWNT / Ni-Porphyrin complex, calculated using M05-2X / 3-21G theoretical level.

Since the energy of formation (binding energy) of the complex ($\Delta E_{complex}$) can be calculated using the following formula[23,24]:

$$\Delta E_{complex} = E_{complex} - (E_{SWNT} + E_{Ni\text{-}por})$$

where $E_{complex,}$ E_{SWNT} and $E_{Ni\text{-}por}$ are the corresponding absolute energies of the complex, SWNT and Ni-porphyrin molecule, respectively. The energy of formation of the SWNT / Ni-Porphyrin complex ($\Delta E_{complex}$) has been calculated using M052X / 321G theoretical level and found equals around -1.36 eV which is larger compared to the energy of formation of SWNT / porphyrin complex (-5.8 eV), implying that SWNT / porphyrin complex is more stable than SWNT / Ni-Porphyrin complex from the energetic point of view.

It worth to mention also that in the optimized geometric structure of Ni-Por / SWNT complex, the Ni-porphyrin ring was bent towards the tube surface with intermolecular distance $d_{SWNT/Por.}$ = 0.3 nm, taking chips shaped like structure or saddle structure (Fig. 6), which is the same with the distance measured for porphyrin / SWNT complex and very similar to the distance obtained for tetraphenylporphyrin (TPP) / C_{60} system[74] which is 3 Å and with TPP / SWNT system[75] which is $3.0 \leq d \leq 3.3$ Å.

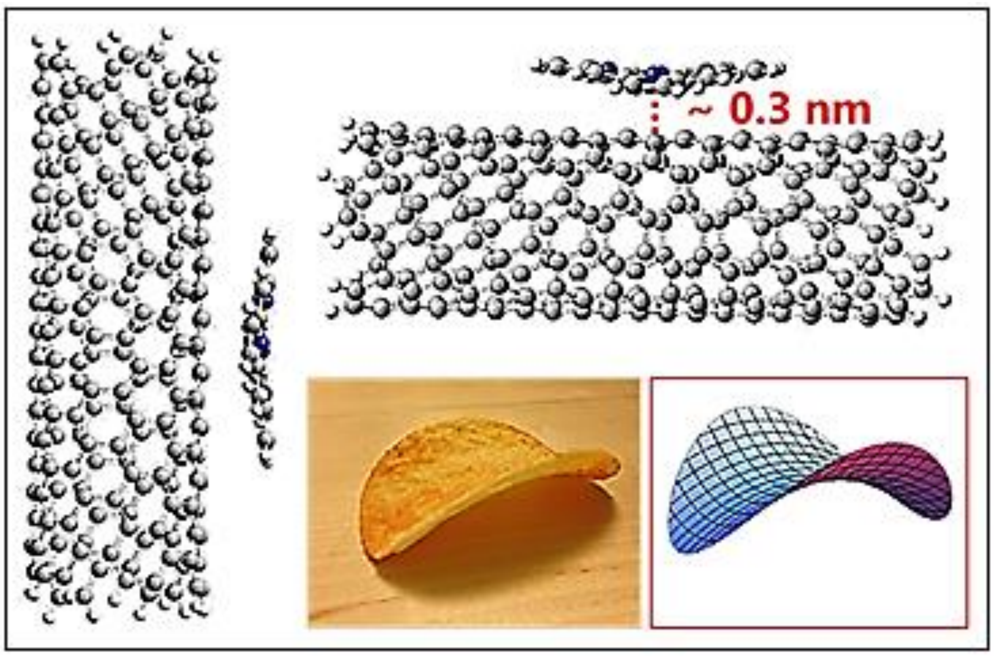

Figure 6. Optimized geometric structure obtained using M05-2X functional with 3-21G basis set for the+ non-covalent interaction of ***P***-(6,5) SWNT / Ni-Por complex in which the Ni-porphyrin ring was bent towards the tube surface (with intermolecular distance $d_{SWNT/Por.}$ = 0.3nm) taking chips shaped like structure or saddle structure.

Some novel supramolecular structures formed on SWNT surface.

As a very interesting unique finding, three novel supramolecular structures have been accidently observed, the first one in which Ni-C12P molecules can't only form a self-assembled mono layer on SWNTs surface, but also can give second layer of arrays above the first layer via π-π staking between porphyrin molecules. This is clearly appeared in Figures 7 and 8; where half of the SWNTs is covered by the second layer of Ni-C12P molecules, in addition one can see the height difference between the two layers which further confirmed by measuring the actual height of the two layers from the topographic profile (Fig. 7c); as first layer height is 0.2 – 0.4 nm, whilst the height of the second layer is 0.6 – 0.7 nm. Figure 7b elucidates a schematic representation for the multi-layered supramolecular structure arrays of Ni-C12P molecules on SWNTs surface.

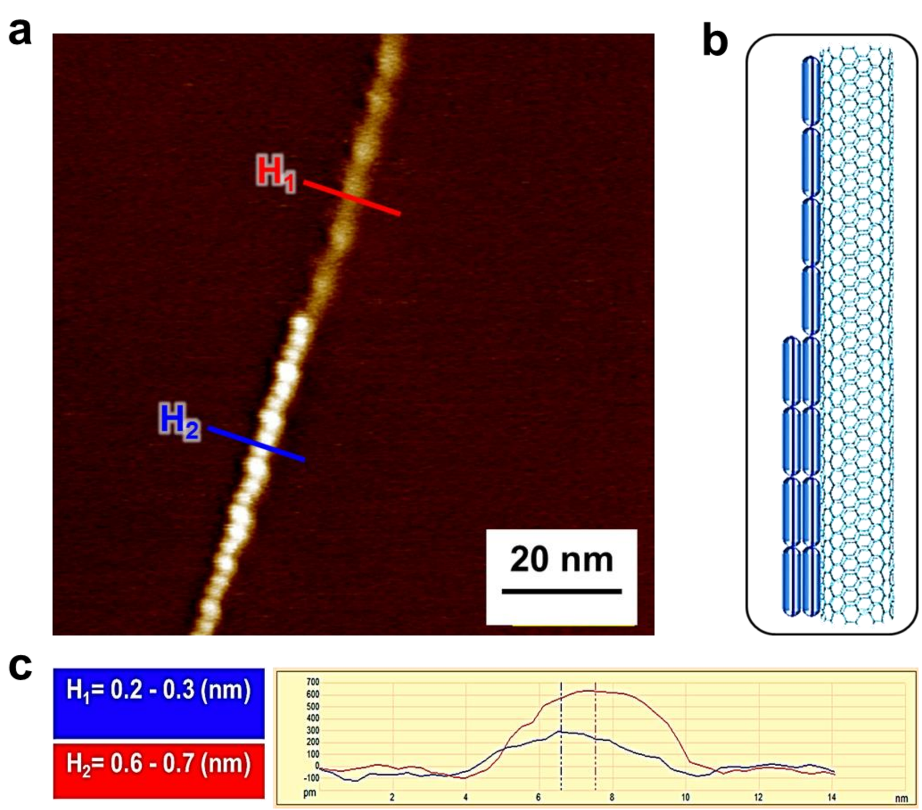

Figure 7. a, STM image of Ni-C12P / SWNTs complex on HOPG surface showing multi-layered supramolecular structure arrays of Ni-C12P molecules on the tube surface (100 nm × 100 nm, first layer, $I_{t} =$ 0.010 nm, V_{sample} = 0.100 V, second layer, I_t = 0.010 nm, V_{sample} = 0.130 V) **b,** Schematic representation illustrating multi-layered supramolecular structure arrays of Ni-C12P on SWNT surface **c**, The topographic profile showing the height of first (H_1) and second layers (H_2) which are 0.2 -0.4 nm and 0.6 – 0.7 nm, respectively.

In order to obtain such kind of these images, the scanning conditions have been modified during STM measuments; this can be shown in Fig. 8 (especially Fig. 8 c and d), as we succeed to image each layer separately. The average molecular length of the second layer molecules was measured and equals around 3.7 nm, however the average center to center distance for the second layer molecules is smaller than the first layer center to center distance, this is may be attributed to Ni-C12P molecules close packing became narrow as the interaction and staking increased between them (Fig. 8d).

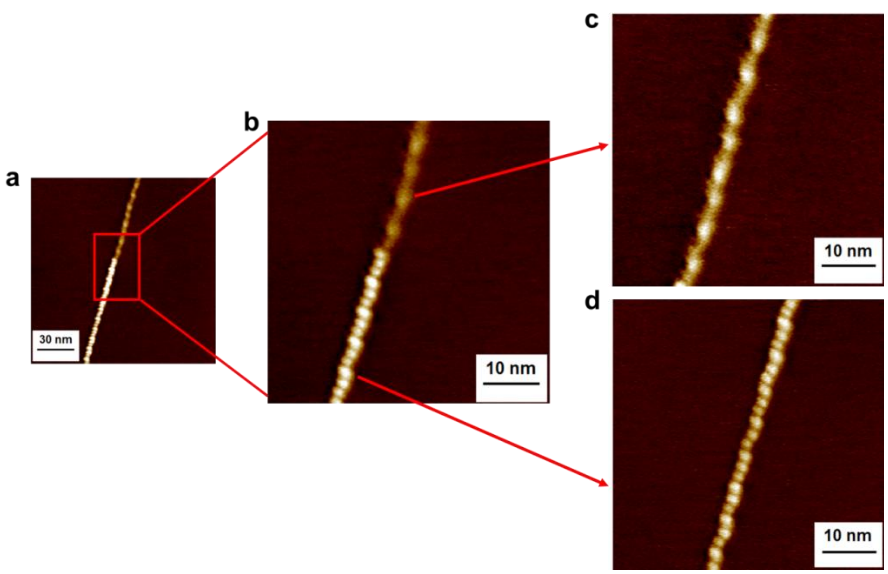

Figure 8. Large scale and high resolution STM images for multi-layered supramolecular structure arrays of Ni-C12P / SWNTs complex on HOPG surface. All images were taken at V_{sample} = 0.100 V and I_t = 0.010 nA for the first layer, and I_t = 0.010 nm, V_{sample} = 0.130 V for the second layer **a**, First and second layers (150 nm × 150 nm) **b,** First and second layers (50 nm × 50 nm) **c,** First layer only (50 nm x 50 nm) **d,** Second layer only (50 nm × 50 nm).

Formation of multi-layers of porphyrin and phthalocyanine derivatives on different flat surface has been reported by many researches[76-81]. We also found that, it is possible for free base porphyrin (C12P) to form a second layer in some sites on HOPG surface (Fig. 5b in chapter 2). However as the best of our knowledge; this is the first work studying multi-layered supramolecular structure arrays on SWNTs (curved) surface.

The second amazing supramolecular structure is depicted in Fig. 9a, in which two SWNTs are superimposed via π-π staking; the lower SWNT (marked as *III*) is bundled with upper SWNT (marked as *II* in) and become totally superimposed at part *I*, as it is illustrated in the schematic representation in Fig. 9b. In addition to one can see clearly the upper SWNT is covered with Ni-C12P molecules (part *II*). For more confirmation the height of sections *III*, *II* and *I* has been measured and equals 0.2 – 0.3 nm, 0.3 – 0.4 nm and 0.6 – 0.7 nm. Similar phenomenon of SWNTs / porphyrin complex superimposable was also reported by our group in a previous study[60].

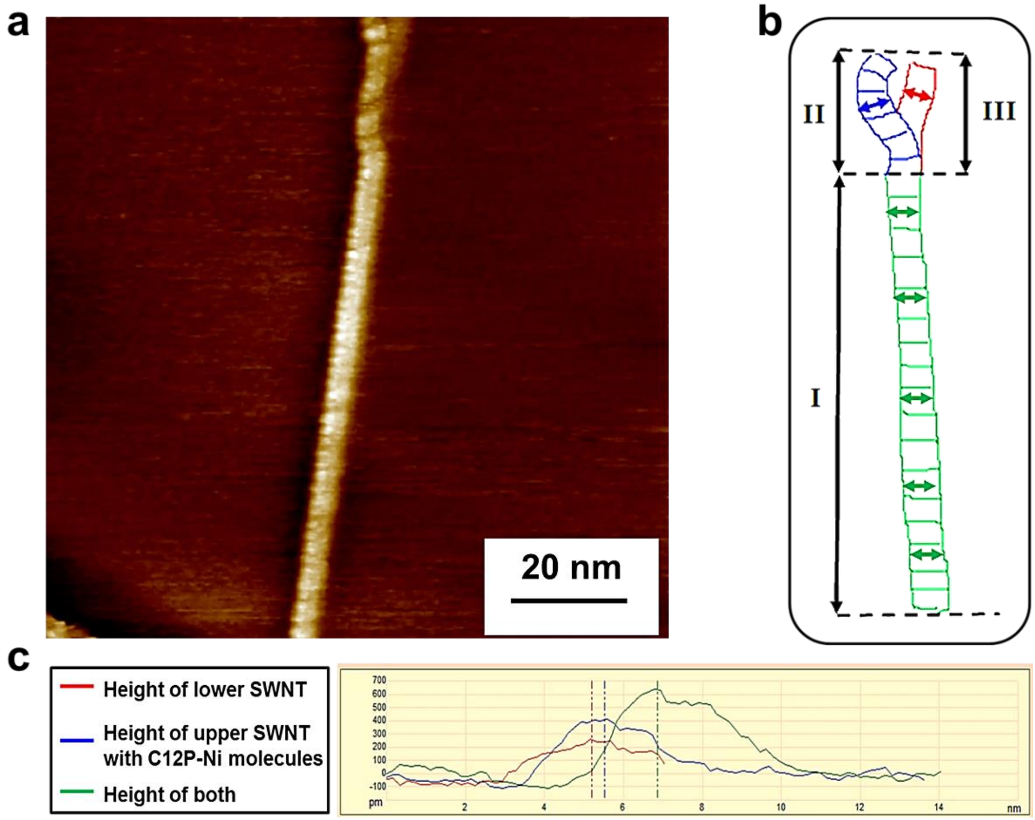

Figure 9. a, STM image of Ni-C12P / SWNT complex on HOPG surface showing supramolecular structure arrays of Ni-C12P molecules on the surface of two superimposed SWNTs (100 nm × 100 nm, $I_{t\,=}$ 0.010 nm, $V_{\,sample}$ = 0.100 V) **b,** Schematic representation illustrating the two superimposed SWNTs with supramolecular structure arrays of Ni-C12P molecules **c**, The topographic profile showing the height of each tube in sections *I, II* and *III*.

The third matchless structure found for Ni-C12P / SWNT complex is distinctly marvelous finding. Figure 10 elucidates an interesting structure of two separately SWNTs covered with Ni-C12P molecules, and at the same time, they are interacting altogether via π-π staking between both molecule-molecule interactions and molecule-substrate interaction in addition to substrate-substrate interactions. Furthermore, the Ni-C12P molecules are aligned in well-organized ordering.

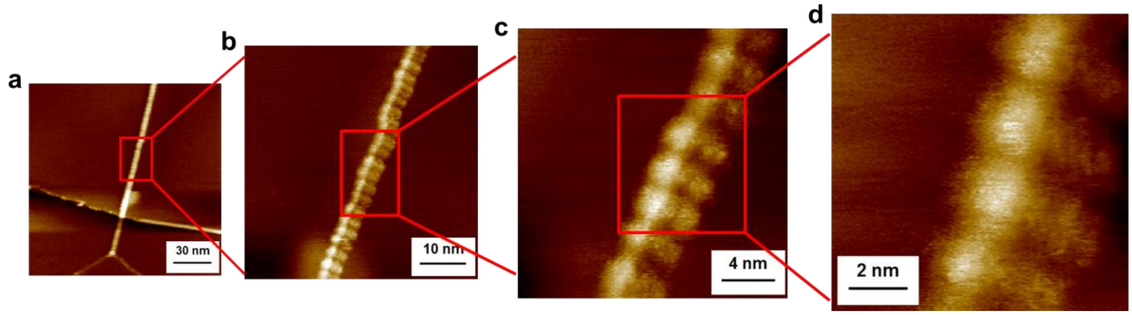

Figure 10. Large scale and high resolution STM images of an interacted supramolecular structure arrays of Ni-C12P / SWNT complex on HOPG surface **a**, (150 nm × 150 nm, I_{t} = 0.010 nm, V_{sample} = 0.100 V) **b,** (50 nm × 50 nm, I_{t} = 0.020 nm, V_{sample} = 0.130 V) **c**, (20 nm × 20 nm, I_{t} = 0.020 nm, V_{sample} = 0.130 V) **d**, (10 nm ×10 nm, I_{t} = 0.020 nm, V_{sample} = 0.130 V).

By measuring the height difference between the two SWNTs, we found it equals around 0.1 nm (topographic profile Fig. 11b). One more interesting point is the molecular length, as it equals around 2.45 nm; this of course, smaller than our molecule (Ni-C12P) length which is 3.7 nm (Fig. 4a), that means Ni-C12P molecules might physisorbed in this situation by different behavior. As the difference in length equals 1.25 nm and this is the same length of one dodecyl alkyl chain; so Ni-C12P molecules might be adsorbed on SWNTs surface by only one dodecyl alkyl chain, whilst the other one may be wrapped around the SWNTs. Adsorption of *meso*-alkyl porphyrin on SWNTs surface by only one alkyl chain was reported by N. Katsonis *et al*[68]. The same situation happened to the other

SWNTs to give this unique supramolecular interacting structure. Such kind of these new structures will be very helpful for building a novel molecular architectonics from SWNTs / porphyrin systems.

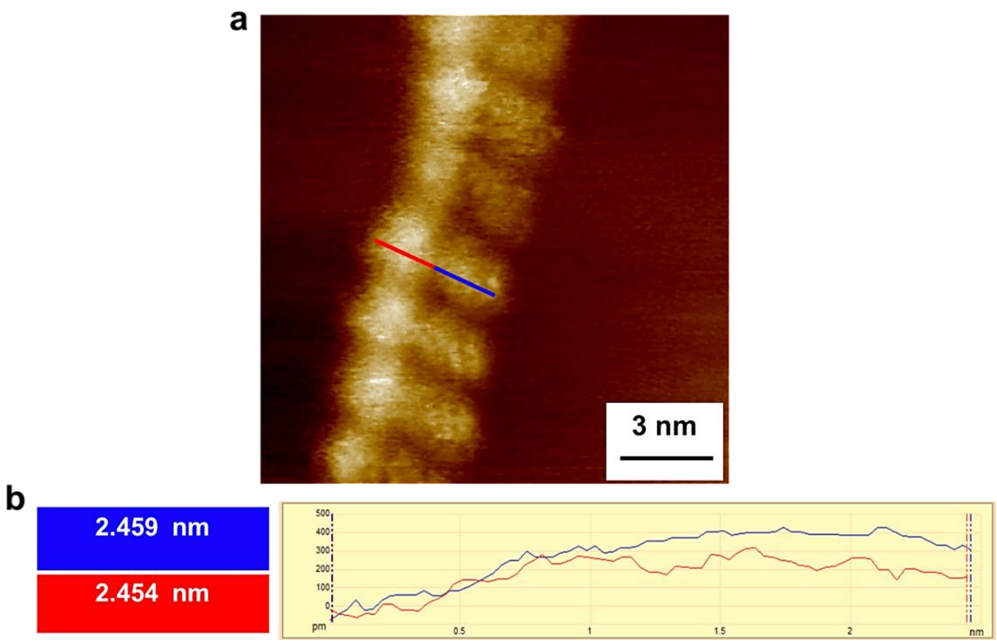

Figure 11. **a**, STM image of an interacted supramolecular structure arrays of Ni-C12P / SWNT complex on HOPG surface (15 nm × 15 nm, $I_{t\,=}$ 0.020 nm, V_{sample} = 0.130 V) **b,** The topographic profile showing the molecular length on the upper and lower SWNTs surface, which equals 2.454 and 2.459, respectively; with height difference between them around 0.1 nm.

4.4. Conclusion

The handedness chirality of single-walled carbon nanotubes (SWNT) has been successfully distinguished using STM imaging technique by using the supramolecular structure of 5,15-bisdodecylporphyrin-Ni (Ni-C12P) which formed on the tube surface. Previously we also succeed to distinguish the handedness chirality of SWNT by STM using free base porphyrin C12P (chapter 2), furthermore in this chapter we succeed to confirm the identification of SWNT handedness chirality using metalized porphyrin indicating that even though by changing the molecular structure of porphyrin molecule i.e. insertion a central metals to the porphyrin ring; the handedness chirality of SWNT still can be recognized using the supramolecular structures of these organic molecules formed on the tube surface. Interestingly two opposite supramolecular structures of Ni-C12P molecules have been observed on SWNT surface, by using a mixture of two different types of chiral SWNTs (right handed ***P*** or plus SWNT and left handed ***M*** or minus SWNT), displaying the marvelous effect of SWNT handedness chirality on the alignment of organic molecules on its surfaces. In addition, surprisingly some novel supramolecular structures of Ni-C12P have been accidently observed on SWNT surface. This vital finding effectively will identify directly the absolute handedness chirality of SWNTs, and being as key point for further understanding and building a new supramolecular architectures on curved nanocarbon surfaces, as well as can be used for designing and fabricating novel molecular architectonics of porphyrin / SWNTs based devices.

References

1 Aviram, A. & Ratner, M. A. Molecular rectifiers. *Chemical Physics Letters* **29**, 277-283 (1974).

2 Metzger, R. M. *et al.* Unimolecular electrical rectification in hexadecylquinolinium tricyanoquinodimethanide. *Journal of the American Chemical Society* **119**, 10455-10466 (1997).

3 Flood, A. H., Stoddart, J. F., Steuerman, D. W. & Heath, J. R. Whence molecular electronics? *Science* **306**, 2055-2056 (2004).

4 Liljeroth, P., Repp, J. & Meyer, G. Current-induced hydrogen tautomerization and conductance switching of naphthalocyanine molecules. *Science* **317**, 1203-1206 (2007).

5 Okawa, Y. *et al.* Chemical wiring and soldering toward all-molecule electronic circuitry. *Journal of the American Chemical Society* **133**, 8227-8233 (2011).

6 Kubatkin, S. *et al.* Single-electron transistor of a single organic molecule with access to several redox states. *Nature* **425**, 698-701 (2003).

7 Staykov, A., Areephong, J., R. Browne, W., L. Feringa, B. & Yoshizawa, K. Electrochemical and photochemical cyclization and cycloreversion of diarylethenes and diarylethene-capped sexithiophene wires. *ACS nano* **5**, 1165-1178 (2011).

8 Vuillaume, D. Molecular nanoelectronics. *Proceedings of the IEEE* **98**, 2111-2123 (2010).

9 Song, H., Reed, M. A. & Lee, T. Single molecule electronic devices. *Advanced Materials* **23**, 1583-1608 (2011).

10 Heath, J. R. Molecular electronics. *Annual Review of Materials Research* **39**, 1-23 (2009).

11 Ratner, M. A. *et al.* Molecular wires: Charge transport, mechanisms, and control. *Annals of the New York Academy of Sciences* **852**, 22-37 (1998).

12 Duong, B., Arechabaleta, R. & Tao, N. In situ AFM/STM characterization of porphyrin electrode films for electrochemical detection of neurotransmitters. *Journal of Electroanalytical Chemistry* **447**, 63-69 (1998).

13 Harima, Y. *et al.* Formation of Schottky barriers at interfaces between metals and molecular semiconductors of p ‐ and n ‐ type conductances. *Applied physics letters* **69**, 1059-1061 (1996).

14 Liu, C.-y., Pan, H.-I., Fox, M. A. & Bard, A. J. Films of the Photoconductor ZnODEP. *Sens. Actuators A* **21**, 193 (1990).

15 Malinski, T. & Taha, Z. Nitric oxide release from a single cell measured in situ by a porphyrinic-based microsensor. *Nature* **358**, 676-678 (1992).

16 Maree, C. *et al.* Photovoltaic effects in porphyrin polymer films and heterojunctions. *Journal of applied physics* **80**, 3381-3389 (1996).

17 Reimers, J., Crossley, M. & Hush, N. Molecular electronic properties of fused rigid porphyrin-oligomer molecular wires. *Nanotechnology* **7**, 424 (1996).

18 Ishii, T. *et al.* Syntheses and electronic structures of macrocyclic metal complexes with fullerene. *Inorganica Chimica Acta* **317**, 81-90 (2001).

19 Guldi, D. M., Taieb, H., Rahman, G. A., Tagmatarchis, N. & Prato, M. Novel Photoactive Single‐Walled Carbon Nanotube–Porphyrin Polymer Wraps: Efficient and Long‐Lived Intracomplex Charge Separation. *Advanced Materials* **17**, 871-875 (2005).

20 Ehli, C. *et al.* Interactions in single wall carbon nanotubes/pyrene/porphyrin nanohybrids. *Journal of the American Chemical Society* **128**, 11222-11231 (2006).

21 Ozawa, H. *et al.* Supramolecular Hybrid of Gold Nanoparticles and Semiconducting Single-Walled Carbon Nanotubes Wrapped by a Porphyrin–Fluorene Copolymer. *Journal of the American Chemical Society* **133**, 14771-14777 (2011).

22 Hirsch, A. Functionalization of single‐walled carbon nanotubes. *Angewandte Chemie International Edition* **41**, 1853-1859 (2002).

23 Basiuk, V. A. & Bassiouk, M. Nanoassembly of meso-tetraphenylporphines on surfaces of carbon materials: initial steps as studied by molecular mechanics and scanning tunneling microscopy. *Journal of nanoscience and nanotechnology* **8**, 259-267 (2008).

24 Basiuk, E. V., Basiuk, V. A., Santiago, P. & Puente-Lee, I. Noncovalent functionalization of carbon nanotubes with porphyrins: meso-tetraphenylporphine and its transition metal complexes. *Journal of nanoscience and nanotechnology* **7**, 1530-1538 (2007).

25 Zhang, X. *et al.* Solvent dependent supramolecular self-assembly and surface reversal of a modified porphyrin. *Physical Chemistry Chemical Physics* **15**, 12510-12515 (2013).

26 Oncel, N. & Bernasek, S. L. The effect of molecule-molecule and molecule-substrate interaction in the formation of Pt-octaethyl porphyrin self-assembled monolayers. *Applied Physics Letters* **92**, 133305 (2008).

27 Ikeda, T. *et al.* STM observation of alkyl-chain-assisted self-assembled monolayers of pyridine-coordinated porphyrin rhodium chlorides. *Langmuir* **20**, 5454-5459 (2004).

28 Ikeda, T., Asakawa, M., Miyake, K., Goto, M. & Shimizu, T. Scanning tunneling microscopy observation of self-assembled monolayers of strapped porphyrins. *Langmuir* **24**, 12877-12882 (2008).

29 Ogunrinde, A., Hipps, K. & Scudiero, L. A scanning tunneling microscopy study of self-assembled nickel (II) octaethylporphyrin deposited from solutions on HOPG. *Langmuir* **22**, 5697-5701 (2006).

30 Shen, Y. *et al.* Self-assembling in fabrication of ordered porphyrins and phthalocyanines hybrid nano-arrays on HOPG. *CrystEngComm* **15**, 5526-5531 (2013).

31 Zheng, L. *et al.* Preparation of cobalt-tetraphenylporphyrin/reduced graphene oxide nanocomposite and its application on hydrogen peroxide biosensor. *Analytica chimica acta* **768**, 69-75 (2013).

32 Auwärter, W., Écija, D., Klappenberger, F. & Barth, J. V. Porphyrins at interfaces. *Nature Chemistry* **7**, 105-120 (2015).

33 Baughman, R. H., Zakhidov, A. A. & de Heer, W. A. Carbon nanotubes--the route toward applications. *science* **297**, 787-792 (2002).
34 Sinha, N., Ma, J. & Yeow, J. T. Carbon nanotube-based sensors. *Journal of nanoscience and nanotechnology* **6**, 573-590 (2006).
35 Teugels, L. G., Avila-Bront, L. G. & Sibener, S. Chiral domains achieved by surface adsorption of achiral nickel tetraphenyl-or octaethylporphyrin on smooth and locally kinked Au (111). *The Journal of Physical Chemistry C* **115**, 2826-2834 (2011).
36 Murphy, B. *et al.* Growth and ordering of Ni (II) diphenylporphyrin monolayers on Ag (111) and Ag/Si (111) studied by STM and LEED. *Journal of Physics: Condensed Matter* **24**, 045005 (2012).
37 Haq, S. *et al.* Versatile bottom-up construction of diverse macromolecules on a surface observed by scanning tunneling microscopy. *ACS nano* **8**, 8856-8870 (2014).
38 Yoshimoto, S. & Itaya, K. Advances in supramolecularly assembled nanostructures of fullerenes and porphyrins at surfaces. *Journal of Porphyrins and Phthalocyanines* **11**, 313-333 (2007).
39 Phan, T. H., Kosmala, T. & Wandelt, K. Potential dependence of self-assembled porphyrin layers on a Cu (111) electrode surface: In-situ STM study. *Surface Science* **631**, 207-212 (2015).
40 Phan, T. H. & Wandelt, K. Self-assembly of metal free porphyrin layers at copper-electrolyte interfaces: Dependence on substrate symmetry. *Surface Science* **607**, 82-91 (2013).
41 Guo, Z. *et al.* Covalently porphyrin-functionalized single-walled carbon nanotubes: a novel photoactive and optical limiting donor–acceptor nanohybrid. *Journal of Materials Chemistry* **16**, 3021-3030 (2006).
42 Baskaran, D., Mays, J. W., Zhang, X. P. & Bratcher, M. S. Carbon nanotubes with covalently linked porphyrin antennae: photoinduced electron transfer. *Journal of the American Chemical Society* **127**, 6916-6917 (2005).
43 Liu, Z. B. *et al.* Enhanced Optical Limiting Effects in Porphyrin‐Covalently Functionalized Single‐Walled Carbon Nanotubes. *Advanced materials* **20**, 511-515 (2008).
44 Sáfar, G. d. A. M. *et al.* Interactions of porphyrins and single walled carbon nanotubes: A fine duet. *Synthetic Metals* **193**, 64-70 (2014).
45 Sprafke, J. K., Stranks, S. D., Warner, J. H., Nicholas, R. J. & Anderson, H. L. Noncovalent binding of carbon nanotubes by porphyrin oligomers. *Angewandte Chemie International Edition* **50**, 2313-2316 (2011).
46 Cheng, F. & Adronov, A. Noncovalent functionalization and solubilization of carbon nanotubes by using a conjugated Zn–porphyrin polymer. *Chemistry–A European Journal* **12**, 5053-5059 (2006).
47 Cheng, F., Zhang, S., Adronov, A., Echegoyen, L. & Diederich, F. Triply Fused ZnII–Porphyrin Oligomers: Synthesis, Properties, and Supramolecular Interactions with Single‐Walled Carbon Nanotubes (SWNTs). *Chemistry–A European Journal* **12**, 6062-6070 (2006).

48 AminuráRahman, G. Electronically interacting single wall carbon nanotube–porphyrin nanohybrids. *Journal of Materials Chemistry* **16**, 62-65 (2006).
49 Tuncel, D. Non-covalent interactions between carbon nanotubes and conjugated polymers. *Nanoscale* **3**, 3545-3554 (2011).
50 Bilalis, P., Katsigiannopoulos, D., Avgeropoulos, A. & Sakellariou, G. Non-covalent functionalization of carbon nanotubes with polymers. *RSC Advances* **4**, 2911-2934 (2014).
51 Guldi, D. M. *et al.* Functional single-wall carbon nanotube nanohybrids associating SWNTs with water-soluble enzyme model systems. *Journal of the American Chemical Society* **127**, 9830-9838 (2005).
52 Satake, A., Miyajima, Y. & Kobuke, Y. Porphyrin-carbon nanotube composites formed by noncovalent polymer wrapping. *Chemistry of materials* **17**, 716-724 (2005).
53 Chen, J. & Collier, C. P. Noncovalent functionalization of single-walled carbon nanotubes with water-soluble porphyrins. *The Journal of Physical Chemistry B* **109**, 7605-7609 (2005).
54 Chitta, R. *et al.* Donor-acceptor nanohybrids of zinc naphthalocyanine or zinc porphyrin noncovalently linked to single-wall carbon nanotubes for photoinduced electron transfer. *The Journal of Physical Chemistry C* **111**, 6947-6955 (2007).
55 Roquelet, C. *et al.* Light harvesting with non covalent carbon nanotube/porphyrin compounds. *Chemical Physics* **413**, 45-54 (2013).
56 Zhong, Q. *et al.* Fused Porphyrin–Single-Walled Carbon Nanotube Hybrids: Efficient Formation and Photophysical Characterization. *ACS nano* **7**, 3466-3475 (2013).
57 Murakami, H., Nomura, T. & Nakashima, N. Noncovalent porphyrin-functionalized single-walled carbon nanotubes in solution and the formation of porphyrin–nanotube nanocomposites. *Chemical Physics Letters* **378**, 481-485 (2003).
58 Hasobe, T., Fukuzumi, S. & Kamat, P. V. Ordered assembly of protonated porphyrin driven by single-wall carbon nanotubes. j-and h-aggregates to nanorods. *Journal of the American Chemical Society* **127**, 11884-11885 (2005).
59 Sarkar, T., Srinives, S., Sarkar, S., Haddon, R. C. & Mulchandani, A. Single-Walled Carbon Nanotube–Poly (porphyrin) Hybrid for Volatile Organic Compounds Detection. *The Journal of Physical Chemistry C* **118**, 1602-1610 (2014).
60 Tanaka, H., Yajima, T., Kawao, M. & Ogawa, T. Electronic properties of a single-walled carbon nanotube/150mer-porphyrin system measured by point-contact current imaging atomic force microscopy. *Journal of nanoscience and nanotechnology* **6**, 1644-1648 (2006).
61 Tanaka, H., Yajima, T., Matsumoto, T., Otsuka, Y. & Ogawa, T. Porphyrin Molecular Nanodevices Wired Using Single‐Walled Carbon Nanotubes. *Advanced Materials* **18**, 1411-1415 (2006).
62 Miyake, Y. *et al.* Entropy-controlled 2D supramolecular structures of N, N′-bis (n-alkyl) naphthalenediimides on a HOPG surface. *Acs Nano* **6**, 3876-3887 (2012).

63 Liu, G. *et al.* Simultaneous discrimination of diameter, handedness, and metallicity of single-walled carbon nanotubes with chiral diporphyrin nanocalipers. *Journal of the American Chemical Society* **135**, 4805-4814 (2013).
64 Komatsu, N. Stereochemistry of carbon nanotubes. *Japanese Journal of Applied Physics* **49**, 02BC01 (2010).
65 Peng, X., Komatsu, N., Kimura, T. & Osuka, A. Improved optical enrichment of SWNTs through extraction with chiral nanotweezers of 2, 6-pyridylene-bridged diporphyrins. *Journal of the American Chemical Society* **129**, 15947-15953 (2007).
66 Peng, X., Wang, F., Bauri, A. K., Rahman, A. M. & Komatsu, N. Optical Resolution of Single-Walled Carbon Nanotubes through Molecular Recognition with Chiral Diporphyrin Nanotweezers. *Chemistry Letters* **39**, 1022-1027 (2010).
67 He, C. *et al.* Turn on fluorescence sensing of vapor phase electron donating amines via tetraphenylporphyrin or metallophenylporphrin doped polyfluorene. *Chemical Communications* **46**, 7536-7538 (2010).
68 Katsonis, N. *et al.* Self-Organized Monolayer of m eso-Tetradodecylporphyrin Coordinated to Au (111). *Journal of the American Chemical Society* **128**, 15537-15541 (2006).
69 Visser, J., Katsonis, N., Vicario, J. & Feringa, B. L. Two-dimensional molecular patterning by surface-enhanced zn-porphyrin coordination. *Langmuir* **25**, 5980-5985 (2009).
70 Plamont, R. *et al.* Nanoscopic Imaging of meso‐Tetraalkylporphyrins Prepared in High Yields Enabled by Montmorrilonite K10 and 3 Å Molecular Sieves. *Chemistry–A European Journal* **19**, 11293-11300 (2013).
71 Gaussian09, R. A. 1, MJ Frisch, GW Trucks, HB Schlegel, GE Scuseria, MA Robb, JR Cheeseman, G. Scalmani, V. Barone, B. Mennucci, GA Petersson et al., Gaussian. *Inc., Wallingford CT* (2009).
72 Zhao, Y., Schultz, N. E. & Truhlar, D. G. Design of density functionals by combining the method of constraint satisfaction with parametrization for thermochemistry, thermochemical kinetics, and noncovalent interactions. *Journal of Chemical Theory and Computation* **2**, 364-382 (2006).
73 Rodríguez-Galván, A., Amelines-Sarria, O., Rivera, M., Carreón-Castro, M. d. P. & Basiuk, V. A. Adsorption and Self-assembly of Anticancer Antibiotic Doxorubicin on Single-Walled Carbon Nanotubes. *NANO* (2015).
74 Basiuk, V. A., Kolokoltsev, Y. & Amelines-Sarria, O. Noncovalent interaction of meso-tetraphenylporphine with C60 fullerene as studied by several DFT methods. *Journal of nanoscience and nanotechnology* **11**, 5519-5525 (2011).
75 Orellana, W. & Correa, J. D. Noncovalent functionalization of carbon nanotubes and graphene with tetraphenylporphyrins: stability and optical properties from ab initio calculations. *Journal of Materials Science* **50**, 898-905 (2015).
76 Li, M. *et al.* Conformation-Dependent Stacking Behavior of Porphyrin Assemblies Observed by Using Scanning Tunneling Microscopy. *The Journal of Physical Chemistry C* **114**, 1881-1884 (2010).

77 Hutin, M., Sprafke, J. K., Odell, B., Anderson, H. L. & Claridge, T. D. A discrete three-layer stack aggregate of a linear porphyrin tetramer: solution-phase structure elucidation by NMR and X-ray scattering. *Journal of the American Chemical Society* **135**, 12798-12807 (2013).

78 Ge, X. *et al.* Controlled formation of an axially bonded Co-phthalocyanine dimer. *Journal of the American Chemical Society* **131**, 6096-6098 (2009).

79 Buchner, F. *et al.* Chemical fingerprints of large organic molecules in scanning tunneling microscopy: imaging adsorbate– substrate coupling of metalloporphyrins. *The Journal of Physical Chemistry C* **113**, 16450-16457 (2009).

80 Vollnhals, F., Wintrich, P., Walz, M.-M., Steinrück, H.-P. & Marbach, H. Electron beam induced surface activation of ultrathin porphyrin layers on Ag (111). *Langmuir* **29**, 12290-12297 (2013).

81 Inose, T. *et al.* Switching of Single ‐ Molecule Magnetic Properties of TbIII–Porphyrin Double ‐ Decker Complexes and Observation of Their Supramolecular Structures on a Carbon Surface. *Chemistry–A European Journal* **20**, 11362-11369 (2014).

Chapter V. Overall Conclusion

This work has been dedicated to study some properties of organic molecule / nano-carbon conjugates for instance investigating and distinguishing the handedness chirality of SWNT using scanning tunnelling microscopic imaging (for the first time) via the supramolecular structures of some porphyrins and metal porphyrins on the tube surface, as well as more understanding the mechanisms by which such kind of these supramolecular structures can be formed on both the flat and curved nanocarbon materials surfaces.

In the first chapter of this thesis, we described briefly some basics and fundamentals of molecular electronics as an effective field in the material science including single molecular rectifier, porphyrins as efficacious components in molecular devices design. In addition to nano-carbon materials (nanocarbons) i.e. highly oriented pyrolytic graphite HOPG and carbon nanotubes (CNTs) including synthesis, classification, properties, functionalization, characterization and applications. As well as, scanning probe microscopy i.e. STM and AFM.

In chapter II, we succeed to investigate the handedness chirality of single-walled carbon nanotubes (SWNT) by using STM imaging technique and DFT calculations for the first time. This is can be achieved using the supramolecular chemistry of some porphyrin derivatives i.e. 5,15-bisdodecylporphyrin (C12P) on the tube surface. Surprisingly, by using two different types of chiral SWNTs (right handed ***P*** or plus SWNT and left handed ***M*** or minus SWNT); two opposite supramolecular structures have been observed showing the marvelous effect of SWNT handedness chirality on the alignment of organic molecules on its surfaces. Based on our results, it has been found that alkyl chain substituted porphyrins can form a well-ordered supramolecular structure on the basal plane of SWNT surfaces that minutely maintains the Grozsek geometry with a little bit deviation. This vital finding explicate that SWNTs handedness chirality plays a crucial role for the molecular orientation of organic molecules on its surface.

In chapter III, the supramolecular structures of different central metal porphyrins i.e. ZnPor, NiPor and CoPor were successfully observed on SWNT (HiPCO raw) surface by using STM imaging technique and further characterized via HR-TEM and UV - Visible spectroscopy, with the purpose for identifying the effect of metalation on the supramolecular structures of porphyrins on SWNT surface. All the metal porphyrins can be adsorbed effectively on the tube surface leading to well-ordered supramolecular structures (especially in the cases of NiPor and ZnPor) on SWNT surface, as well as strong debundling effect (especially in CoPor case) for the nanotubes. Among the three metal porphyrins; NiPor produced the best STM resolution images.

From an energetic point of view, DFT results displayed that the stability of these metal porphyrins complexes with the following order Ni < Zn < Co, additionally all the metal porphyrins complexes took chips shaped like structure or saddle structure with almost the same intermolecular contact distance between the porphyrin and SWNT surface which equal around 3 Å. Consequently by changing the central metal incorporated inside the porphyrin ring; different supramolecular structures can be observed on SWNT surface, which displaying the marvelous effect of different metal centers on the supramolecular structure of porphyrins on SWNT surface.

In chapter IV, we succeed to confirm the identification of SWNT handedness chirality using metalized porphyrin indicating that even though by changing the molecular structure i.e. insertion a central metals to the porphyrin ring; the handedness chirality of SWNT still can be recognized using the supramolecular structures of these organic molecules formed on the tube surface. Interestingly two opposite supramolecular structures of Ni-C12P molecules have been observed on SWNT surface, by using a mixture of two different types of chiral SWNTs (right handed ***P*** or plus SWNT and left handed ***M*** or minus SWNT), displaying the marvelous effect of SWNT handedness chirality on the alignment of organic molecules on its surfaces. In addition, surprisingly some novel supramolecular structures of Ni-C12P have been accidently observed on SWNT surface.

Ultimately, as a whole conclusion, hopefully by the aid of this study and these vital findings, it will be obvious to identify directly the absolute handedness chirality of the SWNTs, and being as key point for further understanding and building a new supramolecular architectures on curved nanocarbon surfaces, as well as can be used for designing and fabricating novel molecular architectonics of porphyrin / SWNTs based devices.

List of Publications

Master Publications

- Fabrication of core/shell hybrid organic-inorganic polymer microspheres via Pickering emulsion polymerization using laponite nanoparticles

Amro K.F. Dyab, Hamad A. Al-Lohedan, Hisham A. Essawy, **Ahmed I. A. Abd El-Mageed** and Fouad Taha.

J. Saudi Chem. Soc. **2014**, *18*, 610.

- Preparation of polystyrene latex particles via emulsion polymerization using Hitenol BC-20 as a surfmer: Why the coating potential is different compared to the presence of emulsifying solid nanoparticles?

Amro K. F. Dyab, Hisham A. Essawy, **Ahmed I. A. Abd El-Mageed,** and Fouad Taha

International Symposium on Materials and Sustainable Development "CIMDD", Université M'Hamed Bougara Boumerdes, Algeria, **2013.**

- Emulsion polymerization of styrene via Pickering emulsification system.

Amro K. F. Dyab, Hisham A. Essawy, **Ahmed I. A. Abd El-Mageed,** and Fouad Taha

Egy. J. of Appl. Sci. **2010**, *25*, 11.

PhD Publications

Chapter II

- First Observation of Handedness Chirality of ***P***- and ***M***- Single Walled Carbon Nanotubes using Scanning Tunneling Microscopic Images.

Ahmed I. A. Abd El-Mageed, Gang Liu, Naoki Komatsu, Tomoko Inose and Takuji Ogawa.

To be submitted.

Chapter III

- Supramolecular Structure of Different Metal Center Porphyrins on Single Walled Carbon Nanotube (SWNT) Surface.

Ahmed I. A. Abd El-Mageed and Takuji Ogawa.

In preparation to submit

Chapter IV

- Confirmation of SWNT Handedness Chirality Identification with Metalized Porphyrins using STM imaging Technique.

Ahmed I. A. Abd El-Mageed, Gang Liu, Naoki Komatsu, Tomoko Inose, and Takuji Ogawa.

In preparation to submit

- Surface Self-Assembly of Trans-Substituted Porphyrin Double-Decker Complexes Exhibiting Slow Magnetic Relaxation

D. Tanaka, T. Inose, S. Shimono, H. Tanaka, T. Tamaki, **Ahmed I. A. Abd El-Mageed**, Amro K. F. Dyab, N. Ishikawa, T. Ogawa.

J. Surf. Sci. Nanotechnol. (JSSN) **2014**, 12, 124.

List of Presentations and Conferences

- The Chemical Society of Japan 96th Annual Spring (CSJ 2016). Period: March 24-27, 2016, Place: **Doshisha University, Kyoto, Japan**. **Oral** Presentation entitled as "First Investigation of Handedness Chirality Effect of SWNTs by the Supramolecular Structures of Porphyrin Derivatives" **Ahmed I. A. Abd El-Mageed,** G. Liu, N. Komatsu,T. Inose, and T. Ogawa.

- The International Chemical Congress of Pacific Basin Societies (Pacifichem 2015). Period: December 15-20, 2015, Place: **Honolulu, Hawaii, USA**. **Oral** Presentation entitled as "Chirality Effects of SWNTs on the Supramolecular Structures of Porphyrin Derivatives on the Curved Surfaces"**Ahmed I. A. Abd El-Mageed,** G. Liu, N. Komatsu,T. Inose, and T. Ogawa.

- The International Chemical Congress of Pacific Basin Societies (Pacifichem 2015). Period: December 15-20, 2015, Place: **Honolulu, Hawaii, USA**. **Poster** Presentation entitled as "Single molecule devices connecting to three carbon nanotube electrodes" Ari Akbar, Murni Handayani, **Ahmed I. A. Abd El-Mageed**, and T. Ogawa.

- Toward to The Third Stage of The Single Molecular Electronics Research, 6th Study Group of Molecular Architectonics. Period: October 23-24, 2015, Place: **Kyoto University, Kyoto, Japan**. **Poster** Presentation entitled as "First Observation of Chirality of SWNTs by the Supramolecular Structures of Porphyrin Derivatives"**Ahmed I. A. Abd El-Mageed**, G. Liu, N. Komatsu,T. Inose, and T. Ogawa.

- International Workshop on Molecular Architectonics "IWMA 2015". Period: August 3-6, 2015, Place: **Shiretoko, Hokkaido, Japan**. **Poster** Presentation entitled as "Chirality Dependent Supramolecular Structures of Porphyrin Derivatives on Chiral Single-walled Carbon Nanotube Surfaces"**Ahmed I. A. Abd El-Mageed**, G. Liu, N. Komatsu,T. Inose, and T. Ogawa.

Scholarships and Awards

- Specially Appointed Assistant Professor (Full time), Chemistry Department, Graduate School of Science, Osaka University, Osaka, Japan. (October 2016 – March 2017).

- Researcher at Chemistry Department, Graduate School of Science, Osaka University, Osaka, Japan. (April 2013 – September 2013).

- MEXT Scholarship, half year fully funded Scholarship, Japanese Government. (April 2016 – September 2016).

- MEXT Scholarship, one year fully funded Scholarship, Japanese Government. (April 2015 – March 2016).

- Joint Supervision Scholarship, two years fully funded scholarship, Egyptian Government. (April 2013 – March 2015).

- Osaka University Scholarship, two years for waiving tuition fee and enrollment fee exemption, Osaka University, Japan. (October 2013 – September 2015).